# Contents

# List of Figures

# List of Tables

eddies behind the RV body before laminar flow through the atmosphere is again reestablished (and the wake "reattaches" to the RV at the lower altitudes). Prior to BLT, the wake is very pronounced (i.e., has so much signal content, as compared to background noise, that it is hard to ignore), is less affected by atmospheric drag but instead is a consequence of the interaction of the atmosphere and the ballistic coefficient of the RV, and moves at a slightly slower velocity than the RV (to the degree broadly indicated in Fig. 1.1).

(U)Prior to Phase 1 BRVAD, it was realized that an active decoy could not just rely on direct playback of an RV signature because the computational storage requirements would just be too great for onboard practicality of implementation (within present and near term projected future technology) to realistically accommodate:

- Variations in radar aspect angle at various points in the ballistic trajectory and for different candidate trajectories;
- Variations with altitude;
- Variations with various threat radar bandwiths and/or signal structure utilized by the threat radar.

(U)Although the BRVAD program of course accounts for emulating the entire RV tip, RV body, and wake behavior, this particular investigation concentrates on realistically replicating only the RV wake and proceeds to look into possible radar range gate-to-gate cross-correlation of radar signal spectral target returns across contiguous gates as a consequence of being illuminated by the threat radar (as illustrated phenomenologically in Fig. 1.2). This is a *major* thrust in this investigation. Accounting for and exploiting to an advantage any cross-correlation that exists across corresponding wake range gates between Principal Polarization and Orthogonal Polarization (PP/OP) components is also a *major* objective of this investigation.

(U)Within the Phase 1 BRVAD program, wake emulation proceeded from estimates of auto-spectra extracted from available Minuteman III Mark 12A RV data, as obtained from S-band/narrowband Tradex signal returns (at an operating frequency of 2.95 GHz) having a bandwith of 10 MHz and, consequently, only a 15 meter range resolution of

$$\Delta r = \frac{c}{2B_e} = \frac{3.0 \times 10^8}{2(10 \times 10^6)} = 15 \text{ meters}, \tag{1.2}$$

known as the Levinson-Wiggins-Robinson (LWR) algorithm and the other being a multichannel approximate generalization of the single channel Burg Maximum Entropy Method.(MEM) [158] algorithm, as further developed and extended to the multichannel case by A. H. Nuttall. Both algorithms are described in Chapter 2. Chapter 3 describes experiments done on simulated data, first to test out the software tools that were implemented for this investigation, with supporting discussions provided in Appendices D, E, F, and G. These tools are then applied to the actual, data. These experiments point out some of the perceived strengths and weaknesses of these two representative algorithms that were encountered in seeking to apply multichannel LP modeling to radar target data. Some general problems that were encountered in applying these Multichannel LP algorithms are pointed out in Appendix F. Considerations for using only Autoregressive (AR) process models here over apparently more general Autoregressive Moving-Average (ARMA) processes are provided in Chapter 4. Chapter 5 and its auxiliary Appendix A discuss how to effectively handle the radar ambiguity function effects that are present, which taint the processing results and, consequently, how to temper final cross-correlation results and conclusions in terms of a computed coherence function representation and associated moderating confidence regions. These techniques are applied to the Tradex RV wake data in Chapter 5 as a further detailed investigation of the cross-correlation present between designated channels representing either contiguous radar range gates and/or PP/OP components of the radar signal returns. Appendix B summarizes the methodology that can be used to explicitly erect accuracy bounds about the AR parameter estimates, which are the focus of this investigation, and the other supporting methodology available to calculate corresponding asymptotic Cramer-Rao lower bounds. After considering certain critical leads provided by the results of the independent 2-D modeling investigation, as reported in Section 6.1, Section 6.2 of Chapter 6 illustrates use of the 1-D modeling approach as it is explicitly applied to a representative sample of the available Tradex data at a particular altitude. It is at this point that the pertinent conclusions of the 2-D processing are folded in to aid in the selection of the most appropriate 1-D state size to use and to decide what states to include in the 1-D model. Concluding results on specifying an appropriate wake model (that is the primary objective of this investigation) are offered in the remainder of Chapter 6. Overall conclusions and a summary are offered in Chapter 7.

(U)In general, technical details are relegated to the Appendices. The contents of Appendices A and B have already been described above. Appendix C describes the emergence of new techniques to gauge proximity to a spectral template that are important in subsequent downstream evaluations to gauge the adequacy of the

approach offered here or the results of this modeling effort in successfully approximating the signature of actual RVs. Appendix D discusses the capabilities designed into the new simulator as well as elaborating on why this redesign was initiated as a way to preserve the cross-channel sensitivity by avoiding previous approximations that tended to obscure simulated cross-channel effects. This is important in validating software implementations of spectral estimation algorithms that are themselves extremely sensitive to the veracity of the multichannel simulator implementation. A discussion is also provided here of each new feature introduced and how it was checked out and validated as having been correctly implemented and how it is presently performing to provide the correct answers. The status of each critical software module and the structured progression of validation and debug efforts/activities are covered in Appendix F, while the specific analytic closed-form test cases used for verification/validation are derived or described in Appendix G along with identification and an explanation of what software feature is to be verified through the use of each test case. Appendix H serves to explicitly remind that 1-D results are not totally comparable to 2-D results even when applied to the same data under almost identical conditions, as illustrated in Chapter 6. Finally, Appendix I concludes by leaving a trail of several technical details being offered as clarification for spectral estimation specialists.

## 1.3 Background on Maximum Entropy Spectral Estimation and Radar Applications

(U)An objection that had been raised in the past [152] was that the superresolution techniques of MEM would probably not be useful for radar applications. The useful exception acknowledged in [152] as being ideal for MEM was for an application where detailed knowledge exists about the target and where the radar operation is not limited by noise or by clutter. Such an unusually pleasant situation is in fact the case for the Tradex modeling application considered here.

(U)LP in a single input/single output linear filter corresponds exactly to maximum entropy spectral estimation for a single channel and is well known in this context for its high resolution capabilities (relative to the Blackman-Tukey (1959) or Cooley-Tukey (1965) FFT-based methods) and its ability to distinguish high peaks that may exist in the spectra. Since all versions of multichannel LP incorporating linear autoregressive parametric models must estimate a fixed number of poles and zeroes, it is important to be aware that certain undesirable phenomena can sometimes be encountered with its use such as line-splitting [233] (as a result

# Chapter 2

# Overview of Multichannel LP Spectral Estimation

## 2.1 Fundamentals of Autoregressive (AR) Complex Random Processes, and the Structure and Properties of the Associated Power Spectra

(U)A multichannel complex time series can be represented by a vector

$$\underline{X}_n = \begin{bmatrix} x_n(1) \\ x_n(2) \\ \cdot \\ \cdot \\ \cdot \\ x_n(M) \end{bmatrix} \tag{2.1}$$

of M-channel samples at time index n where each component has both a real and an imaginary part. For a "coherent" radar application, where phase is also accounted for, such a representation in terms of complex variables is necessary (see [70, Chapt. 4], [88, Sec. 1.41, [48], [164]). For a stationary zero-mean process, the covariance at lag $\tau$ is

$$R_{xx}(\tau) = E\left[\underline{X}_{n+\tau}\underline{X}_n^H\right] = R_{xx}^H(\tau) \tag{2.2}$$

where the "$H$" superscript indicates the Hermitian conjugate (i.e., the complex conjugate transpose).

(U)The associated spectral density of the process is defined by

$$S_{xx}(\omega) = \int_{-\infty}^{+\infty} R_{xx}(\tau) e^{-j\omega\tau} d\tau \tag{2.3}$$

for $R_{xx}(\tau)$ corresponding to a continuous-time representation, or as

$$S_{xx}(\omega) = \Delta t \sum_{k=-\infty}^{+\infty} R_{xx}(k) e^{-j\omega k \Delta t}, \quad \frac{-\pi}{\Delta t} \leq \omega \leq \frac{+\pi}{\Delta t} \tag{2.4}$$

for $R_{xx}(k)$ being expressed in a discrete-time representation. Here ***At*** is the time interval or time-step between successive samples of $\underline{X}_n$ and is chosen to satisfy a Nyquist criterion for the transmitted radar signal of known form.

(U)A multichannel AR process of order P is generated by a random process of the form

$$\underline{X}_n = -\sum_{i=1}^{\mathrm{P}} A_i^{(P)} \underline{X}_{n-i} + \underline{W}_n \qquad \text{for n} = 1, 2, 3, \ldots \tag{2.5a}$$

$$\text{or} \quad \underline{X}_{n-P} = -\sum_{i=1}^{P} B_i^{(P)} \underline{X}_{n-P+i} + \underline{W}_n^B \qquad \text{for n} = 1, 2, 3, \ldots \tag{2.5b}$$

where $A_i^{(P)}$ and $B_i^{(P)}$ are, respectively, the associated forward and backward prediction matrices and $\underline{W}_n$ and $\underline{W}_n^B$ are zero mean Gaussian white noise driving terms. For the scalar case, the collection of $A_i^{(P)}$'s and the collection of $B_i^{(P)}$'s are identical, but differ, in general, for the multichannel case [71]. Via standard input/output properties of linear systems [87, Sect. 10.21, the spectrum of the forward process of Ea. 2.5a is

$$S_{xx}(z) = \Delta t \left[\sum_{i=0}^{P} A_i^{(P)} z^{-i}\right]^{-1} U \left[\sum_{i=0}^{P} A_i^{(P)} \overline{z}^{i}\right]^{-H}, \tag{2.6}$$

where

$A_0 = B_0 = \mathbf{I}$, the identity matrix,
***At*** is the sampling interval,
$U = \mathrm{E}\left[\underline{W}_n \underline{W}_n^H\right]$, the forward residual error covariance, and
$z = e^{j\omega\Delta t}$, and the complex conjugate is denoted by $\overline{z} = e^{-j\omega\Delta t}$.

Equivalently, using the backward representation of Eq. 2.5b, the spectrum of the process is

$$S_{xx}(z) = \Delta t \left[\sum_{i=0}^{P} B_i^{(P)} z^{-i}\right]^{-1} V \left[\sum_{i=0}^{P} B_i^{(P)} \overline{z}^{i}\right]^{-H}, \tag{2.7}$$

where the backward residual error covariance is

$$V = E\left[\underline{W}_n^B (\underline{W}_n^B)^H\right]$$

The associated forward and backward prediction error series are defined to be

$$\underline{Y}_k = \sum_{n=0}^{P} A_n^{(P)} \underline{X}_{k-n} \tag{2.8a}$$

$$\underline{Z}_k = \sum_{n=0}^{P} B_n^{(P)} \underline{X}_{k-P+n}. \tag{2.8b}$$

(U)For complex Gaussian processes such as are encountered in this investigation of the PP and OP components of the reflected radar signal, the underlying state-vector of Eq. 2.5 can be decomposed in terms of its constituent real and imaginary components as

$$\underline{X}(t_k) = \underline{X}^1(t_k) + \jmath \underline{X}^2(t_k) \text{ for } 1 \leq k \leq \mathrm{N} \tag{2.9}$$

and, moreover, for a super-stacked vector

$$\tilde{\underline{X}} = [\underline{X}(t_1), \underline{X}(t_2), \underline{X}(t_3), ..., \underline{X}(t_N)]^T \tag{2.10}$$

with zero mean as

$$E\left[\tilde{\underline{X}}\right] = 0 \tag{2.11}$$

and with

$$Q \triangleq E\left[\tilde{\underline{X}}\tilde{\underline{X}}^H\right] \tag{2.12}$$

and

$$P \triangleq E\left[\tilde{\underline{X}}\tilde{\underline{X}}^T\right], \tag{2.13}$$

the underlying pdf is Gaussian of the form [164, Eq. 1] [1]:

$$p_{\tilde{x}}(\tilde{\underline{X}}) = \frac{1}{\pi^N |Q|^{1/2}} exp\left[-\tilde{\underline{X}}^H Q^{-1} \tilde{\underline{X}}\right]. \tag{2.14}$$

As in most applications of complex Gaussian processes, the underlying complex process that arises in this application is "circularly symmetric" such that

$$P \equiv 0. \tag{2.15}$$

[1]The corresponding **Eq.** 1 of [164] is evidently in error by omitting the squareroot of the determinant of Q that should appear in the denominator as properly shown above in **Eq.** 2.14.

Further, the essentially *stationary* complex Gaussian processes of concern in this application are such that

$$R_{\underline{\tilde{x}}\underline{\tilde{x}}}(\tau) = R^{H}_{\underline{\tilde{x}}\underline{\tilde{x}}}(-\tau) = E\left[\underline{\tilde{X}}(t)\underline{\tilde{X}}^{H}(t+\tau)\right] \tag{2.16}$$

which again can be decomposed by virtue of **Eq.** 2.9 into

$$R_{\underline{\tilde{x}}\underline{\tilde{x}}}(\tau) = R^{C}_{\underline{\tilde{x}}\underline{\tilde{x}}}(\tau) + \jmath R^{S}_{\underline{\tilde{x}}\underline{\tilde{x}}}(\tau) \tag{2.17}$$

where

$$R^{C}_{\underline{\tilde{x}}\underline{\tilde{x}}}(\tau) = R_{\underline{x^1}\underline{x^1}}(\tau) + R_{\underline{x^2}\underline{x^2}}(\tau) \tag{2.18}$$

and

$$R^{S}_{\underline{\tilde{x}}\underline{\tilde{x}}}(\tau) = R_{\underline{x^2}\underline{x^1}}(\tau) - R_{\underline{x^1}\underline{x^2}}(\tau) \tag{2.19}$$

Due to the condition of Eq. 2.15 holding, the following symmetries also must be satisfied [164, Eq. 8]:

$$R^{C}_{\underline{\tilde{x}}\underline{\tilde{x}}}(\tau) = 2R_{\underline{x^1}\underline{x^1}}(\tau) = 2R_{\underline{x^2}\underline{x^2}}(\tau) \tag{2.20}$$

and

$$R^{S}_{\underline{\tilde{x}}\underline{\tilde{x}}}(\tau) = 2R_{\underline{x^2}\underline{x^1}}(\tau) = -2R_{\underline{x^1}\underline{x^2}}(\tau). \tag{2.21}$$

The above expressions will be further utilized in the sequel and are also utilized in the companion report in [187, pp. 9-10 of Chapter 1 and footnote on p. 24 of Chapter 3].

## 2.2 Multichannel MEM Generalizations

(U)The MEM approach to spectral estimation has been utilized for a wide variety of practical applications[98]. While almost all variations of single channel LP are closely related to single channel MEM spectral estimation (as identified following Table 2.1), there are several different versions of multichannel LP that more or less correspond to multichannel MEM. However, it is noteworthy that Burg in [100, Intro., p. xiii] observes that:

> multichannel spectra do not have the necessary structure to permit the correspondingly rich development as occurs in the single channel case. Because of this (situation existing), no simple extension of the Burg technique [158] to the multichannel case is possible

as he thought in 1975.

(U)Since 1975, there has now been considerable prior work in seeking multidimensional MEM generalizations. Lang [91], [94] gave a general and complete presentation of the theoretical issues that arise in the multidimensional MEM spectral estimation problem and suggested an algorithm. Alternatively, the Lim-Malik algorithm for two-dimensional MEM [68] is a type of alternating projection algorithm commonly used in signal processing. It achieves computational efficiency by exploiting the speed of the FFT to an advantage. Johnson [90] reported that for the Direction Finding (DF) application, Lang's version of multichannel MEM performed poorly relative to conventional Maximum Likelihood Method techniques and especially as compared to SVD-based approaches [88, Appendix B] (such as MUSIC [2]) which can better handle the situation for the signal of interest in the DF application consisting of essentially two separate spectral component lines or tones (i.e., sinusoids). (See [92] and [95] for additional evidence of relative performance in evaluating the outcome of alternative algorithms for the common test problems.)

(U)The multichannel LP algorithm of Nuttall [86] provides LP coefficient estimates directly by minimizing a very reasonable error criterion defined directly in terms of the measurement data. At the same time, Nuttall's algorithm also provides a simple model for eventually generating the process by using the recursive model of Eq. 2.5a in reverse as driven by a Gaussian white noise pseudo-random number (PRN) generator as input.

## 2.3 The LWR and the Nuttall algorithms as LP Multichannel Generalizations of Particular Interest in this Tradex Wideband Application

(U)Multichannel LP was used in this investigation because its simple parametric form is suggestive of an autoregressive (AR) solution to the modeling problem, and because efficient algorithmic implementations exist. While there are several alternative methods for obtaining the multichannel LP coefficients, the two approaches investigated here are the "Levinson-Wiggins-Robinson" (LWR) and the "Nuttall" algorithms. LWR is the direct multichannel generalization by Whittle [126] of the single channel Levinson recursive algorithm, which requires intermediate estimation of the covariance matrices by averaging the outer products of the multichannel data

[2]MUltiple SIgnal Classification(MUSIC).

inputs (expressed in vector form), before proceeding to the main goal of estimating the (AR) coefficient matrices of Eq. 2.5 as used in forming the spectrum.

(U)The multichannel LWR algorithm [127] utilizes a recursive representation of the AR coefficients that provides a $\mathrm{P}^{\mathrm{th}}$ order solution in terms of the prior $(\mathrm{P}-1)^{\mathrm{th}}$ order solution. The LWR algorithm can be briefly summarized as (cf., [84], [99, Sec. II] where slightly different but equivalent conventions are used):

$$\text{repeat for p} = 1, 2, ..., \mathrm{P} \begin{cases} \Delta_p = \sum_{n=0}^{p-1} A_n^{(p-1)} R_{(p-n)} \\ A_p^{(p)} = -\Delta_p (V_{p-1})^{-1} \\ B_p^{(p)} = -\Delta_p^H (U_{p-1})^{-1} \\ U_p = (I - A_p^{(p)} B_p^{(p)}) U_{p-1} \\ V_p = (I - B_p^{(p)} A_p^{(p)}) V_{p-1} \\ A_k^{(p)} = A_k^{(p-1)} + A_p^{(p)} B_{p-k}^{(p-1)} \quad \text{for } 1 \le k \le p-1 \\ B_k^{(p)} = B_k^{(p)} + B_p^{(p)} A_{p-k}^{(p-1)} \quad \text{for } 1 \le k \le p-1 \end{cases} \tag{2.22}$$

with initial conditions

$$U_0 = V_0 = R_{(0)}$$
$$A_0^{(k)} = B_0^{(k)} = I \quad \text{for all k.}$$

(U)This algorithm solves the Yule-Walker or normal equations, which minimize the mean squared error (provided that the covariance function used is exact rather than approximate, as it is here). Hence, use of this algorithm in applications where the covariance function must first be estimated leads to a potential vulnerability to error in subsequently estimating the AR prediction coefficient matrices. In order to ensure stability in a LWR mechanization, a triangular (a.k.a. a Bartlett) window is usually utilized [3]. LWR is sometimes alternately referred to in the literature as being the "autocorrelation method" [82].

(U)The Nuttall algorithm invokes the LWR recursion as specified above, except that the reflection coefficient matrix $\Delta_p$ is obtained as the solution to the generalized Lyapunov-like equation:

$$\left[(V_{p-1})^{-1} F_p\right] \Delta_p + \Delta_p \left[(U_{p-1})^{-1} E_p\right] = -2G_p \tag{2.23}$$

[3]Windowing, as used here, has a much less pronounced effect upon the results than it does in conventional FFT-based approaches to spectral estimation but is needed to ensure that a positive semidefinite matrix sequence is obtained, as is necessary in order to rigorously proceed.

where

$$E_p = \frac{1}{N}\sum_{k=P+1}^{N} \underline{Y}_k \underline{Y}_k^H,$$
$$F_p = \frac{1}{N}\sum_{k=P}^{N-1} \underline{Z}_k \underline{Z}_k^H, \qquad (2.24)$$
$$G_p = \frac{1}{N}\sum_{k=P}^{N-1} \underline{Y}_k \underline{Z}_k^H,$$

and $\underline{Y}_k$ and $\underline{Z}_k$ in the above are again the forward and backward prediction error series as defined in Eq. 2.8. The above matrices $E_p$, $F_p$ and $G_p$ can be interpreted, respectively, as being the windowed sample averages of the forward and backward error series, and their respective cross-correlation [4]. By solving for the AR coefficients in this way, the Nuttall algorithm minimizes the weighted error function defined directly in terms of the measured data as

$$\text{trace}\left[U_{p-1}^{-1} E_p + V_{p-1}^{-1} F_p\right] . \qquad (2.25)$$

(U) For a complete derivation of the Nuttall algorithm, see [86]. Compared to the LWR method, this Nuttall algorithm is of much greater computational complexity since on each iteration, $E_P$, $F_P$, and $G_P$ as well as a solution to a steady-state generalized Lyapunov-like equation must be evaluated.

## 2.4 Overview Comparison Between the LWR and Nuttall Algorithms

(U)Table 1 has been constructed as an encapsuled overview of properties associated with the two multichannel algorithms of interest here. The Burg algorithm [158] is essentially identical to the single-channel version of both the LWR and Nuttall algorithms. It is only included in the above table as a familiar reference gauge for comparison purposes.

(U)Note that while windowing is used in the LWR to theoretically guarantee stability, stability still can not be guaranteed if finite wordlength (FWL) arithmetic is being used [93] and sufficient computational dynamic range is not available or

[4] While the representation of $E_p$, $F_p$, and $G_p$ in [84, Section 3] averages by a factor of $\frac{1}{N-P}$ rather than by $\frac{1}{N}$ as done here in Eq. 2.24, extensive numerical experience is that averaging by $\frac{1}{N}$ has been better behaved in providing positive semidefinite matrices as needed to rigorously proceed further.

(U) Table 2.1: Relative Comparison of Properties of Several LP Algorithms

| PROPERTY | LWR (M-channel) | Burg (1-channel) | Nuttall (M-channel) |
|---|---|---|---|
| WINDOWING | necessary | not necessary | necessary |
| STABILITY | guaranteed | guaranteed | guaranteed |
| STABILITY with FWL | not guaranteed | guaranteed | not guaranteed |
| EFFICIENCY | efficient | expensive $(10\times)$ | very expensive $(M^2\times)$ |

UNCLASSIFIED

Table 2.1: Relative Comparison of Properties of Several LP Algorithms (U)

unacceptable truncation and roundoff procedures are being utilized. It is our experience that stability with FWL is also "not guaranteed" for the Nuttall algorithm. Nuttall has proved stability of his technique only in the "ideal" case when it is not encumbered with a finite wordlength arithmetic implementation constraint as is unlikely to be encountered in most practical applications (cf., [75], [76]). Naturally, the situation is usually ameliorated when multiple precision is utilized.

# Chapter 3

# Initial Results of Data Processing to Estimate AR Coefficients and Associated Spectra

## 3.1 Using Simulated Data

(U)This simulated data experiment is designed to verify that our recently modified algorithmic computer program implementations work properly. The spectral estimation programs were first tested using simulated data generated by a known strictly stable $1^{st}$ order 2-channel complex Markov process of the form

$$\underline{X}_n = \begin{bmatrix} 0.34 - j0.22 & -0.75 + j0 \\ 0.65 + j0 & 0.55 + j0 \end{bmatrix} \underline{X}_{n-1} + \underline{W}_n \,, \tag{3.1}$$

where $\underline{W}_n$ is vector Gaussian zero mean white noise of unit variance. Using techniques identical to those demonstrated in Section 3.2, eigenvalues were explicitly calculated from the characteristic equation (associated with the above system matrix displayed in Eq. 3.1) to be $0.4615 + j0.5895(0.75e^{j51.94^\circ})$ and $0.4285 - j0.8095(0.917e^{-j62.10^\circ})$, each being within the unit circle to guarantee the asserted stability of the system of Eq. 3.1. The associated effective time constant for Eq. 3.1 is $\Delta t/ln(0.917) = 11.54\Delta t$, where At is the sampling step size and the highest frequency of Eq. 3.1 ( to which the proper Nyquist sampling in specifying an adequate At is related) is $62.10^\circ(\pi/180^\circ)/\Delta t = 1.08/\Delta t$ [251].

(U)Via Eq. 2.6, the two channel power spectrum associated with the above

Markov process of Eq. 3.1 is:

$$S_{xx}(w) = \Delta t \left[ I_n + \begin{bmatrix} 0.34 - j0.22 & -0.75 \\ 0.65 & 0.55 \end{bmatrix} \frac{1}{z} \right]^{-1} I_n \left[ I_n + \begin{bmatrix} 0.34 - j0.22 & -0.75 \\ 0.65 & 0.55 \end{bmatrix} \overline{z} \right]^{-H} \tag{3.2}$$

$$= \frac{\Delta t \, |z|^2}{\left[z^2 + (0.89 - j0.22)z + (0.6745 - j0.121)\right]\left[z^2 + (0.89 + j0.22)z + (0.6745 + j0.121)\right]} \begin{bmatrix} z^2 + 1.10z + 1 & 0.1z - (0.1025 - j0.165) \\ 0.1z - (0.1025 + j0.165) & z^2 + 0.68z + 0.5865 \end{bmatrix}$$

Computation of the result of Eq. 3.2 involved using the routine properties that the sum, product, and ratio of complex variables are, respectively, the sum, product, and ratio of the conjugates.

(U)The two-channel pole-zero plot of Fig. 3.1 corresponds to Eq. 3.2, each term of which has poles in common of multiplicity two located at $-0.462 + j0.590 (0.75 e^{j128.06^\circ})$ and $-0.429 - j0.810 (0.916 e^{-j117.9^\circ})$, well within the unit circle. All terms have a zero of multiplicity two at the origin. The additional two zeros of the $S_{11}$ term are at $-0.55 + j0.835 (0.9998 e^{j123.37^\circ})$ and at $-0.55 - j0.835 (0.9998 e^{j236.63^\circ})$, both essentially on the unit circle. The additional single zero of the $S_{12}$ term is at $1.025 - j1.65 (1.94 e^{-j58.15^\circ})$ and so is not of minimum phase since it is outside the unit circle. Correspondingly, the additional single zero of the $S_{21}$ term is at $1.025 + j1.65 (1.94 e^{j58.15^\circ})$ and as the conjugate of the $S_{12}$ term zero is also outside the unit circle. The additional two zeroes of the $S_{22}$ term are at $-0.34 + j0.6862 (0.7658 e^{j116.36^\circ})$ and at $-0.34 - j0.6862 (0.7658 e^{j24364^\circ})$, well within the unit circle and therefore being of minimum phase. As indicated in [251], the "effective bandwidth" for each component of this random process is the reciprocal of the integral over the unit circle of the square of the corresponding component of the power spectral density function, as scaled by $2\pi j$. This can be explicitly evaluated using Cauchy's residue theorem for the double poles enclosed.

(U)The true spectra corresponding to Eq. 3.2, as evaluated using $z = \exp[j2\pi \mathrm{f}\, \mathrm{At}]$ for varying values of f, are shown in Figs. 3.2a, b, c. The superimposed dashed line in Fig 3.2c represents the phase while the solid lines represent the standard magnitude of the power spectra. Naturally, autospectra being exclusively real have no phase component. The corresponding outcome of LWR estimation of these simulated spectra, by operating directly on the Monte-Carlo data generated from Eq. 3.1 (following a skipping of the results of the first 100 iterations of Eq. 3.1 to avoid the initial transient prior to entering into a type of steady-state, corresponding to nine time-constants having elapsed, where the process is then sufficiently stationary), is shown in Figs. 3.3a, b, c. Similarly, the outcome of Nuttall estimation for this same test case and conditions is shown in Figs. 3.4a, b, c. All plots have the same scale throughout for ease in unambiguous cross-comparisons.

(U)While both algorithms correctly capture the auto-spectra thus confirming our software implementations of the two algorithms involved, it is observed for this example that the LWR technique, by more closely approaching the actual inflections exhibited in the shape and phase of the true simulated cross-spectrum, appears to be the best performer for this first-order AR process with this length of data of 999 sampled points and a sampling rate of once every second (i.e., $\Delta$=1). (This conclusion is not inconsistent with that of [84] which found the Nuttall algorithm to be the best performer, but that competition was against two other multichannel algorithms). However, we refrain from designating a particular LP algorithm as being "best" because it most likely is situation and application dependent. For a comprehensive comparison of the LWR, Nuttall, and Morf algorithms [1], see [81].

## 3.2 Experiments to Gauge Algorithm Sensitivity to the Data Length

(U)This section consists of an investigation into the degradation incurred by AR-based techniques due to a foreshortened length of available data on which to base spectral estimation. The results of several numerical experiments using simulated data are displayed here for calibrating the anticipated degradation or diminishing in clarity, resolution and/or general performance capabilities of the LWR (and/or Nuttall) algorithms to provide adequate multichannel spectral estimates. We calibrate this effect of limiting the length of data available by roughly identifying at what point the AR coefficient estimates no longer acceptably correspond to those "known" coefficients that we explicitly used in the simulator.

(U)The complex example, Case 4 of Table F.1, was used as the parameterization for the simulator. Then the resulting single sample function that emerged as an output from the simulator, consisting of 898 time samples taken every second, was routed through the AR Estimator (with flag set for the "Nuttall" option) yielding the following estimate of the underlying system cofficient matrix as an output:

$$\hat{A} = \begin{bmatrix} -0.3623 + j0.2046 & 0.7624 - j0.6562 \times 10^{-2} \\ -0.61798 - j0.7521 \times 10^{-3} & -0.5524 + j0.2338 \times 10^{-1} \end{bmatrix} \tag{3.3}$$

[1]This is yet another multichannel LP generalization. This version is based on minimizing the geometric mean of the forward and backward error series. As Morf's later algorithm, it is computationally more efficient than Nuttall's earlier algorithm, as established in [84].

The associated characteristic equation for the above matrix is:

$$0 = (0.66650386 - \jmath 0.12497340) + (-0.9147 + \jmath 0.22798)\lambda + \lambda^2 \, . \qquad (3.4)$$

The above quardratic equation of the form:

$$a\lambda^2 + b\lambda + c = 0 \qquad (3.5)$$

has solutions of the form (still valid even in the complex case):

$$\lambda_{1,2} = \frac{-b \pm \sqrt{b^2 - 4ac}}{2a} \qquad (3.6)$$

Performing the indicated operations for evaluation using the parameters for a, b, and c from Eq. 3.4 yields:

$$\lambda_{1,2} = \frac{-(-0.9147 + \jmath 0.22798) \pm \sqrt{(-0.9147 + \jmath 0.22798)^2 - 4(0.66650386 - \jmath 0.12497340)}}{2}$$

$$= 0.74185799 \, e^{\jmath 50.44^\circ} \text{ and } 0.91407276 \, e^{-\jmath 61.06^\circ} \qquad (3.7)$$

So even though the underlying $\hat{A}$ matrix presented above doesn't look identical to the matrix that was originally used to simulate the data, the resulting eigenvalues that were obtained *are still identical* (as they should be as a confirming check). The **AR** Estimator does not automatically invoke a preferred coordinate system and results obtained can theoretically differ by a similarity transformation; however, the resulting **AR** estimates should still have the same eigenvalues as correctly exhibited here. In fact, it was enough to stop at the point of observing that the characteristic equations were identical since roots of the same common polynomial equation of the same degree are necessarily identical and it is overkill to actually solve it again but informative to do so at least once [2].

(U) Proceeding to investigate the effect of constraining the length of available data on the performance of the LWR version of the AR Estimator by only using 100 equally spaced data samples this time (with the same 1 second time step), rather than the previous 898 data samples, yields the following underlying system matrix (when the "**LWR**" computational option within the software is utillized):

$$\hat{A} = \begin{bmatrix} -0.39511782 + \jmath 0.18683845 & 0.73222971 - \jmath 0.03982116 \\ -0.66155690 - \jmath 0.03186497 & -0.48329157 + \jmath 0.02238195 \end{bmatrix} . \qquad (3.8)$$

[2] Some **grief (induced by hand computation of eigenvalues from the associated characteristic equation with complex coefficients) can be spared by using the Fortran program offered in** [46, **pp. 335-3371 for factoring complex polynomials.**

The associated characteristic equation is

$$0 = \lambda^2 + (-0.\underline{8}784 + \jmath 0.\underline{2}092)\lambda + (0.\underline{6}725 - \jmath 0.\underline{1}022) \; . \qquad (3.9)$$

This is essentially the same characteristic equation as reported above in Eq. **3.4** except that only one or two digit accuracy is now available due to the forshortened data length. This will give rise to slight differences in the calculated eigenvalues from those of Eq. 3.7.

(U) Proceeding to also investigate the effect of constraining the length of available data on the performance of the Nuttall version of the AR Estimator by similarly only using **100** equally spaced data samples, rather than the previous 898, yields the following underlying system matrix when the "Nuttall" computational option is utillized:

$$\hat{A} = \begin{bmatrix} -0.39514713 + \jmath 0.18633008 & 0.73258209 - \jmath 0.04051232 \\ -0.66313660 - \jmath 0.03125645 & -0.484176397 + \jmath 0.02102142 \end{bmatrix} \; . \qquad (3.10)$$

The associated characteristic equation is

$$0 = \lambda^2 + (-0.\underline{8}799 + \jmath 0.\underline{2}074)\lambda + (0.\underline{6}747 - \jmath 0.\underline{1}025) \; . \qquad (3.11)$$

Again, this is essentially the same characteristic equation as reported above in Eq. **3.4** except that again only one or two digit accuracy is available due to the foreshortened data length. Again, the resulting eigenvalues will differ slightly from those of Eq. 3.7.

## 3.3 Using Radar Target Data

(U) As indicated in Fig. 3.5, a burst is designated to be a collection of radar target pulse returns that are in general proximity to one another with an interpulse separation interval or instantaneous pulse-to-pulse repetition interval (PRI) that is less than some prescribed constant, K. On the other hand, strings of radar target pulse returns are declared to be members of a distinctly different pulse train when the time since reception of the last target return pulse exceeds a prescribed maximum allowable time interval, TMAX. The radar data initially investigated here consists of **3** bursts (each containing 32 pulses) that occupy a total of **114** contiguous radar range gates. This situation can be interpreted here as a worst case condition for possible multichannel LP estimation as a vector time series consisting of 32 time

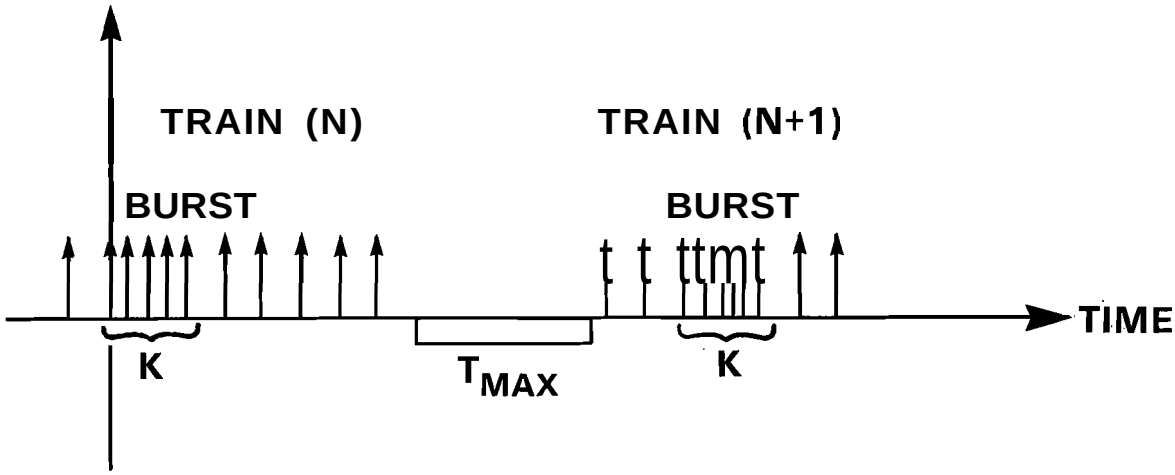


Figure 3.5: Pulse Returns from Test Radar: definition of Bursts and Trains via relative proximity of pulses as gauged by system parameters K and TMAX (U)

samples of a possible, but unlikely, upper limit extreme of 114 vector channels of data. Because of limitations on the amount of computer memory available to us and for other practical considerations to be further discussed below, no more than 10 channels at a time are actually considered here. The radar pulse repetition interval is 14 microseconds. Based on some prior Lincoln Laboratory radar precedents [226] and subsequent follow-ups for the narrowband case of BRVAD Phase 1, a postulated fourth order AR random process model is used for this Tradex radar application to represent the underlying RV wake target effect in each radar range gate.

(U)Fig. 3.6a shows a 1-channel LWR applied to (radar range)gate 1 of the data. Fig. 3.6b depicts the same channel 1 autocorrelation, where a 5-channel LWR is now used (and the other 4 channels are from gates 2-5 of the actual process). Figs. 3.7a and 3.7b depict the results of an identical estimation experiment using the Nuttall algorithm. The obvious degradation in clarity observed in the auto-spectrum estimate as the number of channels is increased has also been observed and documented in [84]. The explanation is that a single-channel MEM needs to estimate only P parameters, but the generalization of MEM must estimate $M^2P$ parameters for M-channel spectral estimation, being a major increase in the scope or number

of parameters to be estimated which occurs while the the number of supporting data points available for information extraction is only modestly increased from N points in the single channel case to M N points in the M-channel case. Therefore, the multichannel estimator can only estimate this larger number of parameters while unfortunately incurring an increased degadation in variance, as pointed out by Marple and Nuttall [84].

(U)This deleterious effect is much more pronounced when the channels considered do not have significant cross-spectral content. It is documented in [81] that for uncorrelated channels, a signal present in one channel may manifest itself as a cancelling of pairs of zeroes in another channel; but because of round-off error incurred in the digital implementation of an otherwise ideal algorithm, the cancellation is not perfect. In these cases, there may be "feed-through" or leakage of some of the auto-spectrum from one channel to another.

(U)Figs. 3.8a, b and 3.9a, b depict the same LWR versus Nuttal algorithm experimental comparisons as performed on another channel being Gate 2 for the radar data that was provided. Notice that the degree of performance degradation in going to 5 channels is different in this case but still present none-the-less.

(U)Figs. 3.10a, b, and 3.11a, b compare 1-channel and 2-channel estimates for primary polarized vs. orthogonally polarized data using LWR versus Nuttal algorithm estimates. The use of 2-channel AR modeling appears to be very suitable here since it is already anticipated from a physical argument and from other experimental precedents with other dual polarization radar applications that the use of orthogonally polarized radar returns from the same target on the two separate channels should be highly correlated. Whether use of an AR-based model structure suffices for RV wake modeling or whether an ARMA-based model structure is required is considered in the next chapter.

# Chapter 4

# Precedents in ARMA Modeling of Targets as well as Use of Standard AR Modeling Techniques

## 4.1 Motivation for Considering ARMA Models

(U)A question arose as to whether the underlying truth model Monte-Carlo simulator for exercising the spectral estimation algorithms should also contain a provision for including a component of additive measurement noise as well as the standard process noise in the final sensor measurement so that it is more properly modeled as consisting of the following sum of two statistically independent components as:

$$y(t) = y_{AR}(t) + v(t), \text{ where } v(t) \sim N(0, r). \tag{4.1}$$

Typical Kalman filter simulators always include a measurement noise simulation capability, so it was initially perceived to be somewhat unusual that some AR simulators don't include this provision or capability. However, an AR process with measurement noise present is essentially an ARMA process, as can be conveniently seen for the scalar case by considering the underlying equivalent correlation function that results from summing an AR process plus additive independent Gaussian white measurement noise, as demonstrated here:

$$\begin{aligned} \phi_{yy}(s) &= \phi_{y_{AR}y_{AR}}(s) + \phi_{vv}(s) \\ &= \frac{q}{D(-s)D(s)} + r = \frac{q + rD(-s)D(s)}{D(-s)D(s)}, \end{aligned} \tag{4.2}$$

where the above left hand fraction represents the correlation function of a pure AR process by having a constant numerator and the above right hand fraction represents the effective equivalent ARMA process that results by having a non-constant numerator. Use of pure AR techniques in situations involving underlying ARMA processes could be a fairly severe model mismatch [149]. A preprint paper on this topic of MEM estimation with white Gaussian measurement noise present, yet to appear in the open literature, is [26]. Other papers on this topic are [30], [150], [179], with asymptotic Cramer-Rao lower bounds having been worked out for this situation in [150].

## 4.2 Overview Summary of ARMA-Based Spectral Estimation Considerations

(U)While as recently as 1981, Kay and Marple observed in [27] that their version of high resolution model-based spectral estimation using an ARMA model was *tractable* only when p, the order of the AR portion is identical to q, the order of the MA portion of the ARMA$(p,q)$ random process. For p to be identical to q is a fairly contrived condition not likely to be usually satisfied in practice for arbitrary situations other than that of a pure AR signal in additive "ideal" white noise. Recently, the approach of [28] has emerged and is advertised to be tractable for arbitrary p and q (as long as the dimensions of p and q are specified beforehand). Nested hypothesis tests on model order values of p and q using the Akaike Information Criterion (AIC) [55] or canonical correlation techniques [51] such as are already typically used in parameter identification for deterministic control systems, and for model order reduction for reduced-order Kalman filter applications [106, Secs. V and VI], [108], are appealing in this new ARMA context. However, despite some apparent successes [169], reservations or limitations on use of AIC for certain applications are expressed in [49, Section 5] where it is claimed that use of AIC yields an estimate for the model order that is not statistically consistent (cf., [173]) and that asymptotically tends to overestimate. Earlier complaints along this same line about use of AIC were raised in [50] and recent critical discussions of AIC appear in [163, Preface].

(U)Several alternative approaches have been proposed for rigorously handling the order determination problem for ARMA processes [52], [151] and for AR processes [53], [54], [57], respectively, both recently and historically [56], [58], [111], [112], [177]. Brief, insightful comments on the fundamental problem encountered in attempting to handle the general ARMA situation is provided in [177] and in the

accompanying author's reply. In this classic historical dialog, the important point that is made is that the criterion to be minimized in determining the numerator and denominator coefficients of an ARMA process is highly nonlinear 'and that the standard methods of parameter identification involve some form of minimization of this or some similar criterion, in which case the calculated values, as obtained by most alternative computational approaches to constrained optimization or function minimization, will likely be merely local minima rather than the global minima that represent the true solution. For additional perspective on the "nasty" nonlinear optimization problem one is faced with in seeking to pursue standard *exact* maximum likelihood approaches to ARMA parameter identification and what rigorous asymptotic results are guaranteed for large sample size, see [231]. There is a suboptimal but extremely tractable approach, which starts with a given sample autocorrelation function (rather than with the preferred unreduced raw data as input) and uses the modified (or extended) Yule-Walker equations in performing subsequent manipulations. For this type of approach, the estimation of the AR and MA parameters is separated out and the resulting estimation equations are rendered benignly linear or at worst quadratic [215, p. 901]. The best approaches to consistent estimation of model order appear to be [116] - [119], [218] as recently claimed in [120]. Now that ARMA-based super-resolution spectral estimation techniques are considerably more tractable and flexible in allowed assumptions than they had been in the past, there may be more impetus to use them in the future but use of these techniques are apparently unnecessary at this time for the BRVAD application of concern to us here as further explained in Section 4.3.

(U)Not too surprisingly, a link has now been revealed between two parallel branches of technology that had previously been developing independently. The modern control theory specialty of parameter identification has objectives of estimating parameters of state-variable models, which can further be of AR, MA, or ARMA structure as special cases [176, pp. 90-95]. The observations of [172], [185] are that the modified Yule-Walker or so-designated normal equations that arise in estimating the AR parameter portion of an ARMA process can be viewed as a special case of the Instrumental Variable (IV) method of parameter identification. Once the spectral estimation intermediate objectives of obtaining adequate AR coefficient estimates are recognized to be identical to the objectives of parameter identification in general, the supporting theory and cross-checks from parameter identification [174], [163] can subsequently be brought to bear on spectral estimation as well. Of particular interest or relevance here are conditions of identifiability and structural identifiability which guarantee that such endeavors or attempts are in fact do-able.

## 4.3 A Novel Result to Allow the Subsuming of ARMA Models Within AR Models for Spectral Estimation

(U)The particular contribution of the present author to this problem of modeling radar target spectra having an underlying model that corresponds either to the more tractable [1] **AR** processes or to the less tractable **ARMA** processes can be found in [187, Sections 4.5 and G.4]. In [187, Section G.4], it is demonstrated using an extremely old, extremely simple trick from ordinary differential equation (ODE) theory (but involving an extremely tedious derivation that is not repeated here for the sake of brevity) in order to show that a *multichannel* or multi-input/multi-output **ARMA** process can be equivalently reformulated as a multichannel **AR** process (being of higher order than the original **ARMA** process but of finite order none-the-less).

(U)The general properties of the original algorithm of [187] that can be invoked to get rid of differentiated input (i.e., to get rid of the MA portion of an **ARMA** process to result in just a pure **AR** process of slightly greater dimension) are now discussed. This approach is formally generalized in [187, Section **G.4** of Appendix G] and demonstrated there to be a totally rigorous approach from which to validly obtain a state variable model which is a minimal realization. The main result that is an outcome of the manipulations in [187, Section **G.4** of Appendix G] are summarized in the remainder of this section.

(U)Consider the scalar constant coefficient linear differential equation of order $n_i$ represented by the following:

$$y^{(n_i)} + a_{(n_i-1)}y^{(n_i-1)} + \ldots + a_0 y = \sum_{s=0}^{n_i}\sum_{j=1}^{r} b_{js}x_j^{(s)} \tag{4.3}$$

or, equivalently,

$$y^{(n_i)} + \sum_{\ell=0}^{(n_i-1)} a_\ell y^{(\ell)} = \sum_{s=0}^{n_i}\sum_{j=1}^{r} b_{js}x_j^{(s)}, \tag{4.4}$$

[1] Tractability here refers to the ease of performing MEM spectral estimation.

where the superscript in parentheses denotes the order of the derivative with respect to time, $t$. Define auxiliary variables $z_i$ (i = 1,...,n;) such that:

$$z_1 = y - \sum_{j=1} k_{1j} x_j, \tag{4.5}$$

$$z_2 = y^{(1)} - \sum_{j=1}^{r} k_{1j} x_j^{(1)} - \sum_{j=1}^{r} k_{2j} x_j = y^{(1)} - \sum_{m=1}^{2} \sum_{j=1}^{r} k_{mj} x_j^{(2-m)}, \tag{4.6}$$

$$\vdots$$

$$z_\ell = y^{(\ell-1)} - \sum_{m=1}^{\ell} \sum_{j=1}^{r} k_{mj} x_j^{(\ell-m)}, \tag{4.7}$$

$$z_{\ell+1} = y^{(\ell)} - \sum_{m=1}^{\ell+1} \sum_{j=1}^{r} k_{mj} x_j^{(\ell+1-m)}, \tag{4.8}$$

$$\cdot$$

$$z_{n_i} = y^{(n_i-1)} - \sum_{m=1}^{n_i} \sum_{j=1}^{r} k_{mj} x_j^{(n_i-m)}, \tag{4.9}$$

where, for each j, the sequence $\{k_{mj}\}_{m=1}^{n_i}$ must yet be specified. Determining just what the sequence $\{k_{mj}\}_{m=1}^{n_i}$ must be in order that all the differentiated input terms of the $x_i$'s be removed so that the resulting differential equation in $z_i$'s may be represented in standard state variable form is the goal. The above represents a change of coordinate axes in the underlying state space.

(U)Notice that from the above, it can be seen that

$$\frac{d}{dt} z_1 = y^{(1)} - \sum_{j=1}^{r} k_{1j} x_j^{(1)} = z_2 + \sum_{j=1}^{r} k_{2j} x_j; \tag{4.10}$$

indeed, the general expression can be seen to be

$$\frac{d}{dt} z_\ell = y^{(\ell)} - \sum_{m=1}^{\ell} \sum_{j=1}^{r} k_{mj} x_j^{(\ell+1-m)} = z_{\ell+1} + \sum_{j=1}^{r} k_{(\ell+1)j} x_j. \tag{4.11}$$

$$\frac{d}{dt} z_\ell = z_{\ell+1} + \sum_{j=1}^{r} k_{(\ell+1)j} x_j \quad \text{for} \quad 1 \le \ell \le (n_i - 1) \tag{4.12}$$

Obtaining expressions for the $y_i$'s from the equations above, we have that:

$$y = z_1 + \sum_{j=1}^{r} k_{1j} x_j, \tag{4.13}$$

$$y^{(1)} = z_2 + \sum_{m=1}^{2}\sum_{j=1}^{r} k_{mj}x_j^{(2-m)}, \tag{4.14}$$

$$\vdots$$

$$y^{(\ell)} = z_{\ell+1} + \sum_{m=1}^{\ell+1}\sum_{j=1}^{r} k_{mj}x_j^{(\ell+1-m)}, \tag{4.15}$$

$$\vdots$$

$$y^{(n_i-1)} = z_{n_i} + \sum_{m=1}^{n_i}\sum_{j=1}^{r} k_{mj}x_j^{(n_i-m)}. \tag{4.16}$$

Using all of the above expressions for the $y^{(\cdot)}$'s and substituting into the original differential equation of Eq. 4.4 , we obtain an expression involving $\frac{d}{dt}z_{n_i}$; this expression is:

$$\frac{d}{dt}z_{n_i} + \sum_{m=1}^{n_i}\sum_{j=1}^{r} k_{mj}x_j^{(n_i+1-m)} = y^{(n_i)} = -\sum_{\ell=0}^{(n_i-1)} a_\ell y^{(\ell)} + \sum_{s=0}^{n_i}\sum_{j=1}^{r} b_{js}x_j^{(s)}. \tag{4.17}$$

Now by working with the above expression to eliminate all expressions involving y's and to maneuver it into a more manageable form by performing changes of the dummy index of sumination and by performing interchanges in the order of summation, the resulting expression is:

$$\begin{aligned}\frac{d}{dt}z_{n_i} = & -\sum_{\ell=0}^{(n_i-1)} a_\ell\left[z_{\ell+1} + \sum_{t=1}^{(\ell+1)}\sum_{j=1}^{r} k_{tj}x_j^{(\ell+1-t)}\right] \\ & + \sum_{s=o}^{n_i}\sum_{j=1}^{r} b_{js}x_j^{(s)} - \sum_{m=1}^{n_i}\sum_{j=1}^{r} k_{mj}x_j^{(n_i+1-m)} \\ & - \sum_{\ell=0}^{(n_i-1)} z_{\ell+1} + \\ & \sum_{j=1}^{r}\left[-\sum_{\ell=0}^{(n_i-1)}\sum_{t=1}^{(\ell+1)} a_\ell k_{tj}x_j^{(\ell+1-t)} + \sum_{s=0}^{n_i} b_{js}x_j^{(s)} - \sum_{m=1}^{n_i} k_{mj}x_j^{(n_i+1-m)}\right]\end{aligned} \tag{4.18}$$

From the analysis of [187, Section G.4, Eq. G.64], we have that:

$$b_{jn_i} = k_{1j} \text{ for each } j. \tag{4.19}$$

Further, from [187], the following recursion equation is available to completely specify all the requisite $k_{mj}$'s as:

$$k_{(n_i-s+1)j} = b_{js} - \sum_{\ell=s}^{(n_i-1)} a_\ell k_{(\ell+1-s)j} \ . \tag{4.20}$$

Thus each of the $k_{mj}$'s for ($1 < m \leq n$;) is now specified for each $j$ via the above finite recursion.

(U)A few representative terms are now found to illustrate how this result is applied. For fixed $j$, we had found from the derivation of [187, Section G.4] that the starting value is:

$$k_{1j} = b_{jn_i} \ ; \tag{4.21}$$

now applying the preceeding recursion results in a complete specification for the $k_{mj}$'s as:

$$\begin{aligned} k_{(2)j} &= b_{j(n_i-1)} - \sum_{\ell=n_i-1}^{(n_i-1)} a_\ell k_{(\ell+1-n_i+1)j} \\ &= b_{j(n_i-1)} - a_{(n_i-1)} k_{(1)j}, \qquad (4.22) \\ k_{(3)j} &= b_{j(n_i-2)} - \sum_{\ell=n_i-2}^{(n_i-1)} a_\ell k_{(\ell+1-n_i+2)j} \\ &= b_{j(n_i-2)} - a_{(n_i-2)} k_{(1)j} - a_{(n_i-1)} k_{(2)j}, \qquad (4.23) \\ &\vdots \end{aligned}$$

(U)The above procedure, as generalized here for handling multiple inputs, allows us to recast or re-represent the general system-describing differential equations of Eqs. 4.3 or 4.4 (having differentiated inputs) in the equivalent state variable form devoid of differentiated inputs as follows:

$$\frac{d}{dt}\begin{bmatrix} z_1 \\ z_2 \\ z_3 \\ \vdots \\ \vdots \\ z_{n_i} \end{bmatrix} = \begin{bmatrix} 0 & 1 & 0 & \cdots & \cdots & 0 \\ 0 & 0 & 1 & 0 & \cdots & 0 \\ 0 & 0 & \ddots & \ddots & & \vdots \\ \vdots & \vdots & 0 & \ddots & 1 & \vdots \\ \vdots & \vdots & \vdots & & 0 & 1 \\ -a_0 & -a_1 & -a_2 & \cdots & \cdots & -a_{n_i-1} \end{bmatrix} \begin{bmatrix} z_1 \\ z_2 \\ z_3 \\ \vdots \\ \vdots \\ z_{n_i} \end{bmatrix}$$

$$\begin{bmatrix} k_{21} & k_{22} & \cdots & k_{2r} \\ k_{31} & k_{32} & \cdots & k_{3r} \\ k_{41} & k_{42} & \cdots & k_{4r} \\ \vdots & \vdots & \cdots & \vdots \\ k_{n_i 1} & k_{n_i 2} & \cdots & k_{n_i r} \\ \left[b_{10} - \sum_{\ell=0}^{(n_i-1)} a_\ell k_{(\ell+1)1}\right] & \left[b_{20} - \sum_{\ell=0}^{(n_i-1)} a_\ell k_{(\ell+1)2}\right] & \cdots & \left[b_{r0} - \sum_{\ell=0}^{(n_i-1)} a_\ell k_{(\ell+1)r}\right] \end{bmatrix} \begin{bmatrix} x_1 \\ x_2 \\ x_3 \\ \vdots \\ x_r \end{bmatrix}, \quad (4.24)$$

where the $k_{mj}$'s are found as specified above (as availed in Eqs. 4.19 to 4.23).

(U)An alternate interpretation can be applied to this very old trick from differential equation manipulation as offered next. Notice that within the realm of random processes (where the inputs to Eq. 4.4 are Gaussian white noises), the straightforward transformation offered here essentially converts a scalar ARMA process into an equivalent vector AR process. Typically, AR processes are usually much simpler to work with (especially with regard to spectral estimation). When this result is used in conjunction with the approach illustrated in [187, Sections 4.2, 4.3, and 4.41, then the method is applicable for converting multi-input/multi-output ARMA processes into AR processes. This is the difference between this new more general method offered for the first time here (and in [187]) and more standard methods for getting rid of differentiated input terms such as that offered in 1987 in [214, Eqs. 1 and 2]. The approach of [214] is only applicable to Single-Input/Single-Output (SISO) transfer functions of the form

$$h_{1,1}(z) = \frac{1 + b_1 z^{-1} + \cdots + b_q z^{-q}}{1 + a_1 z^{-1} + \cdots + a_p z^{-p}}, \quad (4.25)$$

where the numerator and denominator polynomials in Eq. 4.25 are Hurwitz and additionally [214] assumes that p = q to yield the realization result in terms of so-called "phase-variable" or "companion form" [220] that:

$$x_{n+1} = \begin{bmatrix} 0 & \cdots & \cdots & \cdots & 0 \\ 1 & & & & -a_p \\ & \ddots & & & \vdots \\ 0 & & 1 & & -a_1 \end{bmatrix} x_n + \begin{bmatrix} b_{p+1} \\ \vdots \\ \vdots \\ b_1 \end{bmatrix} e_{n+1}, \quad (4.26)$$

$$\text{with } y_n = [0, \ldots, 0, 1]\, x_n,$$

but unfortunately of limited utility to us here because of the above stipulation that p = q and it is only good for SISO, while for the application of interest here we are considering approaches that can handle more general vector channels.

(U)Aspects not previously explicitly addressed in the open literature to this author's knowledge that cannot remain unaddressed here (since it directly pertains

to the efficacy of using this proposed AR equivalence technique for the application of interest) relates to whether the final AR model that results is in fact a "minimal realization". This topic is important for the reasons elaborated on in the first paragraph of Section 4.2 of [187] relating to reducing unnecessary expense of using more integrators than are absolutely necessary and avoiding possible instabilities of the "unobservable" or "uncontrollable" portion of an excessively nonminimal realization, while a minimal realization is always entirely both "controllable" and "observable" and of minimum degree (i.e., uses the least number of integrators for implementation). The approach of [214] above (only being applicable to a scalar or single channel ARMA process) can be seen to be "controllable" because it results in an AR system matrix that is in "phase variable" canonical form (also known as "companion form") and this representation is reasonably well known to be "controllable" ([220]) and being "controllable" and also obviously "observable", it is a "minimal realization", as established by the Kalman/Gilbert results that are reviewed in this context in [187, Section 4.41. The approach of [176, Eqs. 3.9-13 to 3.9-16] offers an equivalent AR model for the (scalar single channel SISO) ARMA process and just "hopes for the best" without being able to prove or establish that the resulting model is well-behaved and satisfactory in this role. This structure, to date, has defied establishing "controllability and observability" for the equivalent AR representation of [176]. The beauty of the present author's approach for multi-input/multi-output (multi-channel) ARMA process re-representation as an equivalent AR process here is that the resulting AR system matrix is also demonstrably "minimal" as ascertained using the theoretical results of [187, Appendix H]. An indication of a minor limitation to the algorithm offered here when the degree of the MA portion exceeds that of the AR portion of an ARMA process (and its subsequent remedy) are provided in [187, last paragraph of Appendix G] (also see [151] for additional perspective).

(U)Again, the obvious further benefit of using the above AR reformulation is that the simpler MEM approaches based on an assumed AR process structure can now be validly used [2] without recourse to the more involved less tractable ARMA

[2]This result also offers a new perspective on a fairly well known historically observed phenomenon that in numerical evaluations or numerical experiments using various hypothesized model orders on the same data, the candidate AR models of higher order ultimately reduced the residual error in estimation (as a figure of merit where smaller means better) even when it was obviously ***of greater order than the known AR process model that was actually used to generate the data*** via Monte-Carlo simulation. Previously, the observed reduction in residuals provided by use of even higher assumed AR model order was perceived as deleterious and was attributed to the "dumb" parameter estimation algorithm "not knowing any better" (by being unable to distinguish the true underlying situation) than to prefer an increase in the assumed model order to better fit the characteristics of

model-based spectral estimation techniques that are frequently plagued by numerical sensitivities due to nonlinearities inherently encountered in most ARMA approaches as reviewed above in Section 4.2. Our approach, as augmented with these new theoretical results of [187, Section G.4], subsumes the ARMA-based approaches without incurring the usual intractability difficulties of ARMA-based spectral estimation approaches but at the price of a slightly enlarged dimension of system order and matrices utilized.

the simulated additive noise. The results of this section demonstrate that the effect of having noise present in the simulation is tantamont to having an AR system present of higher order than the original model order used to generate sample functions. Therefore, the behaviour of the parameter estimation algorithm in seeking a higher order system model was not so "dumb" after all and (by the insights revealed by this analysis) is now justifiable and laudable.

# Chapter 5

# How Much Gate-to-Gate Cross-Correlation is Really There?

## 5.1 Discussion of the Problem that Confronts Us

(U)The question arises of how to distinguish between "real" cross-correlation that may exist between some contiguous radar range gates (due to the presence of the target's smeared out reflected returns) versus de facto correlation as a consequence of the underlying signal structure of the particular test radar (as introduced by the effect of the sidelobes of Tradex's ambiguity function) as it inadvertently diverts some of the energy from the RV body target returns to spill over into range gate returns associated with the wake.

(U)A two dimensional waveform amplitude distribution in both time delay $\tau$ and in frequency displacement $\phi$ in terms of the form of the underlying transmited radar signal waveform is

$$\chi(\tau,\phi) = \int_{-\infty}^{\infty} s(t)s^*(t+\tau)\exp[-j2\pi\phi t]\,\mathrm{dt} \tag{5.1}$$

One of several alternative conventions [115, Chapt. 4], [123, pp. 127-1411, [124, pp. 303-309, pp. 310-3171 (cf., [166, Eq. 3]) is to denote the real quantity $[\chi(\tau,\phi)\chi^*(\tau,+)]$ as the radar ambiguity function of interest. Closed-form expressions for different standard forms of $\chi(\tau,+)$, including FM chirp, are available in [114, Chapt. 3], [122, Eq. 6.341.

(U)Real gate-to-gate cross-correlation that should be universally present between adjacent gates could be exploited to an advantage in performing target detection and, eventually, tracking. To develop universally applicable target models,

it is necessary to adequately evaluate the persisting residual cross-correlation that is independent of the signal structure or ambiguity function of a particular test radar. Therefore, it is desirable to remove the effects due to the test radar's ambiguity function alone. Perhaps this ambiguity function should be replaced by that of the anticipated operational threat radar for additional realism but this is generally not practically feasible for reasons described below. Besides, the threat radar will superimpose the effect of its own ambiguity function and to additionally include it in the modeled emulation would double the effect as an unfortunate but likely discriminator from an actual RV.

(U)While a fairly obvious approach to removing the effect of the known ambiguity function would be to exploit the standard input/output spectral formulation of Eq. 2.6 and pre- and post-multiply in the frequency domain by the inverse of the associated transfer function matrix corresponding to the FFT of the Tradex test radar's ambiguity function. While conceptually correct at the aggregate level, certain random aspects of the radar signal make it difficult to exactly line up and synchronize the pre-recorded ambiguity function with the radar pulse initiation times that correspond to the specific recorded target returns. To attempt to strip off the effect of the radar ambiguity function in this simple manner may actually introduce more fictitious correlation into the successive radar range gates beyond what is nominally present.

(U)In particular, use of the ambiguity function such as that depicted in Fig. 5.1 (as recorded a year earlier), cannot be prudently used to decorrelate the current data without risk of severely misleading results. This situation exists because radar components such as amplifiers, phase-shifters, transmitters, switches, e t ~; age with time and consequently slightly alter the radar's performance. More confidence could be placed in data that was decorrelated using an ambiguity function that was obtained via a calibration sphere measurement just prior to data recording and additionally was confirmed to be unchanged by a subsequent calibration sphere measurement immediately following the mission target tracking, as would all be recorded on tape. In this way, the target data would be bracketed by calibration sphere data and the two sets of calibration-sphere-data-evaluation-of-ambiguity-function could be confirmed to be close enough to be essentially the same throughout the mission. Only by doing this would the above proposed method to decorrelate the effect of the radar ambiguity function be defendable. Besides this effect, slight mis-synchronizations inevitably occur that interfere with exactly cancelling out the effect of the ambiguity function and to attempt to do so in this obvious way may in fact further smear and corrupt the signal of interest. Additionally, for good Primary Polarization (PP) and Orthogonal Polarization (OP) calibration, the radar measurements should be

made using calibration dipoles since spheres are least capable of stimulating OP effects.

(U)It was mentioned above that the effect of the radar ambiguity function was creating a problem by "muddying the water" as we seek to accurately assess the degree of inherent cross-correlation that exists between contiguous range gates due to the presence of a target in our particular application scenario. Recent results that were further pursued in seeking a deeper understanding and a resolution in this area are [31], [32] but to no avail in the problem that faces us here. Instead, coherence-function-based tests of gate-to-gate cross-correlation, hypothesis tests, and distributional tests will be performed and conclusions caveated with a warning on possible tainting of final results by the radar ambiguity function itself.

## 5.2 Use of Statistical Tests of Significance

(U)Use of statistical hypothesis tests of significance will be pursued to verify validity at various stages of the modeling effort. The first cut at this, as offered below, is to seek to use coherence functions as a measure, where gate-to-gate cross-correlation can be tested two-at-a-time. This is also to be used two-at-a-time to test for significant target wake PP and OP cross-correlation, as are expected to be significant based on expectations as forged by past experience. Expressions for the variance and bias (cf.,[14]) to be expected in coherence function calculations, as utilized in Section 5.3, are offered here for possible benefit to others and are derived in Appendix A. Such information is useful in quantitatively caveating conclusions (as via confidence regions or $\alpha$ - probability in the outcome of statistical hypotheses tests) that may otherwise be interpreted too strongly. These recent theoretical results offered in Appendix A can be compared to earlier 1963 SANDIA results [15] along these same lines as well as with more recent results by Ralph Deutsch (in the textbook [16, Appendix]) and NUSC results in coherence function calculation by G. C. Carter, and distributional tests (of Thomas Kailath and Mati Wax from Stanford Univ. as occured in a recent 1986 paper on detection of signals [49]). G. C. Carter just came out with a streamlined high level overview survey of pertinent results and statistics associated with coherence function calculation in [12], so that apparently all the following prior NUSC reports on this topic [5], [6], [7], [62] (also by Carter) are now subsumed and superceded by his more concise overview report [12].

(U)Actually, Kailath and Wax [49, p. 388, para following Eq. 4] claim that the more statistically sophisticated approaches to this same problem by Bartlett

[135] and Lawley [136] based on a sequence of hypothesis tests suffer from having to rely on "subjective" judgement in the selection of decision threshold levels for the various intermediate tests and that the approach of [49] therefore avoids this. These complaints raised in [49] against [135] and [136] could be perceived as being somewhat artificial if a full evaluation procedure is available for specifying the necessary thresholds for each required test in terms of its operating characteristics $\alpha$, $\beta$ (i.e., probabilities of false alarm and correct detection, respectively) and power of the test. While [135] and [136] are somewhat dated by having been published in the middle 1950's, more recent work in this active research area such as are discussed next should be more germane by being more complete.

(U)While hypothesis tests involving two bivariate Gaussians are well-known (e.g.,[137, p. 249], [141, pp. 175-1911, [140, p. 153, ff 190]), a challenging research problem has been how to rigorously handle hypothesis tests involving multivariate Gaussians of unequal variance as evidenced by the historical summary of painfully slow theoretical advances in [137, pp. 257-2581, [138], [139], [140, pp. 154-1551. In general, the problem of known and unequal variances for the multivariable case (even the bivariate case) is very formidable while the case of unknown variances that must be estimated is much worse and usually involves working with a distribution of the Wishardt matrix (see [160]).

(U)In particular, the maximum likelihood estimate of multiple correlation coefficients for an underlying multivariate Gaussian problem has variance and covariances that have a Wishardt distribution [143, pp. 191-192, p. 325], [144, pp. 341,3441, [137, pp. 113-1181, having properties that can be related to tensor products [137, p. 119]. Other approaches to this problem also exist [181, pp. 321-3821. Full statistical rigor may perhaps need to be sacrificed in this particular application in favor of a more tractable more expedient analytical "punt" such as is offered below involving pair-wise tests of significant radar cross-correlations using coherence function evaluation.

## 5.3 Results of Using Coherence Estimation on Available Radar Data

(U)A common presentation format is adhered to for all coherence function estimates to be presented in Figs. 5.2 to 5.7. The mean square coherence (MSC) results portrayed here, as originally estimated in this investigation via Eq. A.3 using conventional Fast Fourier Transform (FFT) techniques (see 2nd and 3rd paragraphs of

two gates away (Fig. 5.4b), and five gates away (Fig. 5.4c). Yet the results of Fig. 5.4 are less likely to be artifact effects due to target body interaction in the radar ambiguity function sidelobes.

(U)Since Gate 5 is less likely to be adversely tainted by the above described radar ambiguity function effects, a cross comparison of the most significant cross-correlation indications, as occurred between Gates 5 and 6, are obvious candidates for further cross-comparisons at the two Altitudes Nos. 1 and 2. This comparison is performed in Figs. 5.5a and 5.5b, where again the greater cross-correlation appears to be at the higher altitude (Altitude No. 1) but both are significant at the lower frequencies of interest due to the likely leaking of RV body energy.

(U)The anticipated supplementary reinforcing effect of using both PP an OP data within corresponding radar range gates, treated as two separate simultaneous channels, is now investigated. Results for Altitude No. 1 are portrayed in Fig. 5.6. The coherence results for Gate 1 PP and OP are displayed in Fig. 5.6a and are comparable to zero for low frequencies yet this time are more significant at higher frequencies but also possibly due to the likely tainting by the effect of the RV body as siphoned off to the wake gates by the ambiguity function. However, for Gates 5 and 10, the primary low frequency components of the target show up as being significant in Figs. 5.6b and 5.6c. The corresponding results at the lower Altitude No. 2 show less significant cross-correlation in Gate 1 PP and OP results (Fig. 5.7a) but more consistent high frequency components of significant cross-correlation for Gates 5 (Fig. 5.7b) and 10 (Fig. 5.7c). Thus, PP and OP results appear to be significantly cross-correlated.

(U)There was more supporting data on coherence function calculation but it is perhaps less convincing because it relies heavily on arguments based exclusively on simulation only. It involves simulating an extremely simple additive measurement noise- free two channel situation with precisely controlled known (and specified) cross-correlation using a specified level of process noise as the common driver. However, this situation appears to be too simple or to be lacking of sufficient generality; so much so that its relevance to the actual radar application is somewhat questionable due to the fact that the simulated system has no dynamics (i.e., no numerator or denominator terms in the associated transfer function between input and output). Ignoring this shortcoming for the moment, however, the further simulation gestures are germane. The result of a controlled simulation experiment, with known controlled cross-correlation, is convolved with the known pre-specified ambiguity function of the radar of this application with its principal sidelobes 30 dB down. The resulting coherence function, a known constant, is estimated and

horizontal two-sided 80%conficence regions are calculated and erected for this situation (as depicted in Fig. 5.2a as horizontal dotted lines and as should also appear in Figs. 5.2b to 5.3c). The coherence function estimate for the lower frequencies, where the significant wake energy lies (as opposed to the higher frequencies, which are noise dominated so they are of little significance to us) are predominantly within this 80%confidence interval strip. This says that the computed coherence for the actual radar data generally falls within the two-sided 80%confidence interval for simulated data of known cross-correlation as affected by the actual radar ambiguity function. In other words, the effect of the radar ambiguity function dominates the situation.

(U)The major difficulty with the above results is that only one run is portrayed in each of Figures 5.2 to 5.7 (rather than being the results of averaging many runs) so that strong conclusions on the coherence trend and therefore on the underlying gate-to-gate cross-correlation can not be inferred from the above without strong reservations. These runs of a year earlier probably need to be redone with considerably more trials included (enough to obtain a representative average as, say, at least 4 and maybe even 10 trials). This is one of the motivations for the further 2-D investigations of this effect that were performed with greater success and clarity than the results of this section and that are reported in Section 6.1 of Chapter 6.

(U)This completes this preliminary investigation of coherence, which is used both as a measure of the inherent gate-to-gate and PP-OP cross-correlation that exists. When the cross-correlation due to just the target (and not an artifact of the RV body effect in the sidelobes of the ambiguity function) is significant, then the gates should be used jointly in a multichannel model of the target's signature as pursued in Section 6.2.

# Chapter 6

# Specifying and Computing Parameters for a Typical 1-D Model Proposed for Wake Emulation

## 6.1 2-D Processing Results that Influence our Further 1-D Modeling Decisions

(U)Historically, according to Aki and Richards [153, p. 613]:

> Burg [157] points out that a 2-D frequency-wavenumber approach to certain applications may give better physical insight..., but the multichannel approach is more practical for filter design.

This somewhat surprising point of view of being willing to sacrifice "physical insight" for "ease of implementation" with the analytical tools currently at their disposal was evidently in vogue during the time frame of the early 1960's. More recent revelations such as [167], [168], and [175] illustrate the current utility and ease of using 2-D techniques, thus reversing the prior practice of shying away from the 2-D approach. Moreover, even in the 1960's according to Aki and Richards [153, p. 613]:

> A detailed illustration of different [2-D versus multichannel] approaches [to the same problem] was given by Schneider et al [155] for a relatively simple two-channel problem ...

of eliminating ghost arrivals from the unrelated problem of reflection seismograms. More recently, connections between the multichannel approaches and certain 2-D Linear Prediction approaches such as that of [109] have been revealed [159] to further expidite 2-D analyses.

(U)An independent sister study was performed by the Naval Postgraduate School (NPS), as monitered, tracked, and reported on in [259], [260], [261], and [262]. A primary observation from the sister study of [224], as representatively depicted in Fig. 6.1, is that (except for the scale) the PP, OP, and cross-spectrum magnitudes are remarkably similar/comparable and, as also depicted in Fig. 6.1, that the PP/OP MSC indicates that a significant level of cross-correlation exists [1]. The similarity of the PP, OP, and cross-power spectra at 20 km, as depicted herein, is typical of what was observed at all altitudes.

(U)A second significant feature of the above mentioned plots is that the spectra are rather broad in the wavenumber direction but not flat (complete flatness would be indicative of white noise with no correlations). This suggests that there is a degree of space-correlation along the gate direction.

(U)An observation that can be made is that the character of the wake spectra does not change drastically over the extensive range of altitudes considered in the study of [224] even though the expanse of altitudes bracket the BLT region. There may be slight changes in the width of the main ridge, as illustrated, but the plots do not depict any consistent broadening or narrowing of this ridge with altitude. No other special features such as subsidiary peaks seem to appear. The subsidairy peaks seen in earlier analyses still appear at <u>all</u> altitudes only when gates close to the RV (i.e., gates 1 through 5 or gates 2 through 5) are also included in the data used for spectral estimates. (Clarification: By previously including gates 1 through 5, energy from the RV itself was, unbeknowst to us at the time, improperly spilling over into the assessment of the wake. This has now been remedied in 2-D processing results and for the l-D modeling/processing results reported in Section 6.2, but is a problem that plagues the results depicted in Section 5.3.) The size of the secondary peak (in the frequency domain) is still larger at the lower altitudes (i.e., below 20 km) but is less apparent now that a logrithmic scale is being used. While pieces did break off of the RV during the mission, the observed uniform presence of the subsidiary peak at altitudes higher than where this flaking off occurred essentially debunks this as a possible explanation for the occurrence of these secondary peaks.

[1] Unlike what may be hoped for as a path for cross-corroboration between the l-D results of Section 5.3 and the 2-D evaluations here of coherence in the frequency domain, Appendix H explains why this type of desired cross-corroboration is *not* possible in general.

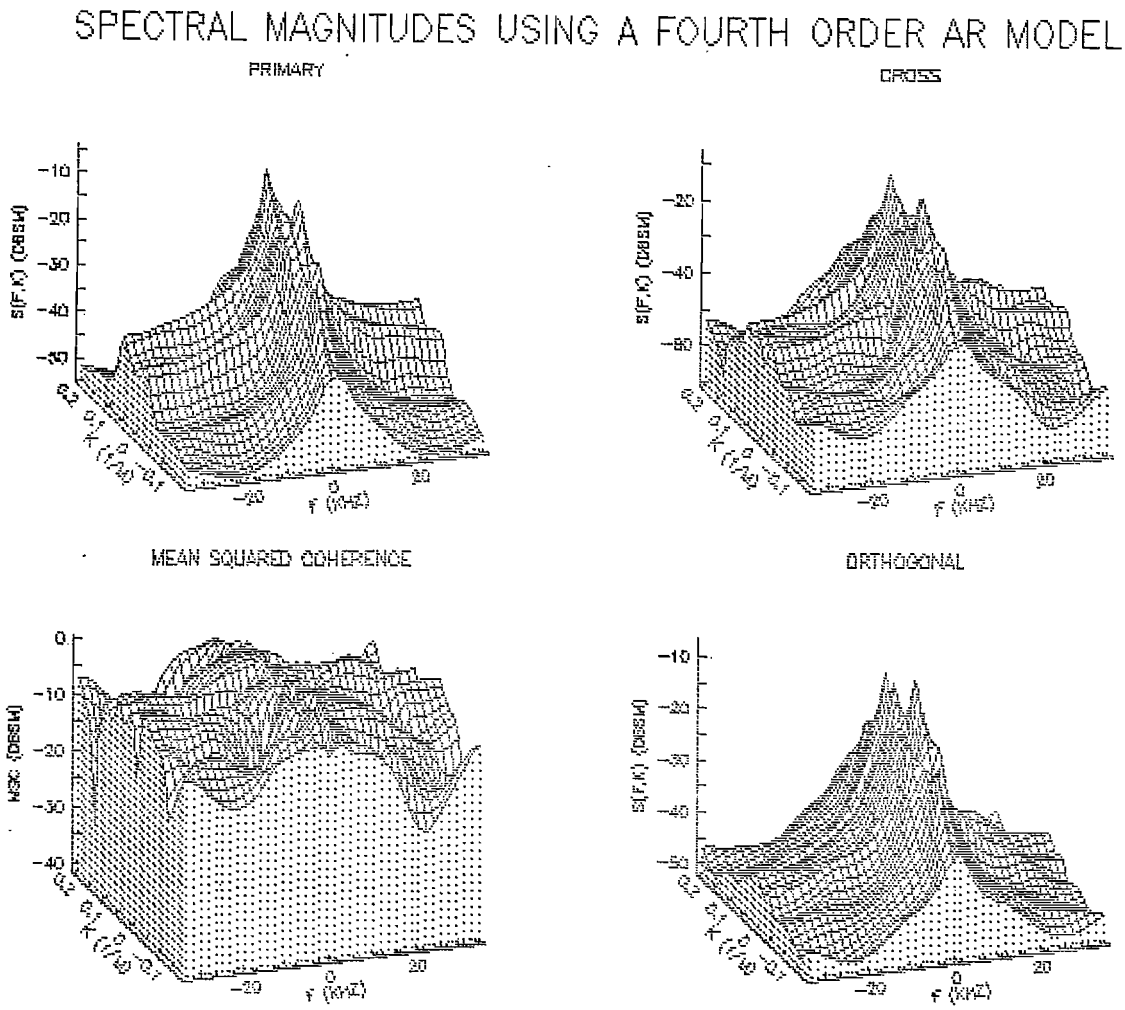


**Figure 6.1: 2-D Plots of PP-, OP-, and Cross-Spectra at 25 km (U)**

Since equally spaced uniform rectangular sampling was utilized throughout, there is no possibility of this effect having appeared because of alliasing occurring due to any deleterious effect in one coordinate spilling over into the other, as had originally been feared.

(U)Finally, the main significant observation from the study of [224] which is immediately useful to us in our 1-D RV wake modeling effort is depicted in the 1-D autocorrelation plot of Fig. 6.2. Here the subsidiary peaks that appear in these range gates within the RV wake most likely represent harmonic spill-over from the RV body due to interaction with the sidelobes of the ambiguity function. Where magnitude dropoff from the first primary peak equals the maximum magnitude of the secondary peak at approximately 3 to 4 gates behind the body while the ambiguity function depicted in Fig. 5.1 decayed at a faster rate. It appears prudent to assume an effective correlation distance of three range gates (that would be used in conjunction with the corresponding three OP range gates) to capture the essence of the significant correlations present as further pursued in a 1-D model as described in the next section.

(U)A 2-D model implementation would ordinarily have a structure as represented in Fig. 6.3. If the application structure is such that it can be demonstrated to be separable, then significant implementation simplifications accrue and 2-D implementation becomes much more tractable in hardware than the fully general implementation depicted in Fig. 6.3.

## 6.2 Demonstrating the Multichannel Spectral Estimation Technique to Obtain a Representative 1-D Model

(U)The results of modeling the RV wake using the 1-D LWR spectral estimation technique is depicted in Fig. 6.4. As motivated by characteristics exhibited by the results of the 2-D investigation, a six channel or six state model was used consisting of three contiguous PP range gates in conjunction with the corresponding three OP range gates. An underlying fourth-order AR model was also assumed [2] based on the historical precedent that it was adequate for Phase 1 BRVAD and also to avoid unnecessary model complexity. The use of three wideband range gates is

[2] As mentioned in footnote 1 on p. 5, an AR model order as high as seven had been used in the past but was later discarded as not being necessary.

also comparable in length to half of a single narrowband range gate, as apparently sufficed for Phase 1 BRVAD. (See end of Appendix F for status of accompanying plots of associated spectra.)

(U)A representative implementation diagram is depicted in Fig. 6.5. Since the wake keeps moving downwards as the RV descends, it is not necessary to consider that correlations from the farthest gate away (i + 2) affect the earlier gates (i + 1 and i), only that the earlier gates affect what occurs in the latter gates. This is a phenomenological argument based on the cause and effect of reentry physics, rather than on having balanced symmetry in the statistical sense of the contents of gate i being correlated with that of gate $i+1$ being equally significant in both directions.

## 6.3 1-D Computational Burden for Implementation

(U)Once the four $6 \times 6$ AR coefficient matrices are estimated, they can be used within a model of the form of Eq. 2.5a for the purposes of RV wake emulation as driven by zero-mean Gaussian white pseudo-random noise, $w(k)$, pre-calculated and inputted from a stored medium. A computational load analysis for an implementation of this approach is considered next. The 1-D mechanization of Section 6.2 (including both PP and OP effects) for each trio of three contiguous range gates is of the form:

$$x(k) = A_1 x(k-1) + A_2 x(k-2) + A_3 x(k-3) + A_4 x(k-4) + w(k), \qquad (6.1)$$

where each indicated matrix-vector product term is equivalent to 36 complex multiplies and 36 complex additions which together with the indicated accumulations across four constituent components on the rigt-hand side of Eq. 6.1 is:

- 4 x (36) = 144 complex multiplies,
- 4 x (36) = 144 complex adds, which accumulate from four matrix-vector products and the driving vector, $w(k)$, as an additional 5 x 6 = 30 complex adds to yield a total of 174 complex adds.

Each complex multiply is equivalent to 4 real scalar multiplies and 2 real scalar adds and similarly each complex add is equivalent to 2 real scalar adds. For emulation, it is likely that the threat radar PRF will be matched. For Tradex, this PRF is $14 \times 10^{-6}$ as the time within which all of the above computations must be made for

the emulation to be credible. Rather than being constrained to an implementation on a classical Von Neumann sequential machine, it is likely that a distributed or parallel processor architecture will be used for emulator implementation. It will likely be able to handle at least 4 sets of 6 complex multiplies and adds simultaneously on 6 separate channels; thus, it initially appears that it must be able to calculate the results for this model of the form of Eq. 6.1 for arround 50 to 200 separate gates as (worst case) as 1 parallel complex multiply every $\frac{\quad}{\quad} = 7 \times 10^{-8}$ seconds and similarly for complex additions, with an assumed "hard-wired" complex accumulator also being utilized. This is pushing the leading edge of small scale portable digital computing technology pretty hard. It will be demonstrated below that this apparent requirement is more severe than actually necessary. The above estimates can be mitigated somewhat if the following structural observations are exploited.

(U)An approach that was initially considered to be extremely lucrative was to reduce the estimated **AR** matrix to its corresponding phase-variable (companion) canonical form [257, pp. 82-85] via the numerical technique of [220], which is much less of a computational burden in the general multichannel case than computing eigenvalues. These companion form matrices are very sparse and are of the form of the left-most matrix of Eq. 4.26. The lure in programming up an Active Decoy emulator using matrices of this form is that it appeared to involve the least number of tap weights to be specified, as a likely considerable savings in programming labor, but would still yield the same multichannel power spectra since it represents merely a "similarity" transformation, as a change of underlying basis vectors. We now refrain from further pursuing use of companion form representation because we *now* recognize that unlike the case of a first order **AR** process, as treated in Sections 3.1 and 3.2, the fourth order **AR** process of the form of Eq. 6.1 must be converted to companion form in one fell swoop from its augmented form as represented next

$$\begin{bmatrix} x(k-3) \\ \cdots \\ x(k-2) \\ \cdots \\ x(k-1) \\ \cdots \\ x(k) \end{bmatrix} = \begin{bmatrix} 0 & \vdots & I_6 & \vdots & 0 & \vdots & 0 \\ \cdots & \cdots & \cdots & \cdots & \cdots & \cdots & \cdots \\ 0 & \vdots & 0 & \vdots & I_6 & \vdots & 0 \\ \cdots & \cdots & \cdots & \cdots & \cdots & \cdots & \cdots \\ 0 & \vdots & 0 & \vdots & 0 & \vdots & I_6 \\ \cdots & \cdots & \cdots & \cdots & \cdots & \cdots & \cdots \\ A_4 & \vdots & A_3 & \vdots & A_2 & \vdots & A_1 \end{bmatrix} \begin{bmatrix} x(k-4) \\ \cdots \\ x(k-3) \\ \cdots \\ x(k-2) \\ \cdots \\ x(k-1) \end{bmatrix} + \begin{bmatrix} 0 \\ \cdots \\ 0 \\ \cdots \\ 0 \\ \cdots \\ I_6 \end{bmatrix} w(k), \tag{6.2}$$

$$y = \begin{bmatrix} 0 & \vdots & 0 & \vdots & 0 & \vdots & I_6 \end{bmatrix} \begin{bmatrix} x(k-3) \\ \cdots \\ x(k-2) \\ \cdots \\ x(k-1) \\ \cdots \\ x(k) \end{bmatrix} \tag{6.3}$$

Having to now deal with a $36 \times 36$ matrix rather than with merely 4 $6 \times 6$ matrices dampens our enthusiasm for using the companion form for this wake modeling application since it would be difficult to unravel even though the underlying lure is still there of only having to perform the same number of nontrivial complex multiplies in hardware implementation of the corresponding companion form as the dimension of the matrices involved (in this case 36). The payoff is still enticing but the burden of getting there is now more taxing since it now goes as $36^2$ rather than the previously expected 4 x $6^2$. It was also feared that by having to deal with larger matrices, the adverse computational effects of roundoff and truncation in converting them to companion form would be more severe, thus diminishing the quality of the final result.

(U)One final structural observation further strengthens the argument against using the companion form in this particular wake emulation application. When converting to the companion form via a transformation that is an effective change of coordinate basis, the original identities of the underlying states are lost. This would ordinarily not be of much concern if just *one set* of three gates was being emulated using the companion form technique in the manner described, but more gates are needed to adequately represent the RV wake. A techniqe is described below for recursive emulation of successive PP and OP radar range gate target return effects. from previously emulated ones using explicit identities of the states (as associated with particular known range gates) once the designated first three contiguous gates behind the RV body are emulated using the structure of Eq. 6.1. The cornerstone of the following approach exploits explicit knowledge of the physical identities of the underlying states, so to convert to companion form (which looses the identities) and then to have to convert back again to recover them would just interfere with the procedure to be described below without providing the benefit of an exclusively companion form implementation. If *the same identical transformation could be used for each sequence of three contiguous gates* to convert Eq. 6.2 to the associated companion form, then this companion form technique and the approach to be described below could be combined, since underlying state identities, while altered, would still be constant. However, this constant transformation result is unlikely to occur.

(U)A more fruitful approach to computational simplifications for hardware RV wake emulation, without seeking recourse to companion form representation, is now discussed. An equation of the form of Eq. 6.1 should be implemented in hardware coresponding to the first three contiguous range gates (i, i+1, i+2), then in seeking to handle the next three contiguous range gates of concern (i+1, i+2, i+3), notice that PP and OP states for gate i+2 and i+3 are in common with the first three contiguous range gates considered [3]. Therefore, it is only necessary to further emulate the new entities representing one additional gate (i.e., the PP and OP components of i+3 using the prior emulation of i+2 and i+3) without emulating the effect of gates i+2 and i+3 a second time, otherwise the effects of gates i+2 and i+3 would be emulated more than once and would be unrealistic for that reason. The additional new gate i+3 can be handled without unsettling redundancy by implementing the following subset of Eq. 6.1:

$$\begin{bmatrix} \dot{x}^{PP}_{i+1}(k) \\ \dot{x}^{PP}_{i+2}(k) \\ \dot{x}^{PP}_{i+3}(k) \\ \dot{x}^{OP}_{i+1}(k) \\ \dot{x}^{OP}_{i+2}(k) \\ \dot{x}^{OP}_{i+3}(k) \end{bmatrix} = \begin{bmatrix} 0 & 0 & 0 & 0 & 0 & 0 \\ 0 & 0 & 0 & 0 & 0 & 0 \\ a_{31} & a_{32} & a_{33} & a_{34} & a_{35} & a_{36} \\ 0 & 0 & 0 & 0 & 0 & 0 \\ 0 & 0 & 0 & 0 & 0 & 0 \\ a_{61} & a_{62} & a_{63} & a_{64} & a_{65} & a_{66} \end{bmatrix} \begin{bmatrix} x^{PP}_{i+1}(k-1) \\ x^{PP}_{i+2}(k-1) \\ x^{PP}_{i+3}(k-1) \\ x^{OP}_{i+1}(k-1) \\ x^{OP}_{i+2}(k-1) \\ x^{OP}_{i+3}(k-1) \end{bmatrix} + \cdots$$

$$+ \begin{bmatrix} 0 & 0 & 0 & 0 & 0 & 0 \\ 0 & 0 & 0 & 0 & 0 & 0 \\ a'''_{31} & a'''_{32} & a'''_{33} & a'''_{34} & a'''_{35} & a'''_{36} \\ 0 & 0 & 0 & 0 & 0 & 0 \\ 0 & 0 & 0 & 0 & 0 & 0 \\ a'''_{61} & a'''_{62} & a'''_{63} & a'''_{64} & a'''_{65} & a'''_{66} \end{bmatrix} \begin{bmatrix} x^{PP}_{i+1}(k-4) \\ x^{PP}_{i+2}(k-4) \\ x^{PP}_{i+3}(k-4) \\ x^{OP}_{i+1}(k-4) \\ x^{OP}_{i+2}(k-4) \\ x^{OP}_{i+3}(k-4) \end{bmatrix} + \begin{bmatrix} 0 \\ 0 \\ w_3(k) \\ 0 \\ 0 \\ w_6(k) \end{bmatrix} \quad (6.4)$$

In this way, new gates are introduced one gate at a time beyond the original first three. The augmenting calculation to handle the next additional range gate beyond the original first three contiguous gates only requires $12 \times 4 = 48$ additional complex multiplications and $12 \times 4 + 2 = 50$ additional complex adds, and two additional pseudo-random variables to be used. Of course the AR coefficients used in the above Eq. 6.4 are as obtained off-line for gates (i+1, i+2, i+3) rather than those obtained for (i, i+1, i+2). The emulation of the effect of including each additional range gate can be handled similarly as a recursive extension with this reduced computational burden of not having to perform each operation implied in Eq. 6.1 to account for

[3] As seen from Fig. 6.6, it wouldn't do to handle gates (i, i+1, i+2) and (i+3, i+4, i+5) as two completely separate implementations because that would miss the important cross-correlation between (i+1, i+2, i+3) and (i+2, i+3, i+4).

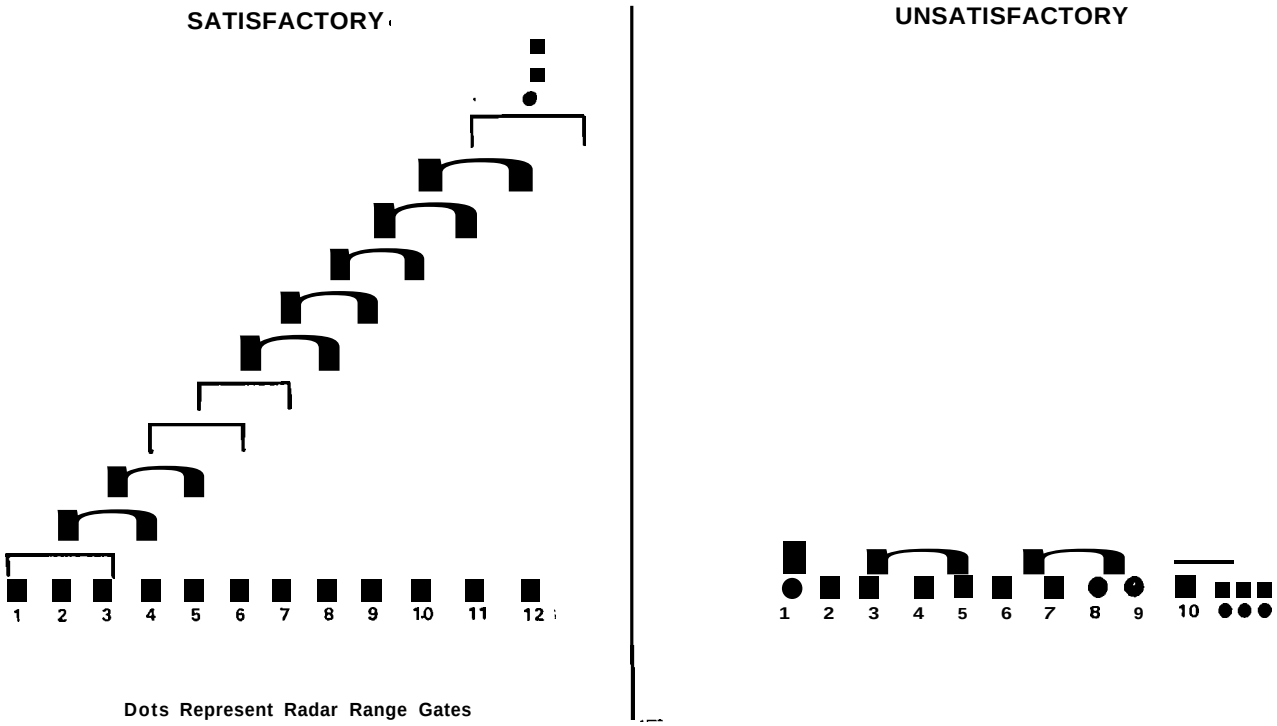


Figure 6.6: Handling Emulation of the Effect of Additional Range Gates without Undue Redundancy

the effect in the other gates handled. Retallying the total computational burden, as calculated from this new perspective, yields a specification of

- 144+N(48) complex multiplies per threat radar cycle,
- 174+N(50) complex adds per threat radar cycle,
- 144+N(48) total memory locations for storing AR coefficients,

where N in the above estimates represents the number of additional gates emulated beyond the initial three contiguous ones represented by **Eq.** 6.1. What N should be for Phase 2 BRVAD needs to be decided as a tradeoff between realism and practicality of implementation. In Section 1.1, it was mentioned in **Eq.** 1.3 that for Phase 1 BRVAD only 14 gates were emulated for the earlier narrow-band case because this number (in conjunction with the radar range gate size of 15) corresponded to a total wake length of 210 meters. In order that emulated RV wakes for the wide-band case of Phase 2 BRVAD be just as long, the number of gates to be included in an emulation should be $\frac{210\text{ meters}}{2.5\text{ meters}} = 84$ or $N = 81$. It is mentioned again for emphasis that many of the calculations should be done in parallel.

data possessing both "real" and "imaginary" components. After demonstrating the utility of this particular modeling approach on a representative multichannel test problem in providing a time-domain state variable model having prescribed auto- and cross-power spectra, the results were documented in [187]. In considering the benefits versus the drawbacks of this MSF-based modeling approach, it was *not* subsequently applied to actual Tradex radar data because it was realized that ***documenting*** a computed solution of general complexity in terms of arbitrary numbers would be a horrendous task [1] and further a significant preliminary step requires that all the data used be first converted into the frequency domain via FFTs in order to proceed. The other two approaches to RV wake modeling, discussed below, can be applied directly in the time domain to sampled data; thus, representing a simplification as they *were* applied to Tradex mission data.

(U)The second approach to RV wake modeling (briefly discussed in Section 6.1 of Chapter 6) was pursued by the Naval Postgraduate School (NPS) subcontractor using relatively recently emerging 2-D random process or random field techniques in now treating the RV wake as a more general 2-D space-time process. Special purpose software was developed and successfully validated with test problems and subsequently applied to Tradex mission data for five (5) different quantized altitudes of interest in providing clear 2-D estimates of spectra and cross-spectra. The benefit of explicitly modeling gate-to-gate cross-correlations was investigated as well as jointly handling Principal Polarization (PP) and Orthogonal Polarization (OP) data as reinforcing information whose simultaneous use more realistically depicts an actual RV wake. As aggreed upon, Mean Squared Coherence (MSC) functions were evaluated in conjunction with this investigation as a convenient, easy to interpret gauge of the inherent cross-correlation present. Results indicated that gate-to-gate cross-correlation that is present is just slightly more than could be reasonably attributed to be due solely to the Tradex ambiguity function alone. It was also necessary to skip five gates behind the RV body to prevent energy from the body from spilling over into the range gates of the wake and unacceptably corrupting/tainting evaluation results. These results are documented in the NPS Report [224]. While the computational burden of implementing a completely general 2-D model for the RV wake modeling application was shown to be very large and probably impractical, the structure of three novel possible simplifications were investigated under the assumption that the RV wake signal returns are a "separable" 2-D process, which has considerably lower implementation demands for wake emulation. It re-

[1] But **not an obstacle for problems with "nice" numbers, such as were used for illustrative purposes in worked (hand calculated) and machine computed examples in [187].**

mains to determine whether the RV wake is in fact truly separable [2]; however, an NPS graduate student is further pursuing this issue along with alternative practical implementation strategies in his thesis research, using this classified data, with conclusions that should be available soon.

(U)The third approach to RV wake modeling, that is the topic of this report, investigated the utility of two linear AR-based [3] spectral estimation approaches, as generalized to the multichannel case, being the Levinson-Wiggins-Robinson (LWR) algorithm and the Nuttall and Strand algorithm (that are described in Chapter 2 with results demonstrated in Chapter 3 and in Section 6.2 of Chapter 6). Between these two AR-based techniques, the conclusion of an earlier investigation [225] was revised based on the evidence to favor use of the LWR implementation as performing better in this particular wake modeling application by having fewer occurrences of spiky cross-channel spill-through and more faithfully estimating phase of the "complex" cross-spectrum. This multichannel approach can be easily generalized without change to encompass many channels if it were demonstrated that the enhancing RV wake target cross-correlation effects exhibited by adjoining additional adjacent radar range gates are significant and worth exploiting by simultaneous inclusion in a more massive joint model; however, to date, use of just three channels appears to suffice and use of a larger model would be a greater computational burden in seeking an implementation, apparently without offering any additional benefit in accuracy or realism. In Chapter 5, variations were considered in how statistical results summarizing the evaluation of gate-to-gate and/or PP/OP cross-correlation effects are best presented and, to that end, MSC function techniques were also utilized. Bounds on expected accuracy had been derived earlier (as reported in Appendix A) as one of the novel contributions of this investigation in order to obtain accurate *one-sided* confidence intervals about the theoretically expected MSC of zero that is anticipated if there were no cross-correlations between range gates beyond that caused by the radar ambiguity function alone. Almost all of the gate-to-gate cross-correlation evaluation results of Chapter 5 fell within this 80%-confidence interval bound except for the prevalent anomalous lower frequency results attributable to RV body energy spilling over into the range gates associated

[2] Seeing [232] when it is finally available may help.

[3] The more computationally challenging and numerically sensitive ARMA-based spectral estimation techniques were ***not*** pursued within this investigation for the reasons detailed in Chapter 4. Instead, a novel approach was provided for reexpressing an arbitrary ARMA process as a more tractable AR process of slightly higher dimension and applied, as explicitly demonstrated in two representative numerical examples in Chapter 4 of [187], for the case of multichannel ARMA processes in order to extract an equivalent "observable" and "controllable" AR process representation of "minimum degree".

with the wake (when five gates behind the body were not skipped as they should have been).

(U)The investigation of this third approach culminates with the illustrative evaluation of AR coefficients in Section 6.2 of Chapter 6 for a six state or six channel model of the RV wake using returns for three (3) contiguous PP range gates in conjunction with OP returns for the same three (3) range gates. An evaluation of corresponding AR-coefficients was performed using the Tradex mission data at a representative altitude. Motivation is provided in Section 6.2 for how this particular model was selected as well as the assumed order of the underlying vector AR process and this report further describes the complete methodology used in the evaluation. This documentation includes a consideration of algorithm selection (Chapter 3 and Sections 1.1, I.3), software implementation (Appendices D, E), software validation history (Appendices F, G), and all other pertinent information that should be useful.

## 7.2 Detailed Considerations and Further Recommendations for the Approach of this Investigation

(U)The computational results displayed in the earlier Chapters 3 and 5 of spectral estimation experiments are those that were originally performed over a year ago. Further more extensive numerical evaluation and step-by-step cross-comparisons between comparable methods or alternative implementations confirmed their correctness of implementation (as discussed in detail in Appendices D, E, F, and G) and also served to fill in missing data relating to signal processing particulars that were needed such as providing the sampling rate that is used and the length of data segments that are processed. With a more detailed scrutiny and sorting through of prior results and placing them in convenient juxtaposition in Chapter 3 to aid in performing a meaningful cross-comparison, the conclusion of an earlier investigation [225] was revised to favor use of the LWR implementation as performing better in this particular wake modeling application by having fewer occurrences of spiky cross-channel spill-through and more faithfully estimating phase of the "complex" cross-spectrum both for simulated data and for Tradex RV wake data. This new resumption of the prior investigation went further to also obtain additional results as well as providing a more refined simulation methodology for initial software algorithm calibration. In particular, the specific AR coefficients, as obtained

as intermediate results from the best performing LWR multichannel spectral estimation approach, are prominently displayed in Section 6.2 of Chapter 6 as our main modeling goal. Although joint multidimensional confidence regions on the coefficient matrices are preferred but are unavailable due to lack of existing techniques, confidence intervals for each row of the AR coefficients can be calculated using one of the recent more tractable techniques of either [19] or as a C-R lower bounding technique either as described in [150] or as a bound based on the "unknown-but-bounded" technique originally developed by F. C. Schweppe ([252], [216, pp. 21-29, ff. 76, ff. 154], [253], [254]) and refined for AR-based spectral estimation by Norton ([213, subsections 8.6.1, 8.6.2], [23]), as summarized in Appendix B.

(U)Results of coherence function calculation, as have already been performed on the available radar data, are displayed in Sections 5.3 and 6.1. Additional data-base experiments are recommended for refined validation of remaining hypothesis about the data, such as will be described below.

(U)One way to determine if range correlation is due entirely to the effect of the radar's transmitted signal is as follows. If the wake is indeed a white noise process, then the wavenumber spectrum is proportional to the squared magnitude of the radar transfer function. Thus, if the wake is truly uncorrelated, we should see the exact same wavenumber spectrum at each altitude and even for different missions! This is a characteristic whose existence can be determined or verified by computing and examining spectra over several different altitudes and/or missions.

(U)An approach for handling the important but temporary turbulent regime of Boundary Layer Transition (BLT) before laminar flow is reestablished and where the associated random process is nonstationary is offered in Section 2.3 of [187] in terms of time-varying Matrix Spectral Factorizations and time-varying linear system realizations, but is probably not too attractive as an easily tractable implementation for emulation. However, a handy approach for handling or faithfully modeling general transitions between altitudes as the RV descends is to use cubic spline interpolation on the reflection coefficients as determined at the quantized altitudes. This "spline interpolation approach" is apparently beneficial even over BLT.

(U)Some considerations and technical perspectives of fairly recent vintage are offered in Appendix C on how to further gauge the goodness of emulated RV wake signatures in quantifying their degree of distinguihability from actual RVs. These can be performed either in terms of standard K-factor evaluation or as refinements in divergence measure evaluation or, more radically, in terms of bispectra and trispectra evaluation criteria that have recently returned to signal processing/hypothesis testing prominence. Practicalities of on-line RV discrimination using these novel

higher moment spectra are briefly discussed in Section C.2.

**ACKNOWLEDGEMENT**

(U)Thanks are due to our consultant, Prof. Arthur Baggeroer of MIT, for many helpful comments and constructive criticisms and to our programmer, Richard T. Bartolomew. Chapter 2 of this report closely follows material in [165] and processing results depicted in Section 5.3 and the description of Appendix A are also largely due to William Huang's work of a year earlier. Thanks are also due to Dr. Paul Fougere of the Air Force Geophysics Laboratory and to Dr. Taikang Ning of Trinity College for making their respective computer implementations of line-split suppression routines for exclusively "real random processes" available to us.

(U)In response to an obvious need for such, a plethora of textbooks with easy to read tutorial discussions of spectral estimation for random processes have recently appeared [46], [47], [71, pp. 82-86, 99-101, 571-5741, [73, Chapt. 4], [74, Chapt. 6], [104, Chapt. 11], [153], [156], [247] which even cover the multichannel case (previously only covered in terse journal or conference articles) along with considerations of efficient algorithmic implementations [72, Chapt. 11]. Even the multidimensional random field case (e.g., 2-D) (with strong links to the multichannel case [109], [159]) has been described in [89, Sect. 6.51. The numerous alternative approaches being available and numerous auxiliary algorithms being offered is similar to the situation that exists in decentralized Kalman filter developments [69, Sec. IV], [113]. The existence of the tutorial discussions mentioned above has made our job easier in sorting through and picking the ones'that we feel are most appropiate for the Tradex radar application.

# Appendix A

# Compensating the Bias of Coherence Estimates and Providing Associated Confidence Regions

(U)The magnitude-squared coherence (MSC) or generalized correlation of two signals x and y (perhaps from different channels representing different polarizations of PP/OP or from different range gates for this radar application) is defined by ([8, pp. 1499-1501], [10],[11]):

$$C = \frac{|S_{xy}(f)|^2}{\sqrt{|S_{xx}(f)|^2 |S_{yy}(f)|^2}}, \text{ where } 0 \leq C \leq 1 \qquad \text{(A.1)}$$

where $S_{xy}(f)$ is the cross-spectrum and $S_{xx}(f)$ and $S_{yy}(f)$ are the auto-spectra. The coherence is a useful quantity in a variety of applications, including time delay estimation [8], [12] so important for sonar and sonobuoy arrays.

(U)In [12, Sect. 2], a generalized framework for cross-spectral power estimation for two stationary processes is postulated as consisting of the following seven steps:

1. Partitioning each time-limited realization of both random processes into N segments, where segments may be overlapped;
2. Multiplying each segment by a time-weighting function (possibly unity or a rectangular weighting or some more exotic rectangular weighting such as, for example, a Hanning weighting);

3. Computing discrete Fourier coefficients (DFC) from each weighted segment via an appropriate algorithm such as the Cooley-Tukey FFT after each segment has been appropriately appended or padded with zeros to achieve a common power of two data length;

4. Multiplying DFCs from one segment by the complex conjugate of the DFCs for the corresponding time sequenced segment of the other process;

5. Averaging of resulting complex products over the N available segments;

6. Fourier transforming the resultant spectral estimates into the correlation or lag domain where they are multiplied by a lag-weighting function (possibly unity);

7. Transforming results back into the frequency domain.

Alternatively, the above steps 6 and 7 may be replaced by convolution in the frequency domain, depending on the application and on which alternative computational path was the lesser computational burden.

(U)Carter then points out in [12] how three existing alternative spectral analysis techniques, being those of :

- Blackman and Tukey;
- Weighted Overlapped-Segment Averaging (WOSA) also referred to as Welch's technique;
- Lag-Reshaping technique of Nuttal and Carter;

each fit into the above described generalized framework. Additionally, [12] points out that these resulting estimates (and others) have the same statistical properties regarding the size of means and variances.

(U)Since much is known about the statistical properties of the MSC [1], the MSC can be used to measure the benefit of including a consideration of the cross-terms in multichannel spectral estimation. Results from previous work by Carter and Nuttall are based on Goodman's distribution as used in [6], which makes several assumptions about the estimated spectra. Additional alternatives not pursued here are discussed in [17].

[1]See [246] for most recent result that avoids need to assume Gaussian statistics for even one of the two channels of concern. Also see [244] and [245].

(U)This Appendix discusses Carter's distribution for the MSC when measured by the method of averaging periodograrns. We verified this implementation for the case of short data length (32 samples – a condition which appears to be so short as to violate the assumptions of Goodman in [6]). We chose to remove the bias by a method that is apparently more reliable than the method in [5] because it guarantees accuracy for all cases (although it is a more severe computational burden). The confidence boundary used here for the MSC estimate differs from that of [62] in that it minimizes the width of the confidence interval. This feature of this confidence boundary may be a desirable aspect favoring its use in hypotheses testing applications of the type pursued here.

## A.1 Estimating MSC by Averaging Periodograms

(U)Let $x_{bp}$, $y_{bp}$, b $= 1, 2, ...N$, $p = 1, 2, ...$M be two signals. For the radar application, b would be the burst number, and p would be the pulse number. In general, N can be considered to be the number of independent data segments, and M is the number of data samples in each segment. When $x_{bp}$ and $y_{bp}$ are jointly stationary, then the coherence can be estimated by the method of averaging periodograms [67]. Let

$$X_b(k) = \sum_{p=1}^{M} W(p) x_{bp} e^{-\frac{j2\pi kp}{M}} \qquad (A.2)$$
$$Y_b(k) = \sum_{p=1}^{M} W(p) y_{bp} e^{-\frac{j2\pi kp}{M}}$$

where $W(p)$ is a windowing function (i.e., $X_b$ and $Y_b$ are the corresponding FFTs of the windowed $x_{bp}$, $y_{bp}$). The coherence estimate is

$$\hat{C}(k) = \frac{|\frac{1}{N}\sum_{b=1}^{N} X_b(k) Y_b^*(k)|^2}{|\frac{1}{N}\sum_{b=1}^{N} X_b(k) X_b^*(k)||\frac{1}{N}\sum_{b=1}^{N} Y_b(k) Y_b^*(k)|} . \qquad (A.3)$$

The estimate in Eq. A.3 requires that N be greater than 1, however, the $\frac{1}{N}$ terms in the numerator and denominator of Eq. **A.3** effectively divide out. Choosing N and M is a tradeoff between achieving stability and having adequate resolution. A data record divided into N segments of M data points each will achieve reasonable

resolution for $\hat{C}(k)$ if M is large, but having too large an N decreases the variance of $\hat{C}$. Nuttall recommended that segments with 50 percent overlap with adjacent segments should be used since apparently segments even with as much as 50 percent overlap still behave as if they are effectively independent.

(U)Carter clarifies the situation in [12, Sec. III.A] with the following explanation of the trade-offs involved:

> Spectral resolution of the estimates varies inversely with the segment length T. Proper weighting or 'windowing' of the T-second segment is also helpful in achieving good sidelobe reduction. On the other hand, for independent segments with ideal windowing, the bias and the variance of the MSC estimate vary inversely with the number of segments, N. Therefore, to generate a good estimate with limited data, one may be faced with conflicting requirements on N and T. Segment overlapping can be used to increase both N and T. When the segments are disjoint, that is, non-overlapping, we call the number of segments $n_d$. As the percentage of overlap increases, however, the computational requirement increases rapidly, while the improvement stabilizes owing to the greater correlation between data segments.

In Figs. 9 and 10 of [12], plots are provided, respectively, of the bias and variance incurred in estimating coherrence as a function of the percentage of overlap utilized.

## A.2 Statistics of $\hat{C}$

(U)Carter [63] gave the form of the probability density function of $\hat{C}$ under the assumption that x and y are stationary, Gaussian, and have M independent (non-overlapping) bursts. (For additional perspective into the utility of pulse trains or bursts in radar applications, see [121].) Assume, in addition, that the number of samples (pulses) is large enough to ensure good spectral resolution, and that the segments are perfectly windowed so that power from the $k^{th}$ frequency bin does not leak into surrounding bins. These assumptions are the same as those invoked by Goodman for his distribution of the spectral density estimates, and the distribution used by Carter in [6] is further derived from Goodman's. If these conditions are satisfied, the probability density function (pfd) for the MSC is (using Drake's notation [64]):

$$f_{\hat{C}}(\hat{C}_0|N,C) = (N-1)\left[\frac{(1-C)(1-\hat{C}_0)}{(1-C\hat{C}_0)^2}\right]^N \frac{(1-C\hat{C}_0)}{(1-\hat{C}_0)^2} {}_2F_1(1-N,1-N;1;C\hat{C}_0)$$

(A.4)

where

$N$ = the number of bursts,
${}_2F_1$ = Hypergeometric function([59], [16, App.], [2], [15], [131, Ch.18])
for $N \geq 2$, simplifies to

$${}_2F_1(1-\mathrm{N}, 1-N; 1; C\hat{C}) = \sum_{n=0}^{N-1} \left( \frac{(1-N)_n}{n!} \right)^2 (C\hat{C})^n \qquad \text{(A.5)}$$

and $(z)_n$ = Pochammer's symbol, defined by
$(z)_0 = 1$
$(z)_n = z(z+1)(z+2)...(z+n-1)$

The corresponding cumulative distribution function (cdf) is as follows:

(A.6)

**Eq.** A.4 applies to **Eq.** A.6 for N strictly greater than 2. Since both

$$0 \leq \hat{C}, C \leq 1, \qquad \text{(A.7)}$$

the general shape of the pdf lies between 0 and 1 and has a peak in the vicinity of C, the true MSC. (Two additional alternative representations of the pdf of comparable complexity also involvingthe hypergeometric function of the same order are provided in [12, Table 1].) Figs. **A.1** and A.2 depict the pdf and cdf of the estimate $\hat{C}$ for the case N = **3,** and for a span of values of C.

## A.3 Unbiasing $\hat{C}$

(U)The $1^{st}$ moment or mean of $\hat{C}$ is [63]:

$$E[\hat{C}] = \frac{1}{N} + C\left(\frac{N-1}{N+1}\right) {}_2F_1(1, 1; N+2; C) \qquad \text{(A.8)}$$

The bias is largest at $C = 0$ (where actual Bias $= \frac{1}{N}$) and decreases monotonically with distance from zero to a minimum of zero when $C = 1$ [12, Sec. III.B]. Nuttall gave an approximate expression for the bias in [5]. However, we observe that the bias can be directly removed by solving for C in the RHS of Eq. A.8. This is much more of a computational burden, but it has the advantage that the error can be guaranteed to be small even in cases where the assumptions in [5] may not be valid. Since $\hat{C}$ and N are known, it follows from Eq. A.8 that

$$\begin{aligned} E[\hat{C}] &= \frac{1}{N} + C\left(\frac{N-1}{N+1}\right)\sum_{n=0}^{\infty}\frac{(1)_n(1)_n}{(N+2)_n}\frac{C^n}{n!} \\ &= \frac{1}{N} + C\left(\frac{N-1}{N+1}\right)\sum_{n=0}^{\infty}\frac{(n!)(N+1)!}{(N+1+n)!}C^n \\ &= \frac{1}{N} + C\left(\frac{N-1}{N+1}\right) + (N-1)N!\sum_{n=1}^{\infty}\frac{n!}{(N+1+n)!}C^{n+1} \end{aligned} \tag{A.9}$$

Since Eq. (A.9) is a polynomial in $C$, we can solve for $C$, the unbiased estimate of the true coherence by truncating the summation at $(M-1)$ terms to yield an $M^{th}$ order polynomial, and then dropping the quantifiable remaining error term so that the absolute error incurred in using this approximation is known. To achieve this goal, a useful decomposition is:

$$E[\hat{C}] = \frac{1}{N} + \frac{N-1}{N+1}C + (N-1)N!\sum_{n=1}^{M-1}\frac{n}{(N+1+n)!}C^{n+1} + ERR \tag{A.10}$$

where

$$ERR = (N-1)N!\sum_{n=M}^{\infty}\frac{n!}{(N+1+n)!}C^{n+1} \tag{A.11}$$

$ERR$ is upper bounded by noting that

$$\frac{n!}{(N+1+n)!} \le \frac{1}{(N+1)!}, \text{ for } n, N \ge 0 \tag{A.12}$$

Equality in Eq. A.12 only occurs when $n = 0$, which never happens in Eq. A.11. Therefore,

$$ERR < \frac{(N-1)N!}{(N+1)!}\sum_{n=M}^{\infty}C^{n+1} \tag{A.13}$$

Since the bias is positive, $C < \hat{C}$, so that all the more:

$$\begin{aligned} ERR &< \frac{N-1}{N+1} \sum_{n=M}^{\infty} \hat{C}^{n+1} \\ &= \frac{(N-1)}{N+1} \left( \frac{\hat{C}^{M+1}}{1-\hat{C}} \right) \end{aligned} \tag{A.14}$$

Eq. A.14 is the desired final form. Solving for Eq. A.14 for M we find that it must be that

$$M > \frac{ln(ERR) - ln\left[\frac{N-1}{(N+1)(1-\hat{C})}\right]}{ln\hat{C}} - 1 \tag{A.15}$$

The M in Eq. A.15 is the minimum order of the polynomial in Eq. A.14 needed to ensure that Eq. A.10 is off by no more than ERR. While a measure of relative error (as absolute error/true coherence value) is perhaps more desirable near zero values of C, it is unfortunately intractable and unavailable. Fig. A.3 shows a plot of the debiased estimate of $\hat{C}$ versus that measured by actually estimating $\hat{C}$ as averaged for various values of N, the number of bursts for this radar application. In [12, Table 2], both exact and approximate expressions are provided for the bias and the variance of $\hat{C}$ in terms of the number of data points N.

## A.4 Verifying Carter's PDF

(U)Standard tests for the goodness-of-fit to a particular postulated pdf are the Kolmogorov-Smirnovand the Chi-Squared test [65]. The Kolmogorov-Srnirnov test is used here because it is known to sometimes yield good results for smaller sample sizes such as we are constrained to consider for this particular radar application. For a brief discussion of the relative merits of using the Kolmogorov-Smirnov test versus the use of Chi-Squared test, see [66]. The Kolmogorov-Smirnov test statistic is the maximum error between the measured cumulative distribution function and the expected cdf (corresponding to the theoretical cdf or "null hypothesis") as

$$\mathrm{D} = \max_{\hat{C}_0} \left| S(\hat{C}_0) - F_{\hat{C}\leq}(\hat{C}_0) \right|; \tag{A.16}$$

where

$$\begin{aligned} \mathrm{D} &= \text{Kolmogorov} - \text{Smirnov statistics} \\ S(\hat{C}_0) &= \frac{\text{number of samples} < C_0}{\text{total number of samples}} \\ F_{\hat{C}\leq}(\hat{C}_0) &= \text{CDF of the null hypothesis} \end{aligned} \tag{A.17}$$

(U) Figure A.4: Kolmogorov-Srnirnov distribution, for large N

$S(\hat{C}_0)$ can be thought of as an estimate of $F_{\hat{C}\leq}(\hat{C}_0)$. Each estimate here is an average of N radar bursts.

(U)Consider Fig. A.4. In the limit as N gets large, $f_D(D_0)$, the pdf of the Kolmogorov-Smirnov test statistic is observed to approach the Chi-Squared distribution. For a set of estimates, if the statistic $D_0$ (defined in Fig. A.4) corresponds to an $a < 0.05$, that set of estimates is said to have failed the test at the 0.05-level of significance (i.e., the conclusion is that the samples were not distributed according to the null hypothesis).

## A.5 2-Sided and 1-Sided Confidence Bounds

(U)In Fig. A.5, consider the pdf for any statistic, $s$, in general and any two points, $s_1$ and $s_2$, selected in such a way that the area of the pdf between them is $(1 - a)$. Then this is a valid $100(1 - a)$ percent confidence bound for s. In reference [62], the confidence bound is selected so that the area of both the left and right tails is $\alpha/2$. For the purpose of relating confidence bounds to hypothesis testing, we are interested in a confidence bound where $f_s(s_1) = f_s(s_2) = p_o$ (see Fig. A.5). For pdf's that have one peak, such as the pdf for $\hat{C}$, this corresponds to choosing a confidence bound that minimizes $|s_2 - s_1|$. The result is shown in Fig. A.6 for

# Appendix B

# Alternative Methodologies for Gauging the Accuracies of AR Coefficient Estimates

(U)The prudent analyst always seeks to quantify the degree of confidence associated with final results. To this end, it is desirable to have variance estimates or confidence regions specified for each of the coefficient matrix estimates, $\hat{A}_i^{(P)}$, that are associated with multichannel LP approaches to spectral estimation similar to those existing bounds of [213, subsections 8.6.1, 8.6.2], [23] for ARMAX (Autoregressive Moving-Average-Exogenous) models. An acceptable alternative as a "test of the entire pudding" would be to quantify the uncertainty incurred in the subsequent calculation of the multichannel spectral estimates for which estimates of the coefficient matrices were necessary intermediate results. As a class, spectral estimation results obtained from one parametric model-based approach to LP should not be drastically different from those of a similar approach to LP (viz., [27]).

(U)Historically, consideration of estimating the bias and variance of spectral estimates has been treated in [20] and [21], respectively. For the particular LP estimation approach of MEM, confidence intervals ([18], [19], [263]) have been developed for the resulting intermediate AR parameter estimates but only for the scalar single channel case. The recent extension in [19] makes such confidence interval calculations more tractable by circumventing the prior requirement in [18] of having to integrate over a two-dimensional generalized Student's-t distribution in transitioning from the underlying joint pdf (being a function of the true but unknown values of the AR parameters being estimated (also see [24])) to the goal of having confidence regions. The results of [19] are also claimed to be applicable to

maximum entropy *wavenumber* estimation as well (of interest if the 2-D modeling approach reported in [224] is adopted) but is still available *only* for the scalar case rather than for the multichannel case as we are faced with in this multichannel radar application.

(U)Historical approaches to using Cramer-Rao (C.-R.) lower bounds to conservatively gauge the uncertainty incurred in AR parameter estimation encountered a barrier of having to perform multitudinous differentiations in order to obtain the intermediate result of computing the associated Fisher information matrix. However, the recent result of [22] circumvents this prior computational burden via a neat identity that allows mere shift-matrix operations to suffice (as long as the underlying process is stationary). Unfortunately, the form of the C.-R. bound utilized in [22] assumes that the AR parameter estimator being utilized is unbiased, which perhaps is not the case for our radar application. (See [107], [110] for discussions of the form of the C.-R. bound that properly acknowledge and handle possible biasness in the estimator.) Another historically exact expression for Cramer-Rao lower bounds on AR coefficient estimation is credited to Donald Tufts [250] and is derived for both the AR and ARMA case in the recent textbook [247, pp. 211-213, 302-3051.

(U)Another augmenting experiment (involving simulated data), beyond what was already presented in Section 3.2, is to determine the effect by calibrating the response of the alternative multichannel AR-based spectral estimation algorithms with respect to varying intensities of additive Gaussian white measurement noise. In this way, the robustness of these high resolution algorithms to the effect of noise being present (and, moreover, its response to actual mismodeling in assuming an AR-process to be present, when, in actuality, it is an ARMA process as discussed further in Chapter 4) can now be gauged as to how well it performs and at what intensity level of the noise do the resulting estimates of the AR coefficients become unacceptably degraded. Results of these numerical experiments (offered in [179], [185], [255], and [256] so that there is no longer a need for us to perform them ourselves[1]. at some expense) can be compared for proximity to the above described asymptotic C.-R. lower bound for additive noise being present, as calculated using the technique of [150]. While the actual radar application of interest here is not noise-limited since target returns have an extremely strong SNR advantage, it is in fact time-limited or of constrained data length. It is proposed that a buy-off of sorts can be performed to still use the C.-R. lower bounds of [150] in this RV wake modeling application, where white additive measurement noise being assumed to

[1] An awareness of the existence of these results avoids the expense of an unnecessary duplication of effort in repeated evaluation.

be present makes the lower bound higher than normal, in place of not being able to have enough data to achieve asymptotic C.-R. bounds, which also makes lower bound results higher than normal. The correspondence could be experimentally calibrated but awaits evaluation by the user who makes the final decision on which of the approaches to use, either 1-D or 2-D; otherwise, it would just be a wasted exercise to determine a 1-D refinement if the 1-D approch was not used. Additional benefits of pursuing the evaluation technique of [150] is that an explicit formula for the lower bound is available that does not involve numerical integration, as most other evaluation approaches require. Indeed, in some applications one is interested not so much in the AR parameters themselves as in some useful function of these parameters such as in the center frequency, bandwidth, and power of narrowband spectral lines. Another beneficial aspect of the results of [150] is in providing a simplified methodology for computing C.-R. lower bounds on such general functions of the AR coefficients (and additive noise intensity).

(U)The "unknown-but-bounded" approach of [252], [216, pp. 21-29, ff. 76, ff. 154], [253], [254] as converted to apply to AR coefficient estimation in [213] is not recommended for further pursuit for the RV wake modeling application for reasons provided in [23] relating to disappointments in performance in practice. Again knowledge of these results avoids unnecessary duplication of effort.

(U)The topics of Appendices B and C, while germane to the task of modeling and evaluating the model for RV wakes, is more in the nature of R & D to be utilized further downstream. The issues in these two Appendices B and C are more like "icing on the cake" and recieve less emphasis in this report than the higher priority primary concerns addressed throughout the remainder of this report.

Another area of concern in the calculation of K-factors is when unequal variance situations sometimes arise, where K-factors are not appropriate (however a standard tractable approximation is to average the two differing variances and take the result to be the common variance that exists for both situations) [239, p. 105], and to then proceed in the usual manner.

(U)New divergence measures have recently been developed or modified to gauge *spectral* proximity of amplitude and phase components to a specified goal or template. Additionally, higher order spectral characteristics are now beginning to be utilized or exploited in practice such as bispectrum and trispectrum methods which relate, respectively, to third- and forth-order moments. Unlike most other statistical and random process techniques, these higher order techniques only apply to processes that are non-Gaussian, as are more likely to be encountered in actual target data rather than by resorting to a perhaps untenable assumption of Gaussianess.

(U)Sophisticated measures for determining whether significant cross-correlation exists between channels (as between contiguous range gates or between primary parallel polarization and orthogonally polarized target returns) can be based on metrics such as the well-known measures of Chernoff coefficient, Bhattacharyya distance, I-divergence measure, and J-divergence measure, all to be further described below.

## C.1 Analytic Formulation of Four New Measures

(U)While the exact evaluation of probability of error in statistical hypotheses testing situations is frequently intractable [1], two well-known bounds that bracket the elusive exact probability of error, $P_e(m)$, based on m-data samples, $x^m$, in decisions associated with signal detection and pattern recognition applications (where $f_1(x^m)$ and $f_2(x^m)$ are the underlying pdfs of $x^m$ under hypotheses $H_1$ and $H_2$, respectively, and $\pi$ and $(1-\pi)$ are the corresponding prior probabilities) are known to be [33]:

$$\frac{1}{2} - \frac{1}{2}\left[1 - 4\pi(1-\pi)\left[B_m(0.5)\right]^{2m}\right]^{\frac{1}{2}} \leq P_e(m) \leq \left[\pi(1-a)\right]^{\frac{1}{2}}\left[B_m(0.5)\right]^m \quad \text{(C.1)}$$

and

$$\frac{1}{2}\min(\pi, 1-\pi)\exp\left(\frac{-J_m}{8}\right) \leq P_e(m) \leq \left[\pi(1-\pi)\right]^{\frac{1}{2}}\left[\frac{J_m}{4}\right]^{-\frac{1}{4}} \quad \text{(C.2)}$$

[1] A detection/hypothesis-testing situation that is surprisingly tractable as a departure from the usual situation where frequently one is elated to be able to evaluate even mere coarse bounds is reported in [248].

where, in the above, $B_m(t)$ is the Chernoff coefficient:

$$B_m(t) \triangleq \left[\int_{R^{3m}} [f_1(x^m)]^t \, [f_2(x^m)]^{1-t} \, dx^m\right]^{\frac{1}{m}} \tag{C.3}$$

for $0 \leq t \leq 1$, and the J-divergence is:

$$J_m \triangleq \frac{1}{m} \int_{R^{3m}} [f_1(x^m) - f_2(x^m)] \log\left[\frac{f_1(x^m)}{f_2(x^m)}\right] dx^m \tag{C.4}$$

(U)The quantity $-m\log B_m(0.5)$ in the above is denoted as the Bhattacharyya distance and a related distance measure is the I-divergence defined as:

$$I_m(f_1, f_2) = \frac{1}{m} \int_{R^{3m}} f_1(x^m) \log\left[\frac{f_1(x^m)}{f_2(x^m)}\right] dx^m \tag{C.5}$$

(U)The above described four measures have already been asymptotically simplified in [33] and can be used to distinguish between two comparably dimensioned, covariance stationary Gaussian processes on the basis of m discrete time samples as further discussed in [33], while other measures are still being further refined [34], that employ a detailed consideration of the adequacy in matching the amplitude and phase component of the spectral function that is the goal. Moreover, higher order spectral characteristics ([35] - [44]) and remnants can also be checked for an adequate match.

## C.2 A Resurgence of Interest in Bispectra and Trispectra Estimation as More Sensitive Discriminators than Just Spectral Estimation

(U)The bispectrum of a stationary process is the Fourier transform of its third moment sequence [39] (which can be utilized in a measure of skewness) and, correspondingly, trispectra can be related to fourth order cumulants (or semi-invariants) [43] which, in turn (as a measure of flattening, excess, or "kurtosis"), relate to fourth moments of the system or random process output sequence. (See [103, pp. 15-20] for a clear treatment of how to handle transitioning between moments and cumulants.) Although these bispectrum techniques have been around since the middle 1960's and before ([40], [41], and [44]), such higher moment techniques

are being increasingly advocated for use in extracting elusive phase information about a random process and in performing more accurate parameter identification of non-Gaussian Autoregressive (AR) processes. Such techniques are being looked into by sonar practitioners [42]. As a reversal of the usual situation for statistical techniques, these new higher moment techniques do not usually work well when the underlying process is Gaussian, but have performance that improves markedly as the underlying random process departs more radically from Gaussianess (as may be explicitly revealed using the techniques of [142], [129] in the same manner as have already been applied via an available FORTRAN program in [132]). Unfortunately, the variances of these higher order spectra for the same length of data are considerably worse by being higher than that of conventional power spectra, as would be expected. In seeking to use higher order spectral techniques, a greater length of data is needed in order to obtain comparable reasonable accuracy of results.

(U)Multichannel higher moment techniques have already been developed (e.g., [39]) but, to date, have internal constraints imposed that the dimension of the output must be identical to that of the input for these multi-input/multi-output (MIMO) systems. However, this excessive constraint will probably be soon lifted in the future since it is not a physical constraint but a mathematical one imposed for the convenience of the analyst in the assumption of [39]. Additional insights and developments on this important topic are still evolving (e.g., [38], [45], [102]). A need apparently exists in how to modify/expand on all of the above bispectra and trispectra results in the manner indicated in [48], [164] in order to obtain comparable results for the complex processes that arise in coherent radar applications involving complex covariance matrices and power spectra. The main obstacle to adequately handling the complex case is to settle on a convention that can be consistently adhered to as in, for example, the handling of conjugation for third moments as discussed further below. While for second moments (as are exclusively used in standard spectral estimation) there is no ambiguity in using the conjugation for the second term in order that the result be all real; however, for third moments, the conjugation can be anywhere between three likely candidate locations with no real preference dictated by any other physical or mathematical constraints being available to invoke, thus recourse must be made to adopting a common convention instead. The appropriate convention to use is still being debated by specialist (as reported by Nikias at the Minisymposium on ASSP in Boston, MA in May, 1987).

# Appendix D

# Capabilities Designed into the New Simulator

(U)Within this investigation a new state-variable based Monte-Carlo simulator for AR process emulation was developed. The new simulator possesses the following ***new*** features:

- Incorporates "exact discrete-time equivalent of continuous-time white noise".
- Offers option of using the more efficient direct calculation of steady-state initial conditions corresponding to stationary behavior of the underlying random process (without having to iterate to steady-state to avoid the nonstationary initial transient).
- Offers option of having additive (stationary white Gaussian) output measurement noise present (thus creating a type of ARMA process).
- Doesn't require use of only diagonal covariances for noises or for initial condition covariances.
- If covariances are not diagonal, the program internally automatically checks to verify that the covariances possess the requisite "positive definiteness" property (via use of the Singular Value Decomposition (SVD) in the manner indicated in [105, p. 504], [178], [108, Section III, p. 713], [106, Section III, p. 63]), otherwise diagonal covariances are merely verified not to have zeroes or negative numbers on the principal diagonal.

- Calculates transition matrix by more accurate Pade approximation (offering two validated options along these lines) rather than through use of a Taylor series expansion.
- Can handle nonzero means for noises and initial conditions.
- Outputs final pseudorandom noise (PRN) seed value to enable continuity of use via allowable dovetailing of output sample functions if further prolonged sample function history is subsequently pursued (which uses this PRN seed during subsequent start-up).

Each of the above mentioned features will be elaborated on further for clarification and to explain why having each new feature is important in this investigation.

## D.1 Discrete-time Equivalent of Continuous-time White Noise

(U)To avoid discrepancies between a continuous-time formulation and the (of necessity) discrete-time implementation on the digital computer, the following refinement was pursued. To ignore the discrepancy or to invoke a rather well-known approximation, discussed at the end of this subsection, would incur an uncalibrated error that would mask the aspects of the software implementation of the spectral estimation algorithms that we seek to verify as our intermediate goal.

For a time-invariant linear continuous-timestate-variable representation in terms of the matrix triple (F, G, C) as

$$\frac{dz}{dt} = F\, z(t) + G\, x(t) \tag{D.1}$$

$$y(t) = C\, z(t) \tag{D.2}$$

with corresponding system transfer function matrix

$$H(s) = C\, (sI - F)^{-1}\, G\,, \tag{D.3}$$

the equivalent discrete-time reformulation in terms of the matrix triple (A, B, M)

$$z(k+1) = A\, z(k) + B\, x(k) \tag{D.4}$$

$$y(k) = M\, z(k) \tag{D.5}$$

with corresponding system transfer function matrix

$$H(z) = M\,(zI - A)^{-1}\,B\,, \tag{D.6}$$

where $z$ in Eq. D.6 is the $Z$-transform variable but in Eqs. D.1, D.2, D.4, and D.5 is just notation for the system state variables with $x(t)$ as the input.

(U)An initial investigation of posing the continuous-time problem as an *exact* formulation in discrete-time proceeds as follows. The form of the solution to the differential equation of Eq. D.1 is:

$$z(t) = e^{F(t-s)}\,z(s) + \int_s^t e^{F(t-\tau)}\,G\,x(\tau)\,d\tau\,. \tag{D.7}$$

In particular, for the upper and lower limits of the above integral being

$$t = (k+1)\,\Delta \tag{D.8}$$

$$s = k\,\Delta \tag{D.9}$$

$$\text{A} = \text{constant incremental step} - \text{size}\,, \tag{D.10}$$

the solution of Eq. D.7 corresponds to the following recursive iteration in discrete-time:

$$z(k+1) = \left[e^{F\Delta}\right]\,z(k) + \int_{k\Delta}^{(k+1)\Delta} e^{F(k\Delta-\tau)}\,G\,x(\tau)\,d\tau \tag{D.11}$$

which, under the further assumption that $x(\tau)$ is essentially constant over the time-step from any k A to any other (k + 1) A, yields:

$$z(k+1) = \left[e^{F\Delta}\right]\,z(k) + \left[\int_{k\Delta}^{(k+1)\Delta} e^{(F(k+1)\Delta-\tau)}\,G\,d\tau\right]\,x(k)\,. \tag{D.12}$$

Upon making the change of variable

$$\tau = \tau' + k\,\Delta \tag{D.13}$$

and substituting into Eq. D.12, yields:

$$\begin{aligned} z(k+1) &= \left[e^{F\Delta}\right]\,z(k) + \left[\int_0^{\Delta} e^{F\Delta}\,e^{-F^T\tau'}\,d\tau'\right]\,G\,x(k) \\ &= \left[e^{F\Delta}\right]\,z(k) + \left[e^{F\Delta}\right]\,\left[\int_0^{\Delta} e^{-F^T\tau'}\,d\tau'\right]\,G\,x(k)\,. \end{aligned} \tag{D.14}$$

The expression in Eq. D.14 is the most general form of the discrete-time formulation that corresponds *exactly* to the continuous-time formulation of Eq. D.7 except for the minor error incurred in assuming $x(\tau)$ to be essentially constant over each small stepsize **A.** In the case where the continuous-time input $x(t)$ is independent, white, Gaussian process noise of continuous-time covariance intensity level, Q, to have *exact* adherence without any approximation incurred, the discrete-time formulation should be

$$z(k+1) = \left[e^{F\Delta}\right]\ z(k) + \left[e^{F\Delta}\right]\ x'(k) \tag{D.15}$$

where

$$x'(k) = \text{zero} - \text{mean Gaussian white noise} \tag{D.16}$$

having discrete-time covariance intensity level. ([234, p. 4-127b], [176, p. 2701]):

$$Q_d = E\left[x'(k)(x'(j))^T\right] = e^{F\Delta}\left[\int_0^\Delta e^{-F\tau}\ G\ Q\ G^T\ e^{-F^T\tau}\ d\tau\right] e^{F^T\Delta}\ \ \delta_{kj} \tag{D.17}$$

where the above Kronecker delta is defined as

$$\delta_{kj} = \begin{cases} 1 & \text{if k=j} \\ 0, & \text{otherwise.} \end{cases} \tag{D.18}$$

The above $Q_d$ in Eq. D.17 is the appropriate discrete-time process noise covariance level to use to have *exact* agreement between the discrete-time mechanization of Eq. D.15 and the the continuos-time formulation of Eqs. D.1 or D.7. A well-known approximation for $Q'_d$ [238, pp. 83-84] (due to Kalman) which is sometimes used is to take

$$Q'_d = \tfrac{1}{\Delta}\ Q\ ;$$

however, the deleterious effect of invoking this approximation is uncalibrated and it can easily be seen to be obviously unsatisfactory by considering the case of a system with a diagonal continuous-time Q, but a nondiagonal system matrix, **F.** The approximate $Q'_d$, defined above, is consequently merely diagonal while the exact $Q_d$ of Eq. D.17 is definitely nondiagonal. See calculations of Eq. G.5 for Test Case 2 in Appendix G as a concrete example.

## D.2 Direct Calculation of Steady-State Initial Conditions

(U)A stationary linear system must not only have a system description that has matrix parameters that are time-invariant, but must also be initialized with the

proper initial conditions that correspond to its steady-state behaviour, otherwise an initial transient occurs within the computations that must first be endured and subsequently skipped before truely stationary behaviour of the system is achieved. Rather than have to iterate Eq. D.15 to steady-state (which is an approach that converges to the desired answer at only a linear rate, thus being fairly expensive in terms of computational resources expended), two different approaches are utilized here for calculating the steady-state mean and covariance associated with the primary iterative mechanization of Eq. D.15 for Monte-Carlo simulation. The approach implemented for the computation of the steady-state covariance is that developed by Kleinman [235], [236]; while the approach implemented for computation of the steady-state mean is original and was developed within this investigation as a novel contribution. Both techniques are described next.

### D.2.1 Steady-State Solution of Covariance

(U)The Kleinman algorithm [235], [236] was developed to solve the following continuous-time Lyapunov equation:

$$\dot{P}(t) = FP(t) + P(t)F^T + GQG^T \tag{D.19}$$

or, equivalently, the discrete-time version of the Lyapunov equation as:

$$P(k+1) = \left[e^{F\Delta}\right]\ P(k)\ \left[e^{F\Delta}\right]^T + Q_d \tag{D.20}$$

(which arise as the primary obstacle that must be computationally overcome within Kleinman's novel approach to steady-state Riccati equation solution) in obtaining the steady-state constant value for

$$P(t) \triangleq E[(z(t) - \bar{z}(t))(z(t) - \bar{z}(t))^T] \ ,$$

being the steady-state covariance associated with the linear system of Eq. D.1 when F is constant and strictly stable. That $P(t)$ satisfies a Lyapunov equation is demonstrated in [234, pp. 165-1671. The rate of convergence of Kleinman's approach to the steady-state solution is better than quadratic [237] and was implemented as one of the available software routines of [197] that was first obtained and then validated with test problems of known solution, as discussed further in Appendix F. The resulting steady-state positive definite solution matrix is first checked for positive definiteness (using the technique discussed in Section D.4), then invoked as the initial condition covariance used to start the recursions of Eq. D.15 that constitute

the Monte-Carlo simulations. By initializing in this manner, the sample functions that immediately emerge correspond exactly to stationary behaviour of the system without having to wait for an initial transient period to end. A detailed explanation of the computational aspects associated with using Kleinman's approach is provided in [240].

### D.2.2 Steady-State Solution of Mean

(U)The original approach to computing the steady-state mean of Eq. **D.l** is discussed now. The implementation of the recursion of Eq. **D.15** in software can be easily accommodated. However, there is a simpler alternative to iterating 1000 times to achieve steady-state operation as was done in the predecessor simulator. Using 1000 iterations can be extremely costly for larger dimensioned state sizes and, although simple and straight forward, is not the computationally efficient way to achieve steady-state operation. For some problems, even 1000 iterations would not be enough to achieve steady-state (i.e., the step-size A must be such that 1000 iterations [1000Δ] is more than 5 times the effective time constant of the underlying system of Eq. **D.l;** if it's not, then steady-state is <u>not</u> achieved even after 1000 iterations. Similarly, if the system matrix, F, in **Eq. D.l** is such that it is only marginally stable rather than being strictly stable, then <u>no</u> steady-state is defined (except for the situation where there is a single pole at the origin while all noises are zero mean; which yields a constant output in steady-state for the corresponding state variables as long as no other state variables are related to it such as being the integral of it, otherwise a ramp results which has no steady-state).

(U)Returning to Eq. **D.l** to focus on the long term effects of providing the linear system with a Gaussian initial condition, having the following statistics for the mean and variance, respectively:

$$E[z(t_o)] = z_o \ , \tag{D.21}$$

$$E[(z(t_o) - z_o)(z(t_o) - z_o)^T] = P_o \ , \tag{D.22}$$

where $P_o = P_o^T > 0$ is positive definite and $E(\cdot)$ denotes total expectation. Notice that in taking the expectation, $E(\cdot)$, throughout **Eq. D.l** yields

$$E[\dot{z}(t)] = F\ E[z(t)] + \underbrace{E[x(t)]}_{=0} \tag{D.23}$$

and under the generally valid condition that differentiation and expectation (interpreted as a Riemann -Stiltjes or Lebesque-Stiltjes integral with respect to the

monotone increasing [and therefore possessing the requisite property of being of bounded variation as needed for this type of integral representation] cummulative distribution function) are interchangable, Eq. D.23 simplifies as

$$\frac{d}{dt}E[z(t)] = F\ E[z(t)] \tag{D.24}$$

or for $\bar{z}(t) \triangleq E[z(t)]$, equivalently,

$$\dot{\bar{z}}(t) = \mathrm{F}\ \bar{z}(t)\ ,\ \text{with}\ \bar{z}(t_o) = z_o\ . \tag{D.25}$$

The above is the describing equation from a continuous-time viewpoint while the equivalent discrete-time equation (obtained by similarly taking expectations throughout Eq. D.15) is

$$\bar{z}(k+1) = [e^{F\Delta}]\bar{z}(k)\ \text{when properly initialized with}\ \bar{z}(0) = z_o. \tag{D.26}$$

For the case of a zero mean:

$$z_o = 0 - \text{vector}\ , \tag{D.27}$$

the need to solve either Eqs. D.25 or D.26 is circumvented entirely. For the case of a nonzero mean:

$$z_o \neq 0 - \text{vector}\ , \tag{D.28}$$

the steady-state mean value (if it exists) is the solution of

$$\bar{z}(\infty) = [e^{F\Delta}]\ \bar{z}(\infty) \tag{D.29}$$

or, equivalently, the solution of

$$[I - e^{F\Delta}]\ \bar{z}(\infty) = 0 \tag{D.30}$$

It is worthwhile to solve for $\bar{z}(\infty)$ because this value (along with the steady-state P) can be used to initialize the Monte-Carlo simulation so that it starts out exhibiting stationary behaviour, rather than having to wait for it to progress through the transient portion. As mentioned above, one solution approach is by recursive iteration as in Eqs. D.25 and D.26, but with better control exercised on the number of iterations utilized than was exhibited in the predecessor simulator. Rather than blindly always using 1000 iterations [1], which is generally ***not*** satisfactory for the reasons already given above, it is better to use knowledge of the system structure

[1] This is satisfactory if the simulator were being used on a one shot basis, which is how it was originally being used over a year ago for the single case of Section **3.1,** but is no longer the case here.

## D.5 Updated Calculation of the Transition Matrix

(U)The calculation of the transition matrix, or matrix exponential as it reduces to for the linear time-invariant system of Eq. D.l, was modernized to take advantage of the most accurate computational techniques that have been relatively recently advertised (and endorsed) by specialist in this area of numerical analysis. A detailed accounting is provided in Appendix E.

## D.6 Handling Nonzero Means for Noises and Initial Conditions

(U)This capability was provided so that situations could be created where a bias is present. It is frequently instructive as a test against reality to find out how well an algorith performs when an unanticipated bias is present. Frequently, analysts tacitly assume biases to be zero for convenience and tractability but the actual physical application may not be so accommodating. There is no technical challenge in including this feature within the simulation capabilities of the new simulator, it was just another item that had to be specified and routinely added in.

## D.7 Outputting of Final Pseudorandom (PRN) Seed Value

(U)In obtaining sample functions from the simulator, it may later become apparent that a longer time record is desired than originally simulated. When the last value of the PRN is outputted from each run as is now done in the new simulator, it can be utilized to initialize a new run starting with the final value of the previous run as the initial starting condition of the new run. In this way, the new run can dovetail with the results of the previous run as effectively one longer run without having to throw away the results of the earlier run that was deemed too short. With the exception of the original technique for specifying the steady-state mean that is offered in Subsection D.2.2, all the other features discussed above are standard techniques that are now used in modern approaches to specialized linear time-invariant Monte-Carlo simulators, as also pursued for this investigation. However, each new feature described in this Appendix D was first implemented using

to specify explicitly the number of iterations required to achieve steady-state. This could be achieved by using the Singular Value Decomposition (SVD) on F to expose the underlying eigenvalues, the longest time constant being the reciprocal of the smallest real part of all the eigenvalues encountered. The required number of iterations would be the interger portion of $\frac{5}{\lambda_{min}\Delta}$.

(U)While the above described solution should work, the preffered solution proceeds as follows. Notice from Eq. D.30 that the steady-state solution of Eq. D.29 is a right singular eigenvector of $e^{FA}$ as

$$(XI - [e^{FA}])\bar{z}(\infty) = 0 \tag{D.31}$$

for

$$X = 1 \tag{D.32}$$

so that all that is computationally needed is to perform an SVD operation on $e^{FA}$ as

$$e^{FA} = U\Lambda V^* , \tag{D.33}$$

where **A** is diagonal and contains the eigenvalues exposed as

$$\Lambda = diag(\lambda_1, \lambda_2, \ldots, \lambda_n) \tag{D.34}$$

in descending order of magnitude, and the associated matrix **V*** contains the corresponding right singular eigenvectors. All that is further required is that the resulting diagonal matrix **A** in Eq. D.33 be searched from left to right to find that eigenvalue that is equivalent to 1 while simultaneously adjusting a corresponding pointer to the rows of V*. If no such eigenvalue exists that is equivalent to 1, then no steady-state exists for Eqs. D.25 or D.26. The "slot" or index value (i.e., value of i = i,) for which

$$\lambda_{i_o} = 1 \tag{D.35}$$

corresponds exactly to the appropriate vector column slot within **V*** of the form

$$\mathbf{V}^* = [v_1 \vdots v_2 \vdots \ldots \vdots v_r] \tag{D.36}$$

such that the steady-state value being sought is:

$$\bar{z}(\infty) = v_{i_o} \tag{D.37}$$

(corresponding to Eqs. D.31 and D.32, together). This is the algorithm that is included in the current simulator. Thus, the steady-state mean can be calculated

(when it exists and this solution approach possesses the additional feature of also automatically checking on the existence of the steady-state solution). This simulator can also be used for Kalman filter applications, where these steady-state initialization features for the mean and covariance will likely be of even greater utility by providing the capability of generating a completely theoretically stationary random process sample function upon entering the normal iteration cycle without the usual "wait for things to settle down".

## D.3 Option of Including Corrupting Additive Output Measurement Noise

(U)A question arose as to whether the underlying truth model Monte-Carlo simulator for exercising the spectral estimation algorithms should also contain a provision for including a component of additive measurement noise as well as the standard process noise in the final sensor measurement so that it is more properly modeled as consisting of the following sum of two statistically independent components as:

$$y(t) = y_{AR}(t) + v(t), \text{ where } v(t) \sim N(0, \mathrm{r}). \tag{D.38}$$

Typical Kalman filter simulators always include a measurement noise simulation capability, so it was initially perceived to be somewhat unusual that some AR simulators don't include this provision. However, an AR process with measurement noise present is essentially an ARMA process, as can be conveniently seen for the scalar case by considering the equivalent correlation function that results from summing an AR process plus additive independent Gaussian white measurement noise, as demonstrated here:

$$\begin{aligned} \phi_{yy}(s) &= \phi_{y_{AR}y_{AR}}(s) + \phi_{vv}(s) \\ &= \frac{q}{D(-s)D(s)} + r = \frac{q + rD(-s)D(s)}{D(-s)D(s)}, \end{aligned} \tag{D.39}$$

where the above left hand fraction represents the correlation function of an AR process by having a constant numerator and the above right hand fraction represents the equivalent ARMA process that results by having a non-constant numerator. Use of pure AR techniques in situations involving underlying ARMA processes could be a fairly severe model mismatch [149]. The motivation for including this feature in the new simulator for this investigation is provided in Sections 4.1 and 4.3.

## D.4 Accommodating More than Just Diagonal Covariance Matrices

(U)Employing only diagonal covariance matrices in a simulator allows an easy check to be utilized to guarantee that such diagonal covariance matrices are positive definite (consisting merely of a verification that every entry on the principal diagonal is positive). However, such a simplistic approach is not general enough for many routine simulator applications.

(U)Because of geometric or other physically induced constraints (such as arise in alinement applications in navigation systems, or in possessing correlated random vector initial conditions-such as result from the method of Section D.2 for initializing the simulation in the steady-state condition, or in having either cross-correlated process noise or measurement noise or both in multichannel applications), the initial condition covariance, $P_o$, the process noise covariance intensity level, $Q_d$, of Eq. D.17, and the measurement noise covariance intensity level, R, can be nondiagonal and usually are nondiagonal. That this is the case can easily be seen for $Q_d$ by examining the structure of the defining equation of Eq. D.17, as pursued next. From Eq. D.17, please observe that when F is not diagonal, which is the prevelant situation, then $e^{FT}$ is not diagonal so even if the continuous-time $Q$ is diagonal, which sometimes occurs, the matrix product of $e^{-F\tau}GQG^Te^{-F^T\tau}$ that appears in the integrand of Eq. D.17 is *not* diagonal, so the discrete-time $Q_d$ is *not* diagonal in general.

(U)In this general case of encountering nondiagonal covariance matrices, it is still prudent to check that these covariance matrices do in fact possess the requisite positive definiteness property in order to proceed with confidence in the knowledge that fundamental structural requirements are in fact satisfied. After first checking for the presence of a degenerately simpler diagonal matrix for which the test may be streamlined in the manner already mentioned above, the "complex variable" form of the SVD subroutine from the International Mathematical Software Library (IMSL), Edition 10.0,(being "LSVCR") is used to decompose any nondiagonal covariance matrix under test (as in Eq. D.33) into

$$U\Lambda V^*$$

and the eigenvalue entries exposed on the diagonal matrix A are checked to confirm that these entries are exclusively positive.

the modern software development techniques of [227], then fully checked out and verified as discussed in Appendix F.

# Appendix E

# Machine Computation of the Matrix Exponential and Verification of its Software Implementation

## E.1 Preliminary Perspectives

(U)As discussed in Appendix D, we have replaced an earlier Monte-Carlo simulation routine with a new version that is upgraded in several important ways so that we know exactly what is being produced by the simulator and to what accuracy. This is extremely important in calibrating the spectral estimation algorithms of primary interest in this investigation. Within our modifications, we had a need to calculate the matrix exponential, which is analytically defined in terms of its corresponding Taylor series as:

$$\begin{aligned} e^{Ft} &= \sum_{k=0}^{\infty} \frac{F^k}{k!} t^k \\ &= I + \frac{F}{1!}t + \frac{F^2}{2!}t^2 + \frac{F^3}{3!}t^3 + \cdots \end{aligned} \tag{E.1}$$

(U)While several historical software implementations [188], [189], [198], [204] pursue evaluation of $e^{Ft}$ using the defining relationship of Eq. E.1, modern implementations use other techniques for this important and fundamental evaluation [190]- [193], [195]- [197], [198]- [203] such as via use of the following two techniques:

### E.1.1 A Chebyshev Approximation:

(U)Makes use of the matrix series analogy to the following scalar relationship:

$$\begin{aligned} e^{2x} &= I_0(2) + 2\sum_{m=1}^{n} I_m(2)T_m(x) \text{ for } |x| \leq 1 \\ &= 1 + \sum_{i=1}^{n} c_i x^i \end{aligned} \tag{E.2}$$

where

$$\begin{aligned} I_m(2) &= \text{modified Bessel function of the first kind} \\ &= \sum_{k=0}^{\infty} \frac{1}{k!(m+k)!} \end{aligned} \tag{E.3}$$

$$\begin{aligned} T_m(\mathrm{x}) &= \text{Chebyshev polylnomial} \\ &= \frac{m}{2}\sum_{s=0}^{2s<m} \frac{(-1)^s}{m-s} \binom{m-s}{s} (2x)^{m-2s} \end{aligned} \tag{E.4}$$

### E.1.2 Pade Approximation:

(U)Makes use of the matrix series analogy to the following scalar Pade approximation to $e^x$ as

$$e^x \approx \frac{N_n(x)}{D_n(x)} \tag{E.5}$$

where

$$N_n(x) = 1 + \sum_{i=1}^{n} \frac{n(n-1)\cdots(n-i+1)}{2n(2n-1)\cdots(2n-i+1)} \cdot \frac{x^i}{i!} \tag{E.6}$$

and

$$D_n(x) = N_n(-x) \tag{E.7}$$

The motivation for deviating from the obvious standard defining Eq. E.1 in computer evaluation or computation is the lure of greater accuracy that can be achieved either via the Chebyshev or Pade approach for an equivalent computational burden to that of using the more direct Eq. E.1.

(U)The computational algorithm depicted in Fig. E.1 (which is based on the defining Eq. E.1) was reported in [199, p. 75], as inherited from the procedure originally used in [188], and serves as the basis of the computational technique used at many universities and aerospace companies. However, Systems Control Technology (previously Systems Control, Inc.) endorses the Pade approach of [192], [193] as being the preferred approach for calculating $e^{Ft}$ since it has greater accuracy in general for the same computer burden [196, p. 7-21]. The Taylor series approach is exact at the point of expansion (as, say, about zero) for up to the number of

derivatives (or terms) retained but drops off in accuracy the further away (i.e., larger) A is from the original point of expansion (being zero for this discussion). However, the error in Pade approximation as the ratio of two polynomials (where, for matrices, the denominator polynomial corresponds to a matrix inversion), has an error that oscillates between being positive and negative all along the baseline from the point of expansion to the point of evaluation, with a net error at the time step A that is considerably less than that measured in using a Taylor series expansion approach.

(U) A so-called "convergence analysis" (for the Method of Fig. E.1) appears in [198] that is based on claimed properties of an "alleged" norm:

$$\|F\| = \min\{\max_i \sum_{j=1}^{n} |f_{ij}| \ , \ \max_j \sum_{i=1}^{n} |f_{ij}|\} \qquad \text{(E.8)}$$

However, the revelations of Kerr [194] demonstrate that the "alleged" norm of Eq. E.8 is in fact bogus and that the "alleged" properties being exploited in the convergence analysis are subsequently compromised but can be patched up using the suggestions of [194], as provided. An independent substantiation or endorsement of the observations of [194] on this topic of the "norm" in vogue being ***bogus*** appeared in [254, p. 798]. Just for perspective and historical appreciation, it is mentioned that the misinterpretation of the intuitively appealing expression of **Eq.** E.8 as incorrectly being a norm was asserted in [188], [198] and propagated by several others [189], [203] including seasoned numerical analysts (e.g., [205], [206]) in this evaluation area.

(U) Correct calculation of the transition matrix, $e^{Ft}$, for time-invariant linear systems is of fundamental importance in the computational solution of linear differential equations, in Kalman filtering applications, in optimal control and guidance applications, in related signal processing applications, and in those nonlinear applications where the solution approach is to first linearize over short duration time intervals over which the system may be reasonably approximated as having constant parameters. Obviously computational considerations are "bread and butter" issues for companies and practioners engaged in such evaluations. Having been personally following the development and evolution of computer algorithms for evaluating $e^{Ft}$ for the last twenty years, I feel compelled to archive the following neat test problems (and their derivation) as discussed in the next section for the possible benefit of others seeking such a definitive cross-check for software implementation and verification just as we had originally been faced with. We used the test problems of the next section, to quickly verify the accuracy of the two different algorithmic versions of $e^{Ft}$ calculation that have been implemented in the new simulator. One version

is entitled MEXP, which is based on the Cheyshev approximation approach [190], and was obtained from David Kleinman(University of Connecticut) as a *DLK.LIB* software subroutine [197], while the other version is entitled *PADE8* and is based on the Pade approximation approach of Ward [192], [193] and the version that we have utilized in the new simulator was implemented by Ward himself.

(U)At Lincoln Lab, certain enhancing pre- and post-processing modifications have been made for both algorithms to make the form of input entry and output reading be easier, more user friendly, and less human error prone, by appending a matrix format structure (originally adopted by TASC in the 1970's) that makes reading large matrices more convenient from a human engineering viewpoint. An example of this format for a $46 \times 46$ matrix is depicted in Fig. E.2. Row numbers are indicated at the left followed by a single right parenthesis. The row entries are 10 per line, with the excess folded around underneath. The alternative to using this convenient format when dealing with matrices of dimension greater than 10 (as I have personally increduously witnessed) is for people to wall paper office walls with the matrices they are working with! Such wall papering is highly inconvenient for stacked-case runs that alter some parameter values and elements within those matrices for a sensitivity analysis of results over a range of likely parametric values.

## E.2 Slick Test Cases and Their Derivation

(U)Certain matrices known as "idempotent" matrices have the unusual property that

$$A \cdot A = A \tag{E.9}$$

While I'm not aware of any prior really fruitful use made of idempotent matrices, the present application of software verification, as now described, is a neat application of idempotent matrices as used to construct test matrices for verifying the transition matrix algorithic implementations that we are using for computer computation of $e^{Ft}$. The utility of these test matrices is that the resulting analytically derived expressions for $e^{Ft}$ is conveniently in closed-form for $F = A$. Hence the performance of a general $e^{Ft}$ subroutine implementation can ultimately be gauged by how close it comes to achieving the known ideal exact solution.

(U)Another benefit of dealing with idempotent test matrices, $A$, is that the Kalman "rank tests" for "controllability" and "observability" also degenerate into much more tractable expressions such as, for example, in having to check only the

considerably smaller matrix

$$\left[A \vdots AG\right] \tag{E.10}$$

to see if it is of rank n rather than having to check the generally much larger but in this case equivalent Controllability Grammian matrix:

$$\left[A \vdots AG \vdots A^2G \vdots \cdots \vdots A^{n-1}G\right] \tag{E.11}$$

to see if it is of rank n to confirm that the linear system under investigation is in fact controllable; thus use of the former expression results in considerable simplification. A similar simplification in testing for "observability" can be exploited in applying Kalman's rank test to Observability Grammians.

(U)Returning to the definition of Eq. E.1, with **A** in Eq. E.9 substituted for F in Eq. E.1 and time-step **A** used for scalar time, t, in Eq. E.l, yeilds

$$\begin{aligned} e^{A\Delta} &= \textstyle\sum_{k=0}^{\infty} \frac{A^k}{k!}\Delta^k \\ &= I + \tfrac{A}{1!}\Delta + \tfrac{A^2}{2!}\Delta^2 + \tfrac{A^3}{3!}\Delta^3 + \cdots \\ &= I + A(\tfrac{\Delta}{1!} + \tfrac{\Delta^2}{2!} + \tfrac{\Delta^3}{3!} + \cdots) \\ &= I + A(1 + \tfrac{\Delta}{1!} + \tfrac{\Delta^2}{2!} + \tfrac{\Delta^3}{3!} + \cdots - 1) \\ &= I + A(e^{\Delta} - 1) \end{aligned} \tag{E.12}$$

where the expression within the first set of parentheses resulted by repeated application of the property of Eq. E.9, where the quantities +1 and -1 were added within the second set of parentheses without altering the sum, and the series within the second set of parentheses is recognized to be $\mathbf{e^A - 1}$. The final expression in the last line of Eq. E.12 checks since for $\mathbf{A} = 0$, the correct result of 1 is obtained. Thus, the closed-form expression for the transition matrix of idempotent matrices is as depicted in the last line of Eq. E.12.

(U)To obtain non-vacuous idempotent matrices is the next issue. Obviously, the zero matrix and the identity matrix satisfy Eq. E.9, however, these are not useful for our purposes of testing software routines. Two useful examples will be given below but first motivation is offered for how they were obtained (i.e., they definitely were not just plucked from the air as a lucky guess). Consider the problem of seeking to solve the following algebraic equation for $x(n \times 1)$, given $y(m$ x 1) and C(m x n):

$$\underline{y} = C\,\underline{x} \tag{E.13}$$

Independent of rank conditions on C and dimensions of $\underline{y}$ and $\underline{x}$, it is reasonably well-known (see [106, Appendix A, Section A.1] and [207, p. 417]) that a solution to Eq. E.13 is of the form

$$\underline{x} = C^{\dagger}\underline{y} + (I_n - C^{\dagger}C)\underline{w} \tag{E.14}$$

for arbitrary $\underline{w}$ and that the term within parenthesis in Eq. E.14 is idempotent (where $C^{\dagger}$ in Eq. E.14 is the Moore-Penrose pseudoinverse). In forming two counterexamples in [108], [106], the following two matrices and their respective pseudoinverses were obtained (as derived in [106]):

$$C_1 = \begin{bmatrix} 1 & 2 \\ 2 & 4 \end{bmatrix} \quad ; \quad C_1^{\dagger} = \frac{1}{25}\begin{bmatrix} 1 & 2 \\ 2 & 4 \end{bmatrix} \tag{E.15}$$

and

$$C_2 = \begin{bmatrix} 1 & 2 & 1 \\ 1 & 1 & 0 \\ 1 & 1 & 0 \end{bmatrix} \quad ; \quad C_2^{\dagger} = \begin{bmatrix} -\frac{1}{3} & \frac{1}{2} & \frac{1}{2} \\ \frac{1}{3} & 0 & 0 \\ \frac{2}{3} & -\frac{1}{2} & -\frac{1}{2} \end{bmatrix} \tag{E.16}$$

Therefore via Eq. E.14, the following two matrices are idempotent

$$\begin{aligned} A_1 &= (I - C_1^{\dagger}C_1) \\ &= \begin{bmatrix} 1 & 0 \\ 0 & 1 \end{bmatrix} - \tfrac{1}{25}\begin{bmatrix} 1 & 2 \\ 2 & 4 \end{bmatrix}\begin{bmatrix} 1 & 2 \\ 2 & 4 \end{bmatrix} \\ &= \begin{bmatrix} 1 & 0 \\ 0 & 1 \end{bmatrix} - \tfrac{1}{25}\begin{bmatrix} 5 & 10 \\ 10 & 20 \end{bmatrix} \\ &= \begin{bmatrix} \frac{4}{5} & -\frac{2}{5} \\ -\frac{2}{5} & \frac{1}{5} \end{bmatrix} \end{aligned} \tag{E.17}$$

and

$$\begin{aligned} A_2 &= (I - C_2^{\dagger}C_2) \\ &= \begin{bmatrix} 1 & 0 & 0 \\ 0 & 1 & 0 \\ 0 & 0 & 1 \end{bmatrix} - \begin{bmatrix} -\frac{1}{3} & \frac{1}{2} & \frac{1}{2} \\ \frac{1}{3} & 0 & 0 \\ \frac{2}{3} & -\frac{1}{2} & -\frac{1}{2} \end{bmatrix}\begin{bmatrix} 1 & 2 & 1 \\ 1 & 1 & 0 \\ 1 & 1 & 0 \end{bmatrix} \\ &= \begin{bmatrix} 1 & 0 & 0 \\ 0 & 1 & 0 \\ 0 & 0 & 1 \end{bmatrix} - \begin{bmatrix} \frac{2}{3} & \frac{1}{3} & -\frac{1}{3} \\ \frac{1}{3} & \frac{2}{3} & \frac{1}{3} \\ -\frac{1}{3} & \frac{1}{3} & \frac{2}{3} \end{bmatrix} = \begin{bmatrix} \frac{1}{3} & -\frac{1}{3} & \frac{1}{3} \\ -\frac{1}{3} & \frac{1}{3} & -\frac{1}{3} \\ \frac{1}{3} & -\frac{1}{3} & \frac{1}{3} \end{bmatrix} \end{aligned} \tag{E.18}$$

both of which check as being idempotent by satisfying Eq. E.9 as an identity. In considering the step-size to use in the evaluation of Eq. E.12, convenience in using just a scalar multiplying factor of one half times the matrix in Eq. E.12 would dictate using

$$\mathbf{A} = 0.405 \tag{E.19}$$

since from Burlington's mathematical tables [210]

$$(e^{\Delta} - 1) = (e^{0.405} - 1) = (1.50 - 1) = 0.50 \tag{E.20}$$

Therefore, the two evaluations corresponding to invoking Eq. E.12 are

$$\begin{aligned} e^{A_1 \Delta} &= I + \tfrac{1}{2} A_1 = \begin{bmatrix} 1 & 0 \\ 0 & 1 \end{bmatrix} + \tfrac{1}{2} \begin{bmatrix} \frac{4}{5} & -\frac{2}{5} \\ -\frac{2}{5} & \frac{1}{5} \end{bmatrix} \\ &= \begin{bmatrix} 1.40 & -0.20 \\ -0.20 & 1.10 \end{bmatrix} \end{aligned} \tag{E.21}$$

and

$$e^{A_2 \Delta} = I + \frac{1}{2} A_2 = \begin{bmatrix} 1.16\overline{6} & -0.16\overline{6} & 0.16\overline{6} \\ -0.16\overline{6} & 1.16\overline{6} & -0.16\overline{6} \\ 0.16\overline{6} & -0.16\overline{6} & 1.16\overline{6} \end{bmatrix}. \tag{E.22}$$

The results of Eq. E.21 and E.22 are the now known closed-form solutions to $e^{AA}$ evaluation of the matrices of Eqs. E.17 and E.18, respectively, with $\mathbf{A} = 0.405$. These two solutions [1] along with several other test cases from [203] were used to successfully verify the correct performance of both *PADE8* and ***MEXP*** (after a few locally-induced minor transition rehosting bugs were found and removed). This is the first time that I have seen test problems for validating correct software performance of $e^{Ft}$ calculation routines constructed in such a novel way. Hopefully, this technique will be useful to others as well, which is why I have bothered to document it. A further benefit in having the closed-form expression of Eq. E.12 for

[1] Copious examples of idempotent matrices and/or important associated structural observations are offered in [209, pp. 106-107, p. 121, and especially on p. 340]. It is observed in [207, p. 66, Example 7.2] that the eigenvalues of a "projector matrix" such as that of Eqs. E.17 and E.18 (being constructed as on the right hand side of Eq. E.14) as symmetric idempotent matrices are always all either zero or one (and so always correspond to an ***unstable*** system). In [211, p. 277, Exercise 5] some observations are made on representing certain special matrices as the sum of two "nilpotent" and "idempotent" components as further introduced in a matrix exponential calculation; however, Nering's result is different and is not as clean and useful for computational verification/validation as the result offered for the first time here as Eq. E.12. Evidently statisticians routinely encounter idempotent matrices.

the matrix exponential of an idempotent matrix A is offered below. Consider the expression of Eq. D.17 that must be calculated in software in order to obtain the "discrete-time equivalent of continuous-time white Gaussian process noise". Using the result of **Eq.** E.12 for idempotent matrices within the more general expression of Eq. D.17 allows this expression for the required discrete-time process noise covariance Eq. D.17 to be evaluated analytically in closed-form as:

$$
\begin{aligned}
Q_d &= \left[I + A(e^{\Delta} - 1)\right] \int_0^{\Delta} \left[I + A(e^{-\tau} - 1)\right] GQG^T \left[I + A^T(e^{-\tau} - 1)\right] d\tau \left[I + A^T(e^{\Delta} - 1)\right] \\
&= \left[I + A(e^{\Delta} - 1)\right] \\
&\quad \int_0^{\Delta} \left[GQG^T + (AGQG^T + GQG^TA^T)(e^{-\tau} - 1) + AGQG^TA^T(e^{-2\tau} - 2e^{-\tau} + 1)\right] d\tau \\
&\quad \left[I + A^T(e^{\Delta} - 1)\right] \\
&= \left[I + A(e^{\Delta} - 1)\right] \\
&\quad \left[\mathrm{GQG^T}\Delta + (\mathrm{AGQG^T} + \mathrm{GQG^TA^T})(1 - \mathrm{e}^{-\Delta} - \Delta) + \mathrm{AGQG^TA^T}(-\frac{3}{2} - \frac{1}{2}\mathrm{e}^{-2\Delta} + 2\mathrm{e}^{\Delta} + \Delta)\right] \\
&\quad \left[I + A^T(e^{\Delta} - 1)\right]
\end{aligned}
\tag{E.23}
$$

This is a new result that is also useful as a confirming check for software implementations (as used in preparing Test Case 1 of Appendix G and Table F.1).

(U)Other less complete approaches exist to constructing test problems with nice numbers based on relationships between similarity transformation (via Eigenvalue/Eigenvector calculation [208]) to Jordan Cannonical form as

$$
E^{-1}FE = J = \begin{bmatrix} \lambda_1 & 0 & 0 \\ 0 & \lambda_2 & 0 \\ 0 & 0 & \lambda_3 \end{bmatrix} \tag{E.24}
$$

(where in the above E is the matrix of eigenvectors of $F$ and $\lambda_1$, $\lambda_2$, $\lambda_3$, are distinct eigenvalues of $F$) utilizes the standard reverse relationship

$$
e^{F\Delta} = E \begin{bmatrix} e^{\lambda_1\Delta} & 0 & 0 \\ 0 & e^{\lambda_2\Delta} & 0 \\ 0 & 0 & e^{\lambda_3\Delta} \end{bmatrix} E^{-1} \tag{E.25}
$$

(but the appropriate expressions are even more complicated than those of Eqs. E.24 and E.25 if the eigenvalues of $F$ are ***not*** unique or do not break separately). A procedure is provided in [208], where Eigenvalue/Eigenvector calculations (as needed

for the transformations of Eqs. E.24 and E.25) can be done entirely in terms of "nice numbers", as is desirable for conveniently tractable test problem formulations. This alternative approach of [208] still needs further work or augmenting use of an exploratory computer program in order to take it to fruition, while the approach offered in this Appendix of using idempotent matrices is complete as it already stands.

(U)We further validated the above mentioned two $e^{FA}$ computational algorithms, PADE8 and MEXP, on the 9 x 9 example depicted in Fig. **E.3** (with $\mathbf{A} = 1.5$) just to be conservatively certain that the accuracy in the results of these new algorithms is not severely degraded with increasing problem dimensions.

(U)Through the cooperation of AFGL, Lincoln procured a free copy of Paul Fougere's nonlinear MEM and line-split supression software although it was not in the original task. This software had been hosted on AFGL's CDC **7600** machine and we had to convert it to our target IBM **3081** machine. The original purpose for obtaining the AFGL software was merely to speed up validation of our recently modularized software implementations of the LWR and Nuttall algorithms by comparisons in benchmark tests to the outputs (for the same "real variable" test problems) of a respected existing program with a certified established track record such as is possessed by this ten year old AFGL software. During the conversion process to Lincoln's IBM **3081** as host, we became aware of the fact that many more changes were needed than we originally expected, thus interfering with or invalidating use of AFGL's rehosted software as a test gauge. These changes related to:

1. use of random number generator (with output that is computer wordlength dependent),
2. conversion to IBM double precision to approximately match the CDC's **60** bit word in single precision,
3. replacement of older CALCOMP Plotter usage, and
4. replacement of dummy temporary scratch pad storage with disk scatch pads,

and all this without recourse to valid CDC intermediate outputs that could perhaps have served as a reasonable basis for "apples-to-apples" comparisons at various critical points during the transition. Two additional aspects that contributed to a diminishing in our enthusiasm to use Paul Fougere's Line-Split Suppression program [96] as a cross-check in the BRVAD application are the following:

1. We had originally seen what we thought at the time was evidence of line-splitting in the Tradex wake spectra; however, when Paul Fougere saw some of our unidentified data (in our May **1987** draft paper for possible open literature publication) corresponding to the figures depicted within Section **3.3** of Chapter **3** (but devoid of intelligible coordinate scales), he suspected that they were evidence instead of cross-channel feed-through which looks similar to line-split to an extent. The clincher was that line-split is much more of a worrisome phenomena in tones or sinusoidally random data (e.g., of say diurnal earth-rotation periods, yearly earth-revolution related periods, **11** year

**rates, and lengths of data, ..., as now provided in this report to complete the puzzle and salvage many previously evaluated results without having to duplicate them.**

sunspot activity, and 88 year sunspot cycles such as AFGL is concerned with [98] or rotating machinery and generators in ASW applications such as NUSC is concerned with) rather than in our non-sinusoidal data.

2. Paul Fougere's programs were only for "real variable" data and so were not sufficiently general enough to accommodate the "complex" case that we need to handle Tradex data, with its coherrent phase processing requirements.

In lieu of not being able to use a rehosted AFGL program to do cross-comparisons to it as an established reference using just "real" data in order to verify on a *relative* basis the new Lincoln implementation of the LWR and Nuttall algorithms, we instead used more test cases and relied instead on a simulator for fuller test coverage to exercise and verify these newer programs on an *absolute* basis.

(U)Using a background in modern control and Kalman filtering and filter related concerns (such as failure detection, event detection, and maneuver detection) but not in spectral estimation per se, there was still considerable direct carry-over of prior experience to the problem of spectral estimation [2]. However, debug within the exclusive regime of the spectral estimator proper (instead of in the simulator portion, which was already familar) was difficult and challenging dispite the existence of a recent paper [184] on this aspect [3]. (The technique that was eventually homed-in on of using the consistency of eigenvalues of "what was simulated" to "what was estimated" as a measure of goodness in validating the correctness of «simulator/power spectrum estimator" will be discussed further below.) Debugging is where prior experience really pays off. There are some obvious similarities between debugging of Kalman filter algorithms and debugging spectral estimation algorithms since both deal with random processes and accompanying second order statistics. One particular difficulty in the BRVAD application that most Kalman filter practicioners don't normally encounter and so are usually inexperienced with

[2] Particularly relating to the carryover and dovetailing of topics of "positive definiteness testing" [105], [178] and "reduced-order modeling" [106], [108] as well as several other numerical algorithms that these apparently diverse topics have in common.

[3] To illustrate what a "can-of-worms" this can be, the newer fast resolution spectral estimation algorithms (such as Cadzow's algorithm which has had spectacularly good performance on exceptionally short lengths of data) can even yield counter-intuitive indications of negative power spectral densities as an output (as documented in [215, p. 900]) even from correctly coded versions. While another standard check case would be to see if the area under the PSD curve was in fact the variance of the process (as possibly scaled by $2\pi$, depending on the convention of FFT's being used); however, one of the Burg algorithm-based multichannel generalizations doesn't even theoretically satisfy this usual sanity check [184] so we can't use this usually desirable feature as a numerical check on the correctness of the software implementation.

these test cases will be examined in the next section during the discussion of the results of each test.

## F.2 Results of Structured Testing for Validating All Software Used

(U)The first test was performed on the two transition matrix calculation modules that we obtained as discussed in Appendix E. The correct answers were obtained as expected for both alternative implementations based on use of Pade approximations instead of use of the Taylor series for calculating the matrix exponential.

### F.2.1 Verifying the Simulator Proper

(U)The overall structure of the new simulator is simply depicted in Fig. F.1. Using the parameters of Test Case 1, as depicted in Table F.l (briefly discussed in Section G.l, and derived in Appendix E), the intermediate outputs provided by the software implementation were verified to be correct. The specific features of the software implementation that were confirmed using Test Case 1 are detailed in the second column from the left in Table G.1. These activities for Test Case 1 are summarized in Fig. F.2. Actual sample functions obtained for the underlying known unstable system that was convenient to use to check detailed intermediate internal software calculations are depicted in Fig. F.2.

(U)Using the parameters of Test Case.2, as depicted in Table F.l (discussed in detail and derived in Section G.2), the intermediate outputs provided by the software implementation were verified to be correct. The specific features of the software implementation that were confirmed using Test Case 2 are detailed in the third column from the left in Table G.1. These activities for Test Case 2 are summarized in Fig. F.3. Actual sample functions obtained for the underlying known benign stable system that was also convenient to use to check detailed intermediate internal software calculations are depicted in Fig. F.3.

(U)Using the parameters of Test Case 3, as depicted in Table F.l (discussed in detail and derived in Section G.3), the intermediate outputs provided by the software implementation were verified to be correct. The specific features of the software implementation that were confirmed using Test Case 3 are detailed in the fourth column from the left in Table G.1. These activities for Test Case 3 are summarized in Fig. F.4. Actual extremely regular essentially *deterministic* sample

functions obtained for the underlying known unstable system that was convenient to use here to check that the output is exactly correct at a high level are depicted in Fig. F.4. Besides confirming the outputs of the simulator with an easily recognizable expected answer (as contrasted to Test Cases 1, 2, and 4 which only provide random noise corrupted sample functions that can only be confirmed at the aggregate level from statistical properties), this Test Case 3 also allowed the programmer to calibrate (and correct his plot routines, his scales from linear to dB, and to confirm or more accurately *straighten out* use of the WMH convention [249] for the intermediate input/output disk files used between each separate program module.

(U)Using the parameters of Test Case 4, as depicted in Table F.1 (briefly discussed in Section G.4, and derived in Section 3.1), the intermediate outputs provided by the software implementation were verified to be correct. The specific features of the software implementation that were confirmed using Test Case 4 are detailed in the fifth column from the left in Table G.1. These activities for Test Case 4 are summarized in Fig. F.2. Actual sample functions obtained for the underlying known unstable system that was convenient to use to check detailed intermediate internal software calculations are also depicted in the previously mentioned Fig. F.3.

### F.2.2 Verifying the Performance of the Simulator and AR Coefficient Estimator Software Together

(U)An obvious test that comes to mind of seeking to validate proper performance of a new spectral estimation software implementation using complex sinusoids (generated from a simply simulated known signal of the form $e^{\sim ?}$) to see if the spectral estimator under scrutiny can identify the correct amplitude and frequency was not pursued here for the following less obvious but nevertheless valid reasons. First, sinusoids or simple tones are best estimated by a software implementation of algorithms that differ drastically in structure from the ones used here (as described in Chapter 2) such as by using the modified Prony methods [84, pp. 367-371], by using the Pisarenko harmonic decomposition method [84, pp. 371-374], or by using one of the other eigenvector decomposition methods (e.g., [242], [243]); however, the Tradex RV wake modeling application exhibits *no* such sinusoidal structure but does exhibit the Markov signal structure that matches our simulator structure and structure of our particular spectral estimation techniques utilized. Hence, we select both the tool and the software validation procedure that best matches the application at hand-that of RV wake modeling. Second, it is fairly well known that even

## VALIDATION OF SIMULATOR (Cont'd)

- DEGENERATE TEST CASE (with all noises present but cranked down to be miniscule) OF LINEAR RAMP OF KNOWN SLOPE AND INTERCEPT YIELDED CONFIRMING OUTPUT

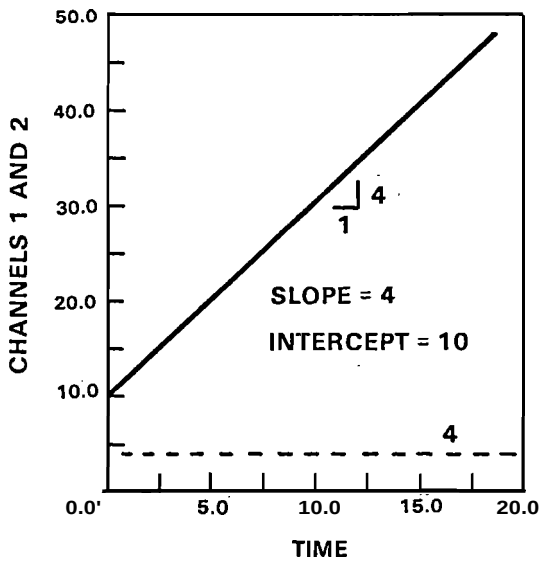


(U) Figure **F.4:** Handling Test Case **3**

Correctly implemented "maximum entropy"-based spectral estimation software is frequently plagued with line-splitting, where proper estimation of the underlying tone is instead split into two lines, neither of which occurs at the proper frequency, but which do occur in general proximity of the true tone, sometimes bracketing it; and, additionally, the associated amplitudes similarly differ from what was actually present or simulated.

(U)A siminal investigation of the problem of line-splitting occurring when "maximum entropy"-based spectral estimation techniques are used is reported by Fougere (1977) [96] and is revisited by Fougere (1985) in a follow-up study in [233]. One of the interesting counterintuitive aspects of line-splitting that Fougere uncovered is that line-splitting is frequently aggrevated with decreasing magnitude of additive measurement noise rather than with an increasing level of such noise and that the phase of the underlying sinusoid also plays a role [233] in the tendency for line splitting to occur.

(U)The validation that was actually used to confirm the performance of the AR Coefficient Estimation software utilized Test Case 4 of known solution as exhibited in Section **3.1.** The steps that were followed are as depicted in Fig. F.5. The confirmation Technique for the eigenvalues of the Coefficient Matrix is identical to what was used in Section 3.2. Thus, this was a confirming check on both the simulator and the AR Coefficient Estimator working in concert. We had no reservations in using this software on Tradex data to evaluate AR coefficients as reported in Section 6.2.

### F.2.3 Status in Verfying the Concatenated Performance of Simulator, AR Coefficient Estimator, and Spectral Estimator

(U)While the simulator and AR Coefficient Estimator were both validated as performing correctly, the results from all the software modules together as depicted in Fig. F.6 were initially somewhat puzzling and unsettling. There are two components of an explanation that satisfactorily accounts for the apparent discrepancy exhibited here of the two power spectral density plots of Fig. F.6 not being identical. One aspect relates to the IMSL FFT routine used, the other is the way the asserted true situation depicted in Fig. 3.2 was originally obtained over a year ago in [225] by merely turning down the noise and making the Test Case 4 to be essentially deterministic and ostensibly obtaining exactly the same structural form and

**VALIDATION OF COMBINED SIMULATOR AND AR COEFFICIENT ESTIMATOR**

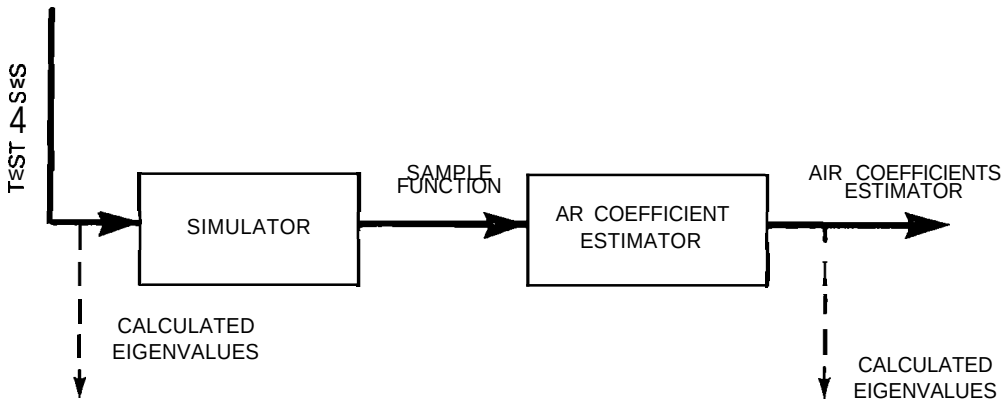


- TEST CASE PARAMETERS OF "COMPLEX" EXAMPLE (of known statistical response) WERE SUPPLIED TO SIMULATOR
- AR COEFFICIENT WAS ESTIMATED WITH HIGH ACCURACY (from long data length)
- EIGENVALUES WERE CALCULATED FOR EACH PATH AND FOUND TO BE IDENTICAL (as a confirming consistency check) INDICATIVE OF PROPER SPECTRAL SIGNATURE CONFORMANCE

(U) Figure F.5: Validating AR Coefficient Estimator by Confirming That the Estimated Coefficient Matrices Have Eigenvalues Identical to What was Simulated

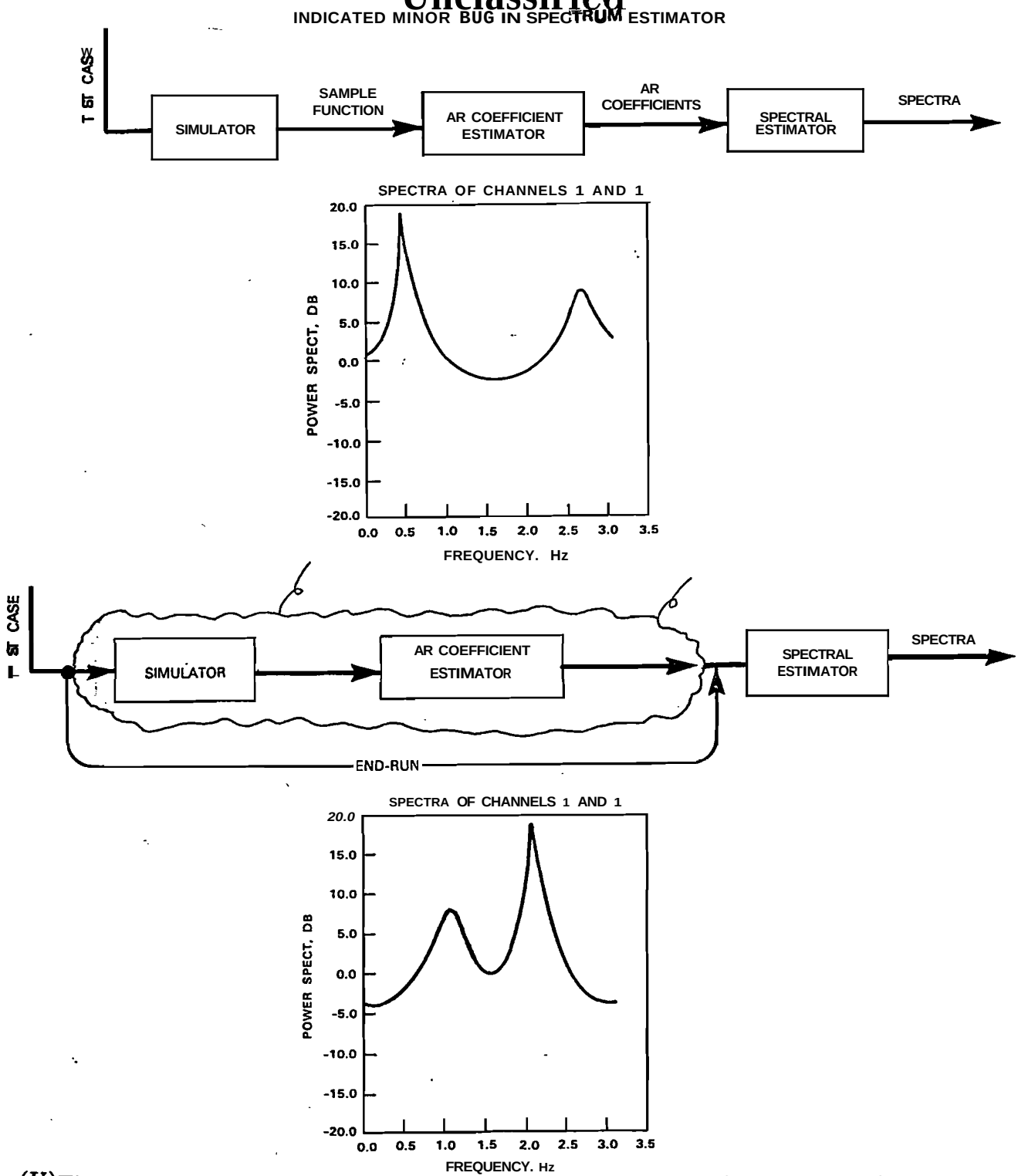


(U) Figure F.6: Steps Toward Validating Spectral Estimation Software by Confirming That the Estimated Coefficient Matrix and the Original Coefficient Matrix (of the Simulator) Yield Identical Power Spectral Density Plots

parameter values for the estimated AR coefficient Matrix as possessed by the original matrix of Eq. **3.1** that was simulated. More detail on these aspects is provided below.

(U)Originally, a point of some consternation was how the ideal curves of Figs. 3.3 and 3.4 were obtained in [225]. This question has now been answered. Through an interview it was found that, during the prior investigation, the noise was essentially initially zeroed out in the simulation, and the earlier version of the multichannel spectral estimation technique that had been implemented in software was allowed to estimate these unknown parameters. Remarkably, the estimated AR matrix was comparable to the orginal matrix in that all the parameters were very close to the matrix that was entered for simulation. Theory specifies that the estimated AR matrix should agree with what was started with in the simulator to within a "similarity" transformation; but of the infinite number of representation possibilities, the AR estimation scheme evidently selected exactly the same coordinate basis as was used in the simulator to represent the AR coefficient matrix. Thus, when both the corresponding simulated and estimated power spectra were plotted using a common software implementation of Eq. 2.6 for the case of $A_0 \equiv \mathbf{I}$, and an almost common $A_1$, the results appear identical since a common IMSL FFT routine entitled "FFTCC" (ostensible applicable to any length "complex" data sequence) [4] was used throughout the software that was inherited and used although apparently less trustworthy than the more common IMSL FFT routine, "FFT2C", that is usually used in the role of FFT-ing "complex" data structures (of a length that is constrained to be a power of two), as are encountered here, and the proper performance of FFT2C is more generally familar to Lincoln Laboratory personnel (as ascertained from an informal poll of several users). The recently released Edition 10.0 of IMSL software offers only "FFTCF" as a subroutine to compute FFTs of 1-D "complex" data thus removing the ambiguity of Edition 9.0 IMSL surrounding which complex FFT subroutine can be safely used, but Edition 10.0 IMSL FFTs became avalible too late to help us in this investigation.

(U)One final aspect remains to be dicussed regarding software before the status report on our RV wake modeling software is completed. The initial version of the plotter "PLADY2" documented in [249] was set up to plot out only a sin-

[4] An initial fear in this area was that power spectra were being generated by a routine that was originally developed to compute the spectra of purely "real" processes and where it was normally enough to evaluate the FFT in the expression merely for $w$ between zero and $\pi$ since the remainder for $\pi$ to $2\pi$ radians would be identical for real processes by symmetry, but not so for the "complex" processes of this application. However, a careful line-by-line check revealed no such discrepancy here since the **1024** point FFTs are evaluated over the full $2\pi$ radians around the unit circle.

gle output binary file (created using the so-designated WMH format described in [249]). Correspondingly, the initial version of the spectral estimation routine "ARTOSP" documented in [249] was set up to only output one file (in WMH format), either an autospectrum or a cross-spectrum, but only one, even though all were calculated simultaneously within the software in the computation of **Eq.** 2.6, with $z = \exp j2\pi f\Delta t$ via a 1024 point FFT. This was not much of a problem when we were just investigating computations associated with the 2 channel analytic closed-form test problem of known solution in Sections 3.1 and 3.2, since it was just a slight waste to recalculate something (that had actually already been calculated previously) in order to plot the two 1-1 and 2-2 autospectra and the 1-2 cross-spectrum. Being constrained to use the programs in this way forced the same intermediate calculation of the Power Spectral Matrix to be performed each time a single scalar matrix component entry was to be plotted out. However, this was deemed to be an ***unacceptable waste*** when the six state model of Section 6.2 was being tackled. The number of distinct entries of the 6 x 6 power spectral matrix to be plotted out is $\frac{n(n+1)}{2}=21$, so to avoid the waste of 20 unnecessary recalculations of a common intermediate quantity that was now expensive to calculate in the 6 x 6 case that had been relatively inexpensive to recalculate in the 2 x 2 case, a modification of the software of [249] was undertaken under fairly tight time constraints of less than a week. Additionally, all the modules discussed in [249] had a built in maximum upper limit of 5 for the matrices and vectors to be handled while the application of Section 6.2 was for 6. Therefore, this maximum allowable size had to be opened up to accommodate these larger vectors and matrices. The openning-up was initiated and completed sucessfully to yield the 6 x 6 results depicted in Section 6.2 and the last-minute modification of "ARTOSP" and "PLADY2" were initiated but have yet to be demonstrated to perform properly. We were debugging this aspect when the clock stopped. The $6 \times 6$ test cases of Sections G.5 and G.6 had been developed to aid in this checkout and bebug effort.

# Appendix G

# Derivation of Test Case Examples

(U)Because the programmer was unfamiliar with spectral estimation applications and for that matter with software implementation of general matrix operations, it was necessary to develop closed-form examples to be used as confirming test cases at every critical step. In order to know what the correct answers should be (as used in Appendix F for confirming checks on the output of the computer programs), certain analytic closed-form results and some intermediate and final answers werk derived to be test cases. These originally derived Test Cases 1 to 4 are documented and explained here and all the specific parameter values used for each of these primary test cases are summarized in Table F.l in Section F.2 of Appendix F. The second phase augmenting test cases used just prior to the computer runs of Chapter 6 in order to upgrade the software to handle the six channel case are also addressed here as Test Cases 5 and 6. All these test cases may be useful to others in validating similar software implementations.

## G.1 Test Case 1

(U)A complete description of this continuous-time state variable system is depicted in the second column of Table F.1 in Section F.2 of Appendix F. As motivated in Appendix E, Section E.2, the continuous-time system matrix, $F_1$, of Eq. E.18, the time-step $\mathbf{A} = 0.405$ (chosen for convenience, as explained in Section E.2, **Eq.** E.20), and the corresponding continuous-time transition matrix (from Eq. E.22) are as indicated in the second column of Table F.1. The 2 x 3 obsevation matrix, $H_1$, indicated in Table F.1 was chosen so that the system is properly observable (cf., Eqs. E.10 and E.11), and the process and measurement noise covariance intensity

levels are chosen to be unity identity matrices for convenience in their simplicity. The initial condition is taken to be zero-mean but the associated initial covariance is taken to be nondiagonal as a known positive definite matrix [1] that can be used to excercise the new software that is designed to handle nondiagonal covariances as well as the less challenging standard diagonal ones.

## G.2 Test Case 2

(U)A complete description of this continuous-time state variable system is depicted in the third column of Table F.1 in Section F.2 of Appendix F. The eigenvalues of this system can be obtained from

$$\det(\lambda\, I - F_2) = \det \begin{bmatrix} \lambda + 5 & 1 \\ -6 & \lambda \end{bmatrix} = \lambda^2 + 5\lambda + 6 = (\lambda + 3)(\lambda + 2) \qquad \text{(G.1)}$$

and therefore are $\lambda = -2,\ -3$ corresponding to a *stable* system. In the frequency domain, the corresponding resolvent matrix is

$$\begin{aligned} (s\, I - F_2)^{-1} &= \frac{1}{(s+3)(s+2)} \begin{bmatrix} s & -1 \\ 6 & s+5 \end{bmatrix} \\ &= \begin{bmatrix} \frac{3}{(s+3)} - \frac{2}{(s+2)} & \frac{1}{(s+3)} - \frac{1}{(s+2)} \\ \frac{-6}{(s+3)} + \frac{6}{(s+2)} & \frac{-2}{(s+3)} + \frac{3}{(s+2)} \end{bmatrix} \end{aligned} \qquad \text{(G.2)}$$

that corresponds in the continuous-time domain (by inverse Laplace transforming elementwise each partial fraction exposed in Eq. G.2) to the following transition function matrix:

$$e^{F_2\, t} = \begin{bmatrix} (3e^{-3t} - 2e^{-2t}) & (e^{-3t} - e^{-2t}) \\ (-6e^{-3t} + 6e^{-2t}) & (-2e^{-3t} + 3e^{-2t}) \end{bmatrix}. \qquad \text{(G.3)}$$

[1] On one occasion, the programmer included an incorrect negative sign on one of the principal diagonal terms of the initial covariance which served to demonstrate that the new SVD-based positive definiteness test (from [105, p. 504]) that was implemented in the new simulator also correctly complains when a nondiagonal covariance matrix departs from being properly positive definite.

For the time step-size of $\mathbf{A} = 0.5$, Eq. G.3 becomes the corresponding exact discrete-time transition matrix as

$$e^{F_2 \Delta} = \begin{bmatrix} (3e^{-\frac{3}{2}} - 2e^{-1}) & (e^{-\frac{3}{2}} - e^{-1}) \\ (-6e^{-\frac{3}{2}} + 6e^{-1}) & (-2e^{-\frac{3}{2}} + 3e^{-1}) \end{bmatrix} = \begin{bmatrix} -0.0664 & -0.1447 \\ 0.8685 & 0.6574 \end{bmatrix}. \tag{G.4}$$

From Eq. D.17, the exact discrete-time equivalent to continuous-time white Gaussian process noise has a covariance intensity level of

$$\begin{aligned} Q_d &= e^{F_2 \Delta} \left[ \int_0^{\Delta} e^{-F_2 \tau} Q e^{F_2^T \tau} \, d\tau \right] e^{F_2^T \Delta} \\ &= \begin{bmatrix} -0.0664 & -0.1447 \\ 0.8685 & 0.6574 \end{bmatrix} \begin{bmatrix} 8.48 & -9.30 \\ -9.30 & 11.24 \end{bmatrix} \begin{bmatrix} -0.0664 & 0.8685 \\ -0.1447 & 0.6574 \end{bmatrix} \\ &= \begin{bmatrix} 0.0940 & 0.01647 \\ 0.01647 & 0.634 \end{bmatrix}, \end{aligned} \tag{G.5}$$

which is easily verified to be positive definite by Sylvester's "principal minor" test [105], [178].

(U)Now the steady-state solution of the discrete-time Lyapunov equation (cf., Eq. D.20) is obtained from the following:

$$P = \left[ e^{F_2 \Delta} \right] P \left[ e^{F_2 \Delta} \right]^T + Q_d$$

$$\begin{aligned} \begin{bmatrix} p_{11} & p_{12} \\ p_{12} & p_{22} \end{bmatrix} &= \begin{bmatrix} -0.0664 & -0.1447 \\ 0.8685 & 0.6574 \end{bmatrix} \begin{bmatrix} p_{11} & p_{12} \\ p_{12} & p_{22} \end{bmatrix} \begin{bmatrix} -0.0664 & 0.8685 \\ -0.1447 & 0.6574 \end{bmatrix} + \begin{bmatrix} 0.094 & 0.016 \\ 0.016 & 0.634 \end{bmatrix} \\ &= \begin{bmatrix} (0.0044p_{11} + 0.0192p_{12} + 0.0209p_{22}) & (-0.058p_{11} - 0.169p_{12} - 0.095p_{22}) \\ (-0.058p_{11} - 0.169p_{12} - 0.095p_{22}) & (0.754p_{11} + 1.142p_{12} + 0.432p_{22}) \end{bmatrix} + \begin{bmatrix} 0.094 & 0.016 \\ 0.016 & 0.634 \end{bmatrix}. \end{aligned} \tag{G.6}$$

It is easily seen that the solution of the above steady-state Lyapunov equation must satisfy the following system of linear algebraic equations:

$$\begin{bmatrix} -0.996 & 0.0192 & 0.0209 \\ -0.058 & -1.169 & -0.095 \\ 0.754 & 1.142 & -0.568 \end{bmatrix} \begin{bmatrix} p_{11} \\ p_{12} \\ p_{22} \end{bmatrix} = \begin{bmatrix} -0.094 \\ -0.016 \\ -0.634 \end{bmatrix}, \tag{G.7}$$

which, by applying Cramer's rule, yields the following answer:

$$p_{11} = \frac{-0.08747}{-0.75436} = 0.116,$$

$$p_{12} = \frac{0.061801}{-0.75436} = -0.0819,$$

$$p_{22} = \frac{-0.82105}{-0.75436} = 1.08.$$

(U)A cross-check of sorts is available by solving the corresponding continuous-time Lyapunov equation for its steady-state solution (cf., Eq. D.19) from

$$\begin{aligned} 0 &= F_2 P + P F_2^T + Q \\ &= \begin{bmatrix} -5 & -1 \\ 6 & 0 \end{bmatrix} \begin{bmatrix} p_{11} & p_{12} \\ p_{12} & p_{22} \end{bmatrix} + \begin{bmatrix} p_{11} & p_{12} \\ p_{12} & p_{22} \end{bmatrix} \begin{bmatrix} -5 & 6 \\ -1 & 0 \end{bmatrix} + \begin{bmatrix} 1 & 0 \\ 0 & 1 \end{bmatrix} \\ &= \begin{bmatrix} (-10p_{11} - 2p_{12}) & (6p_{11} - 5p_{12} - p_{22}) \\ (6p_{11} - 5p_{12} - p_{22}) & 12p_{12} \end{bmatrix} + \begin{bmatrix} 1 & 0 \\ 0 & 1 \end{bmatrix}, \end{aligned} \tag{G.8}$$

which has the following solution (similarly obtained as the previous solution of linear equations of Eq. G.7, but now not requiring use of Cramer's rule, and also being in basic three significant figure agreement with the above discrete-time solution outcome):

$$P = \begin{bmatrix} 0.116 & -0.083 \\ -0.083 & 1.11 \end{bmatrix}. \tag{G.9}$$

Both of these closed-form results can be used as an independent check on the outcome of the DLK.LIB software calculation as obtained along a different route via the recursive algorithm of Kleinman (discussed in Section D.2.1) to yield the steady-state solution of the Lyapunov equation.

(U)Returning to use the upper compact form of the result of Eq. G.2 within the following well-known continuous-time analog to the discrete-time input/output power spectral density matrix relationship of Eq. 2.6 being:

$$S_{yy}(s) = (sI - F_2)^{-1} Q (-sI - F_2)^{-T}, \tag{G.10}$$

(valid only for sytem matrices having eigenvalues with exclusively negative real parts [241, Section 2] as is the case here) yields the output power spectral density matrix to be

$$S_{yy}(s) = \frac{1}{(s+3)(-s+3)(s+2)(-s+2)} \begin{bmatrix} s & -1 \\ 6 & s+5 \end{bmatrix} \begin{bmatrix} -s & 6 \\ -1 & -s+5 \end{bmatrix}$$

$$= \frac{1}{(9-s^2)(4-s^2)} \begin{bmatrix} -s^2+1 & 7s-5 \\ -7s-5 & 61-s^2 \end{bmatrix} . \quad \text{(G.11)}$$

This result can be used to corroborate the outcome of the multichannel spectral estimation algorithm software implementation and to serve as a training exercise as the plot package is initially modified to provide final outputs in units of decibels. To this end, the per channel numerical results (in the frequency domain) should agree with the following results (obtained from Eq. G.11 by substituting $s = \jmath\omega$):

$$[S_{yy}(\jmath\omega)]_{11} = \frac{\omega^2+1}{(\omega^2+9)(\omega^2+4)} , \quad \text{(G.12)}$$

$$[S_{yy}(\jmath\omega)]_{12} = \frac{\sqrt{49\omega^2+25}}{(\omega^2+9)(\omega^2+4)} e^{\jmath \arctan\frac{-7\omega}{5}} , \quad \text{(G.13)}$$

$$[S_{yy}(\jmath\omega)]_{22} = \frac{\omega^2+61}{(\omega^2+9)(\omega^2+4)} . \quad \text{(G.14)}$$

Upon taking logarithms to the base 10 and multiplying by 10 in the above, respectively, yields these final results expressed in dB for cross-comparison with comparable software magnitude plots of the spectra

$$10\log_{10}[S_{yy}(\jmath\omega)]_{11} = 10\left[\log_{,,}(\omega^2+1) - \log_{,,}(\omega^2+9) - \log_{10}(\omega^2+4)\right] , \quad \text{(G.15)}$$

$$10\log_{10}[S_{yy}(\jmath\omega)]_{12} = 10\left[\frac{1}{2}\log_{10}(49\omega^2+25) - \log_{10}(\omega^2+9) - \log_{10}(\omega^2+4)\right] , \quad \text{(G.16)}$$

$$10\log_{10}[S_{yy}(\jmath\omega)]_{22} = 10\left[\log_{10}(\omega^2+61) - \log_{10}(\omega^2+9) - \log_{10}(\omega^2+4)\right] , \quad \text{(G.17)}$$

and the phase of the above cross term $[S_{yy}(\jmath\omega)]_{12}$ is

$$\text{phase}([S_{yy}(\jmath\omega)]_{12}) = \frac{180^o}{\pi \text{ (radians)}} \cdot \arctan\left(\frac{-7\omega}{5}\right) , \quad \text{(G.18)}$$

where the above phase relationship has been converted from radians to a more familiar representation in terms of degrees by multiplying by the appropriate standard conversion factor.

(U)The first two test cases considered above are analytically tractable to an extent and are useful for testing certain specific software computations such as

transition matrix calculation, $Q_d$ calculation, intermediate computations within the positive definiteness tests for diagonal and nondiagonal covariance matrices, and computational solution of the steady-state Lyapunov equation; however, the correct output of the simulator for both Test Cases 1 and 2 are just sample functions that have a random character [2]. While the correspondence of these random sample functions to the specified underlying parameters can be verified only after further processing to obtain spectral estimates (in the case of those sample functions corresponding to a stationary system) and then further comparing the computed results to the analytically derived closed-form expression that is the known answer, it is highly desirable to have some essentially deterministic check at the output of the simulator proper in order to confirm at-a-glance at the aggregate level that what is being output here is correct before going further to also encompass the next software module of the Spectral Coefficient Estimator in conjunction with the associated software module Spectral Estimator (and its associated plotting program) before we have all the ingredients of a confirming check. To this end, we offer the extremely simple Test Case 3, where we seek a simulator output with characteristics that are immediately confirmable as corresponding directly (and exactly) to a known expected output response.

## G.3 Test Case 3

(U)A complete description of this continuous-time state variable system is depicted in the fourth column of Table F.1 in Section F.2 of Appendix F. From Newton's $2^{nd}$ Law,

$$\frac{\mathrm{d}}{dt}(mv) = \text{force}, \tag{G.19}$$

[2]While the sample functions that are obtained for Test Cases 1 and 2 are both random, only the random process of Test Case 2 corresponds to a stationary process (since the eigenvalues of the system matrix have real parts that are strictly negative), and the random process of Test Case 1 is nonstationary (since the eigenvalues of the idempotent system matrix do not have negative real parts, as discussed in the footnote of Section E.2). Moreover, only Test Case 2 admits a steady-state solution to the Lyapunov equation in order to obtain a steady-state initial condition via the technique discussed in Section D.2.1. It is well-known [105, Eqs. 10-12] that the Lyapunov equation has a steady-state solution if and only if $[F,\Gamma]$ is a controllable pair, where $Q = \Gamma\Gamma^T$ *and* the eigenvalues *all* have negative real parts. The property of Test Case 1 that precludes a steady-state solution of the Lyapunov equation from existing is the lack of eigenvalues with exclusively negative real parts since Test Case 1 is easily shown to possess the requisite controllability.

where for constant mass, m, and a random force, $u(t)$, Eq. G.19 simplifies as

$$m \frac{dv}{dt} = u(t) , \tag{G.20}$$

Assigning state variables as

$$x_1 = x, \; x_2 = \mathrm{x} , \tag{G.21}$$

thus yielding the following two differential equations

$$\begin{aligned} \frac{dx_1}{dt} &= x_2 \\ \frac{dx_2}{dt} &= v(t) = \frac{1}{m} u(t) , \end{aligned} \tag{G.22}$$

which in vector form is

$$\frac{d}{dt} \begin{bmatrix} x_1 \\ x_2 \end{bmatrix} = \begin{bmatrix} 0 & 1 \\ 0 & 0 \end{bmatrix} \begin{bmatrix} x_1 \\ x_2 \end{bmatrix} + \begin{bmatrix} 0 \\ \frac{1}{m} \end{bmatrix} u(t). \tag{G.23}$$

From Eq. D.14, the recursive discrete-time solution to Eq. G.23 is

$$\begin{bmatrix} x_1(k+1) \\ x_2(k+1) \end{bmatrix} = e^{F_3 \Delta} \begin{bmatrix} x_1(k) \\ x_2(k) \end{bmatrix} + \int_{k\Delta}^{(k+1)\Delta} e^{F_3(t-\tau)} \begin{bmatrix} 0 \\ \frac{1}{m} \end{bmatrix} u(\tau) \, d\tau . \tag{G.24}$$

Now for $F_3$ as in **Eq.** G.23 with $\mathbf{A} = 0.5$, from **Eq.** E.1, we have that the discrete-time transition matrix is

$$\begin{aligned} e^{F_3 \Delta} &= I + \begin{bmatrix} 0 & 1 \\ 0 & 0 \end{bmatrix} \Delta + \begin{bmatrix} 0 & 1 \\ 0 & 0 \end{bmatrix}^2 \frac{\Delta^2}{2} + \cdots \\ &= \begin{bmatrix} 0 & \Delta \\ 0 & 1 \end{bmatrix} \end{aligned} \tag{G.25}$$

(U)Notice from Eq. G.23 that the system matrix is strictly unstable since the characteristic equation is

$$\lambda^2 = 0, \tag{G.26}$$

and has zero eigenvalues of multiplicity two. Consequently, the solution that emanates from Eq. G.24 as a function of time is unstable (i.e., it grows with time) and the random process with increasing trend is obviously nonstationary.

(U)The mean of the solution should be of the form (corresponding to the solution of Eq. D.24):

$$E\begin{bmatrix} x_1(t) \\ x_2(t) \end{bmatrix} = \begin{bmatrix} 1 & t \\ 0 & 1 \end{bmatrix} E\begin{bmatrix} x_1(0) \\ x_2(0) \end{bmatrix}$$

$$= \begin{bmatrix} 1 & t \\ 0 & 1 \end{bmatrix}\begin{bmatrix} a \\ b \end{bmatrix} = \begin{bmatrix} a+bt \\ b \end{bmatrix}, \qquad \text{(G.27)}$$

where the values $a$ and b in the above were inherited from the initial condition. For concreteness, let

$$a = 10, \qquad \text{(G.28)}$$

$$b = 4. \qquad \text{(G.29)}$$

In order that the output be essentially deterministic and that the above response represent more than just the mean trend, we make the process and measurement noises (that must be present in a Markov process simulator of this type) essentially zero by making them both to have zero mean and with covariance intensity matrices that are extremely small (in comparison to the primary signal) by taking them to be all diagonal with elements that are $10^{-8}$. The observation matrix, $H_3$, is taken to be the identity matrix so that the measurements are identical to the underlying state variables themselves and $y_1$(t) should then be

$$y_1(t) = 10 + 4\,t, \qquad \text{(G.30)}$$

a straight line with intercept 10 and slope 4, while $y_2(t)$ should be

$$y_2(t) = 4\,, \qquad \text{(G.31)}$$

a horizontal line with intercept 4. Thus these easy-to-check predictable responses should emerge from the simultor when the parameters of Test Case 3 are used.

## G.4 Test Case 4

(U)A complete description of a discrete-time "complex" process as Test Case 3 is depicted in the fifth and last column of Table F.1 in Section F.2 of Appendix F. A detailed consideration of various aspects of the state variable model of Test Case 4 and the discrete-time analytic closed-form expression for its associated power spectral density matrix are provided in Section 3.1, while the associated eigenvalue

calculation methodology used for this "complex" case is discussed in Section 3.2. Except for having a small dimension of two, it is Test Case 4 that is closest in structure to the anticipated "complex process" models to be developed for this BRVAD application (in Chapter 6) owing to the presence of coherent phase processing. Test Case 4 directly utilizes $\Phi_4$ and $Q_d \equiv \mathbf{I}$ as discrete-time inputs without requiring the preliminary software calculation of $\Phi$ and $Q_d$ as done in Test Cases 1 to 3.

(U)Since Test Case 4 doesn't test out any of the other new features of the simulator that haven't already been checked other than the ability to handle the proper calculation of "complex variables", its use was logically postponed until after the three prior test cases had already been run to verify all the important intermediate software computations for the "real variable" case. Only after satisfactorily passing all the previously mentioned preliminary benchmark tests as the first hurdle was the sotfware simulator upgraded to handle this complex case (and the previous Test Cases 1 through 3 rerun and this time merely reviewed at an aggregate level [which now suffices since detailed intermediate verification had already preceeded and the exact same step-by-step final results couldn't logically be obtained unless all the intermediate results are exactly the same also]) to verify that the answers were still correct in now treating the "real variable" case as merely a special subset of the general "complex variable" case. Completeing this confirmation, the expected results for Test Case 4 proper, as analyticaly obtained in Section 3.1, are verified against the software outputs.

## G.5 Test Case 5 (Not Shown in Table F.1)

(U)In Chapter 7, the dimension of the state variable model that is decided upon to represent the random process of this application is six while the state variable models of the previous simulator test cases were of considerably lower dimensions by being either two or three. If the computer implementation language had been PL/1, the transition between dimensions would not have been a problem at all since

1. The matrix operations are identical in structure and completely generalize when the dimension of the underlying matrices is larger.

2. PL/1 routinely allows run time dimensioning as one of its standard features.

However, Fortran was used as the design and implementation language in this investigation in order to match all subroutines utilized (e.g., Kleinman's DLK.LIB routines [197], IMSL routines, and the data handling convention which adopted the

FORTRAN-based so-designated WMH format throughout all the subsequent sequentially run programs that had already been developed). While Lincoln's version 4.1 of FORTRAN for the IBM 3081 mainframe computer ostensibly allows dynamic run-time dimensioning, this was a feature that the programmer never could get to work properly [3] so it was abandoned in the interest of saving time and fixed dimensions were employed instead at known specified locations so that they could be quickly and easily changed to accommodate any later cases encountered that might need a different dimension. This use of FORTRAN without run-time dimensioning was also true of all the existing spectral estimation program modules that are to be subsequently used on the outputs of the simulator. In converting the spectral estimation modules over to handle six dimensional problems involving six channels as considered in Chapter 6, it was necessary to modify these existing spectral estimation software modules that we inherited and that had previously been hardwired with a maximum dimension of five to now be opened up to accommodate six channels. In order to confirm that the spectral estimation software could now correctly accommodate six channels following this upgrade, the following state variable model was derived as Test Case 5.

(U)In order to have six channel simulator data to test the spectral estimation modules that had been recently modified by us to accommodate six channel data (as a practice prelude before use of actual six channel Tradex data), the following model was conceived of to give at-a-glance verification of the six channel output of the simulator. It was decided to use a pseudo-deterministic example in the same vein as that of Test Case 3; however, instead of using a straight line which gave a different expected result in each of two channels as in Test Case 3, this Test Case 5 is to consist of a quintic polynomial which will give a different expected result in each of six channels! For convenience of tractability, it was decided that the desired polynomial would be easily recognizable by having five real "zeroes" or roots of the polynomial located at -2.0, -1.0, 1.0, 3.0, and 4.0, and would be adequately represented as the following time response:

$$\begin{aligned} y(t) &= (t+2)(t+1)(t-1)(t-3)(t-4) \\ &= (t+2)(t^2-1)(t-3)(t-4) \end{aligned}$$

[3] **The use of FORTRAN run-time dimensioning apparently required nominal use of the largest dimension anticipated for the programs and reserved this maximum storage amount for the associated matrices even for test case runs of considerably smaller dimensions. Such a practice would make the Test Case runs deplorably more expensive than necessary and contradicts the appealing philosophy espoused in Section F.1 of using low dimensional Test Cases to keep the expense of software debug down.**

$$
\begin{aligned}
&= (t^2-1)(t^2-t-6)(t-4) \\
&= (t^3-4t^2-t+4)(t^2-t-6) \\
&= t^5-5t^4-3t^3+29t^2+2t-24\,, \qquad \text{(G.32)}
\end{aligned}
$$

From knowledge of standard polynomial behaviour between roots, Eq. G.32 is recognized to have relative maxima at $t$ = -1.5 and 1.5 and relative minima at $t$ =0 and 3.5, while shooting up rapidly without any further change in character beyond $t$ =4 and similarly shooting down rapidly below $t$ =-2.0. A state variable differential equation that would offer such a solution can be obtained by differentiation to yield the following "primitive" as offered below:

$$
\begin{aligned}
y(t) &= t^5-5t^4-3t^3+29t^2-24, \\
y'(t) &= 5t^4-20t^3-9t^2+58t+2, \\
y''(t) &= 20t^3-60t^2-18t+58, \\
y'''(t) &= 60t^2-120t-18, \\
y^{(iv)}(t) &= 120t-120, \\
y^{(v)}(t) &= 120. \qquad \text{(G.33)}
\end{aligned}
$$

Let state variables be assigned as

$$
\begin{aligned}
x_1 &= y, \\
x_2 &= y', \\
x_3 &= y'', \\
x_4 &= y''', \\
x_5 &= y^{(iv)}, \\
x_6 &= y^{(v)},
\end{aligned}
$$

which correspond to the following summary overview state variable matrix model for Test Case 5 being

$$
\frac{d}{dt}\begin{bmatrix} x_1(t) \\ x_2(t) \\ x_3(t) \\ x_4(t) \\ x_5(t) \\ x_6(t) \end{bmatrix} = \begin{bmatrix} 0 & 1 & 0 & 0 & 0 & 0 \\ 0 & 0 & 1 & 0 & 0 & 0 \\ 0 & 0 & 0 & 1 & 0 & 0 \\ 0 & 0 & 0 & 0 & 1 & 0 \\ 0 & 0 & 0 & 0 & 0 & 1 \\ 0 & 0 & 0 & 0 & 0 & 0 \end{bmatrix} \begin{bmatrix} x_1(t) \\ x_2(t) \\ x_3(t) \\ x_4(t) \\ x_5(t) \\ x_6(t) \end{bmatrix} + \begin{bmatrix} u_1(t) \\ u_2(t) \\ u_3(t) \\ u_4(t) \\ u_5(t) \\ u_6(t) \end{bmatrix}, \qquad \text{(G.34)}
$$

where $u(t)$ is the zero-mean white Gaussian process noise, and the appropriate initial condition mean in order to obtain the desired quintic polynomial solution as

a function of the independent variable time, t, is

$$\begin{bmatrix} x_1(0) \\ x_2(0) \\ x_3(0) \\ x_4(0) \\ x_5(0) \\ x_6(0) \end{bmatrix} = \begin{bmatrix} -24 \\ 2 \\ 58 \\ -18 \\ -120 \\ 120 \end{bmatrix} \tag{G.35}$$

In order that this example be essentially a deterministic output yet still retain the requisite Markov process structure utilized in the new simulator, the inital condition covariance as well as the covariance intensity matrices of both the process noise and the measurement noise are made to be diagonal with principal diagonal entries of $10^{-8}$. The Gaussian white measurement and process noises are both taken to be zero-mean. The $6 \times 6$ observation matrix is taken to be the identity matrix. In this way, all the various known derivatives of the quintic polynomial will be exposed as measurements, $\mathbf{y}(t)$, as a confirming check on the six output channels of the simulator. Finally, the time step-size should be $\mathbf{A} = 0.25$ and the above continuous-time form of the system matrix should be entered as input and the transition matrix for this step size should be internally computed as $\Phi = e^{F_5 \Delta}$. Using this Test Case 5 [4], the existing spectral estimation program modules, as altered to accommodate six channels, were sucessfully checked for compatibility with the six channel simulator outputs.

## G.6 Test Case 6 (Not Shown in Table F.1)

(U)For a state size of 6 and an output dimension of 6, the following discrete-time model was conceived of as another simple essentially deterministic at-a-glance test of the output of the simulator, but this time for confirming the exercising of the full capabilities requested in the official simulator specification of being able to handle an $m^{th}$-order vector autoregressive process [5]. In order to simply do so, the structure of the known solution of Test Case 3 was exploited again but in a slightly different

[4] Use of this test case revealed that the associated separate modular plot package was set up to output only two channels of data at-a time and had to be modified and enlarged to handle all six channels. This modification was initiated by the programmer but never successfully confirmed.

[5] The attempted use of this test case revealed that the simulator program had not included the feature requested in the official specification of being able to handle a general $m^{th}$-order vector autoregressive process (with details on how to do so also provided in the specification) but can merely handle a $1^{st}$-order vector process, as arise in Test Cases 1 to 4. Since the purpose of the

form. The test case consisted of a state variable model partitioned as indicated below:

$$x(k) = \begin{bmatrix} x_1(t) \\ x_2(t) \\ \cdots \\ x_3(t) \\ x_4(t) \\ \cdots \\ x_5(t) \\ x_6(t) \end{bmatrix}, \qquad \text{(G.36)}$$

where the novel construction offered below is used this time to construct the $4^{th}$ order vector autoregressive process from the simple model of Test Case **3** as

$$x(k) = \begin{bmatrix} \Phi_3 & \vdots & 0 & \vdots & 0 \\ \cdots & \cdots & \cdots & \cdots & \cdots \\ 0 & \vdots & 0 & \vdots & 0 \\ \cdots & \cdots & \cdots & \cdots & \cdots \\ 0 & \vdots & 0 & \vdots & 0 \end{bmatrix} x(k-1) + \begin{bmatrix} 0 & \vdots & 0 & \vdots & 0 \\ \cdots & \cdots & \cdots & \cdots & \cdots \\ 0 & \vdots & \Phi_3 & \vdots & 0 \\ \cdots & \cdots & \cdots & \cdots & \cdots \\ 0 & \vdots & 0 & \vdots & 0 \end{bmatrix} x(k-2)$$

$$+ \begin{bmatrix} 0 & \vdots & 0 & \vdots & 0 \\ \cdots & \cdots & \cdots & \cdots & \cdots \\ 0 & \vdots & 0 & \vdots & 0 \\ \cdots & \cdots & \cdots & \cdots & \cdots \\ 0 & \vdots & 0 & \vdots & \Phi_3 \end{bmatrix} x(k-3) + \begin{bmatrix} 0 & \vdots & 0 & \vdots & 0 \\ \cdots & \cdots & \cdots & \cdots & \cdots \\ 0 & \vdots & 0 & \vdots & 0 \\ \cdots & \cdots & \cdots & \cdots & \cdots \\ 0 & \vdots & 0 & \vdots & 0 \end{bmatrix} x(k-4) + \begin{bmatrix} u_1(t) \\ u_2(t) \\ u_3(t) \\ u_4(t) \\ u_5(t) \\ u_6(t) \end{bmatrix} \qquad \text{(G.37)}$$

where the matrix multiplying $x(k-1)$ in the above will be interchanged with that multiplying $x(k-4)$ in a subsequent run. In the meantime, the output of the first two states should be the same as Test Case **3,** the output of the next two states should be the same as Test Case **3** but at twice the step size as in Test Case **3,** and the output of the last two states should be again the same as Test Case **3** but at three times the step-size, and $\mathbf{\Phi_3} \equiv e^{F_3 \Delta}$ as in **Eq.** G.25. The appropriate initial

simulator is merely to checkout the revised spectral estimation software implementation (which Cases 2 and 4 do test), this oversight is forgivable. Additionally, at the expense of incurring additional vector dimensions, the continuous-time technique of [176, pp. 91-92, Eqs. 3.9-13 to 3.9-16] can be invoked to still successfully simulate an $m^{th}$-order scalar autoregressive process within this sparser software computer program framework of only accommodating $1^{st}$-order vector processes.

conditions are again as in Test Case **3:**

$$x(0) = \begin{bmatrix} 10 \\ 4 \\ \cdots \\ 10 \\ 4 \\ \cdots \\ 10 \\ 4 \end{bmatrix} . \qquad \text{(G.38)}$$

The observation matrix, $H_6$, should be the 6 x 6 identity matrix and the Gaussian white noises are to again be zero-mean having diagonal covariance intensity matrices with all nonzero entries being $10^{-8}$ and similarly for the covariance matrix of the initial condition. Thus, each of the pertinent aspects of the simulator was to be tested for conformance to the specifications provided and was to have had its performance validated.

## G.7 Summary of Test Coverage Analytically Provided Here

(U)An overview of the complete software test coverage offered here through selective use of analytic closed-form "Test Cases of known solution" is provided in Table G.1. This completes the contribution of this Appendix. The use of these results is illustrated in Appendix F in Sections F.2 and **F.3** in establishing the status of the software under development for this wake modeling investigation. All items indicated in Table G.l were successfully validated.

# Appendix H

# Impediments to Direct Cross-Comparison of 1-D and 2-D Evaluation Results

(U)Relations between 2-D and 1-D power spectra are not as simple as one might at first think (as conveyed in this section authored by C. W. Therrien). Since the power spectrum is the Fourier transform of the *autocorrelation* function, not the data itself, drawing inferences from 2-D about 1-D spectra and vice versa can be tricky. This note discusses those relations for the simple periodogram.

(U)The relations between the 2-D and 1-D amplitude spectrum of a 2-D signal are straightforward. Let $x(n_1, n_2)$ represent a discrete time-space 2-D signal where $n_1$ is the time index and $n_2$ is the spatial index (relative range or range-gate). The frequency wavenumber spectrum is defined by

$$X_{2D}(\mathrm{f}, \mathrm{k}) = \sum_{n_1=0}^{N_1-1} \sum_{n_2=0}^{N_2-1} x(n_1, n_2) e^{-j(2\pi \mathrm{f} n_1 - \mathrm{k} n_2)} , \qquad \text{(H.1)}$$

where $N_1$ and $N_2$ are the number of samples in the time and range directions, respectively. The 1-D spectrum for a given fixed range gate $n_2$ is defined by

$$X_{1D}(\mathrm{f}; n_2) = \sum_{n_1=0}^{N_1-1} x(n_1, n_2) e^{-j2\pi \mathrm{f} n_1} \qquad \text{(H.2)}$$

From Eq. H.1, we can write

$$X_{2D}(\mathrm{f}, 0) = \sum_{n_2=0}^{N_2-1} \left( \sum_{n_1=0}^{N_1-1} x(n_1, n_2) e^{-j2\pi \mathrm{f} n_1} \right) , \qquad \text{(H.3)}$$

therefore it is clear that

$$X_{2D}(\mathrm{f},0) = \sum_{n_2=0}^{N_2-1} X_{1D}(\mathrm{f};n_2)\ . \tag{H.4}$$

That is, the amplitude spectrum of the signal along the k = 0 axis in 2-D is essentially an average of the 1-D amplitude spectra computed at all the range gates.

(U)In like manner, we have that

$$X_{2D}(0,\mathrm{k}) = \sum_{n_1=0}^{N_1-1} X_{1DW}(n_1,\mathrm{k})\ , \tag{H.5}$$

where $X_{1DW}$ are the wavenumber amplitude spectra computed at the various points in time.

(U)For the power spectral density of a random process, the relations are not so straightforward. Let $R_{2D}(\ell_1,\ell_2)$ and $R_{1D}(\ell;n_2)$ be the estimated 2-D and 1-D correlation functions defined, respectively, according to

$$R_{2D}(\ell_1,\ell_2) = \frac{1}{N_1N_2}\sum_{n_1=0}^{N_1-|\ell_1|-1}\sum_{n_2=0}^{N_2-|\ell_2|-1} x(n_1+|\ell_1|,n_2+|\ell_2|)x^*(n_1,n_2) \tag{H.6}$$

$$R_{1D}(\ell;n_2) = \frac{1}{N_1}\sum_{n_1=0}^{N_1-|\ell|-1} x(n_1+|\ell|,n_2)x^*(n_1,n_2) \tag{H.7}$$

Correspondingly, the 2-D power spectral density estimate is defined as

$$S_{2D}(\mathrm{f},\mathrm{k}) = \sum_{\ell_1=-N_1+1}^{N_1-1}\sum_{\ell_2=-N_2+1}^{N_2-1} R_{2D}(\ell_1,\ell_2)e^{-j(2\pi\mathrm{f}\ell_1-k\ell_2)} \tag{H.8}$$

By analogy with Eqs. H.l to H.4, it follows that

$$S_{2D}(\mathrm{f},0) = \sum_{\ell_2=-N_2+1}^{N_2-1} S'_{1D}(\mathrm{f};\ell_2)\ , \tag{H.9}$$

where

$$S'_{1D}(\mathrm{f};\ell_2) = \sum_{\ell_1=-N_1+1}^{N_1-1} R_{2D}(\ell_1,\ell_2)e^{-j2\pi\mathrm{f}\ell_1} \tag{H.10}$$

However, the quantity $S'_{1D}$ does not have much physical significance. We would prefer, instead, to relate $S_{2D}(\mathrm{f},\mathrm{k})$ to the 1-D spectra computed for each point in space as

$$S_{1D}(\mathrm{f};n_2) = \sum_{\ell=-N_1+1}^{N_1-1} R_{1D}(\ell;n_2)e^{-j2\pi \mathrm{f}\ell} \tag{H.11}$$

but such a direct relationship can not be rigorously substantiated as being appropriate.

(U)To pursue this point further, one can use the fact that the estimates of Eqs. H.8 and H.11 (with the definitions of Eqs. H.6 and H.7) are actually the same as the periodogram estimates

$$S_{2D}(\mathrm{f},\mathrm{k}) = \frac{1}{N_1 N_2}|X_{2D}(\mathrm{f},\mathrm{k})|^2 \tag{H.12}$$

and

$$S_{1D}(\mathrm{f};\mathrm{n2}) = \frac{1}{N_1}|X_{1D}(\mathrm{f};n_2)|^2 \tag{H.13}$$

Therefore, from Eqs. H.4, H.12, and H.13, it follows that

$$\begin{aligned} S_{2D}(\mathrm{f},0) &= \frac{1}{N_1 N_2}|X_{2D}(\mathrm{f},0)|^2 = \frac{1}{N_1 N_2}|\sum_{n_2=0}^{N_2-1} X_{1D}(\mathrm{f};n_2)|^2 \\ &= \frac{1}{N_2}\left\{\sum_{n_2=0}^{N_2-1}\frac{1}{N_1}|X_{1D}(\mathrm{f};n_2)|^2 + \text{ crossterms }\right\} \\ &= \frac{1}{N_2}\left\{\sum_{n_2=0}^{N_2-1} S_{1D}(\mathrm{f};n_2) + \text{ crossterms }\right\} \end{aligned} \tag{H.14}$$

Thus, the 2-D spectrum even on the $\mathrm{k} = 0$ axis is not a simple combination of the 1-D spectra. The crossterms can potentially result in various phenomena that do not necessarily occur in the 1-D spectrum.

(U)The crossterms in Eq. H.14 are what prevent us from having a simple direct relation between the 2-D and 1-D power spectral estimates. If the signal were independent of range (i.e., if the signals in each radar range-gate were identical functions of time), then each of the crossterms would be equal to $S_{1D}$ and so a simple relation would exist. However, for realistic situations where the signals at each range gate are *different*, it appears that the presence of these crossterms could be responsible for some differences that appear between the shape of the 1-D spectum and the shape of the 2-D spectrum as viewed along the k=O axis.

(U)The above analysis was carried out by NPS for spectral estimates based on periodograms and is relevant to this investigation since differences were observed in attempted comparisons of 2-D and 1-D periodogram spectral estimates. Note that the analysis here does not directly apply to MEM or 2-D AR spectral estimates per se. However, it does suggest that for any type of spectral estimates, differences between the 2-D and 1-D spectra may occur and therefore caveats must accompany any attempted inferences from cross-comparisons between the two forms.

# Appendix I

# A Concise Roadmap of Technical Details for The Spectral Estimation Specialist

## I.1 On "Optimum Approaches" to Multichannel Spectral Estimation

According to Ning and Nikias [99, Intro.], except for their computationally unwieldy "optimum approach" [1], no previously existing (prior to 1987) Multichannel Linear Prediction (LP) is an exact generalization of maximum entropy estimation to more than one channel but merely an approximation. Since all versions of multichannel LP incorporating linear autoregressive parametric models must estimate a fixed number of poles and zeroes, certain undesirable phenomena can be encountered with its use such as line-splitting [233] (as a result of the algorithm assuming that more poles are there than are actually present) and cross-channel feed-through can occur (corresponding to imperfect pole-zero cancellation occuring near the unit circle that underlies the processing considerations). A scalar MEM remedy to the single channel line-splitting problem is the approach of [96] [2] which involves addi-

[1] Since it is claimed to be computationally equivalent to a "Dynamic Programming" implementation, the so-designated "optimum approach" has been implemented for ***only*** two channels and *only* for "real" processes by Ning and Nikias, a severe limitation for the Tradex wideband signal application which has associated signal processing that coherently sums PP and OP phase returns as a "complex" process having both "real" and "imaginary" components and that requires use of more channels for realistic models as further pursued in Chapter 6.

[2] Also only currently implemented by Fougere for "real" processes.

tional optimization operations and, as such, is a greater computational burden.

(U)Recently, another approach to multichannel maximum entropy spectral estimation has emerged [258] that also claims to be an optimal implementation but to also have tractable more practical algorithms as subroutines to be implemented. This new approach also has not yet beeen posed for the "complex" case of interest in this Tradex application.

(U)Since there are several algorithms for multichannel LP that are similar, both in structure and in beneficial efficiency, to the highly regarded Levinson-Durbin recursion technique, it is reasonable to use multichannel LP as a simple way to model a multichannel stochastic time series for either estimation or subsequent sample function emulation of auto- and cross-spectra. This report provides a detailed look at the results of applying Nuttall and LWR techniques, as two multichannel spectral estimation approaches.

## 1.2 Cornnients on Forwards and Backwards Markov Models Disscussed in Section 2.1

(U)While some discussions such as [71, **Eq.** 8.2.73] don't bother to use different notation to make the fine distinctions between the underlying processes in forwards and backwards models such as is done using $\underline{W}_n^B$ in Eq. 2.5b, other discussions do. (For more explanation of the properties and interrelationships between forwards and backwards Markov models and an indication of historical misconceptions and their proper resolutions, see [133], [134].[3])

## 1.3 More on ARMA Spectral Estimation and its Attendant Difficulties

(U)A recent IEEE ASSP award winning investigation [161] looked into what order AR, MA, and ARMA model can match a specified $(L + 1)$ length (positive definite) correlation sequence. We are also forewarned by being cognizant of recent revelations in [78] that the earlier adaptive lattice implementations of ARMA ([78], [82]) that involve unequal forward and backward reflection coefficients suffer by

[3]These **aspects are also important in reverse time Kalman filtering and Kalman smoothing applications** [170], [171].

not being robust in noisy situations and that it also does not conform to previous analytically calculated bounds on anticipated output power.

(U)The problem of estimating the AR and MA parameters of a (scalar) $\mathrm{ARMA}(p,q)$ model for the special case where p = q (so there are exactly the same number of unknown AR terms as there are unknown MA terms to be estimated and where the model order p is assumed to be given or specified a priori) is equivalently reformulated in [214] in terms of a one-step predictor and utilizes Riccati equation solutions within an associated Kalman filter context. This unusual approach (extremely palatable to Kalman filter theorists) is pursued in [214] to completely solve this ARMA parameter estimation or modeling problem for the AR parameters (arbitrarily in either transient or steady-state operating conditions) and for the MA parameters (only in the steady-state). Unlike most other approaches to ARMA estimation, which usually estimate the AR portion first and then the MA portion afterwards (as a highly numerically sensitive possibly nonlinear function of the AR portion), Alengrin and Zerubia claim in [214, p. 1115, first bullet in remarks under proof of Theorem 2] that the reverse is true by the AR portion in their technique being instead dependent on the MA estimates (but the solution approach that they recommend appears to defy or contradict this claim). At any rate, their solution equations do exhibit nice linearity throughout.

## I.4 Some Needs for ARMA Models in Radar Processing

(U)Upon examining samples of our radar data, the sample paths were observed to be spiky, which is indicative of measurement noise being present as compared to the fairly smooth trajectories of a Markov process that would be expected for a pure AR process. Since the spikiness was small as compared to the general trends, it would appear that it could be subsumed as additive white measurement noise of relatively small magnitude (i.e., small variance and zero mean) that had been superimposed. Theoretical and physical justification for such treatment of measurement noise being present is that a radar receiver is in fact a measurement sensor with thermal or shot noise and a corresponding noise figure. Obviously, radar receivers are not noise-free. Other measurement degradations present could be due to minor effects of the atmosphere and other background environmental effects which contribute a component to the effective measurement noise.

(U)There is already a precedent by Simon Haykin in [29] which asserts that:

> "ARMA processes are more appropriate as stochastic models of airport surveillance radar returns (of cooperating benign targets in clutter), where AIC-based selection algorithms to determine the appropriate p and $q$ of the associated ARMA process were utilized"

despite the warnings against AIC techniques in [49, Section V], [50] as noted above. These ARMA techniques are of less interest to us here because RV reentry tracking by radar is clutter-free and for a different frequency range and in a more sensitive target resolution environment and uses the more potent special purpose Tradex radar. We are somewhat satisfied with using just an AR model with perhaps the slight wrinkle of additive white measurement noise being assumed to be present. Recent techniques of [63], [160], and [163] are now available and may perhaps be more appropriate for Haykin's thornier problem of determining the most appropriate ARMA model order and assumed model structure for his C-band air traffic control radar in heavy ground clutter.

## 1.5 On Use of IMSL at Lincoln

Regarding use of Edition 10.0 IMSL subroutines as discussed in Section F.2.3, a somewhat unsettling aspect, recently uncovered (in June 1988), is that some (but not all) Edition 10.0 IMSL routines on the IBM 3081 mainframe here *require* use of the Lincoln Laboratory 4.1 FORTRAN compiler (which still has a status classified as being experimental). No memo has yet been circulated as a warning to general users on this potentially sensitive topic. Information on this sensitive topic is apparently only disseminated serendipitously.

## 1.6 Closing Remarks

Although, at times, it may appear that the'reader is thrust into the midst of a raging technical debate, it was felt that, rather than cover up controversy, it is better to take the "bull by the horns" by acknowledging it and addressing it directly. This approach was used in addressing certain topics, such as when discussing use of Akaike's Information Criterion (AIC) for estimating system model order. Here we have a battle of the titans so to speak with both IEEE Fellows Thomas Kailath [49] and Simon Haykin [29] using AIC without reservations, but with careful and thoughtful IEEE Fellow Kashyap [50] expressing concerns that others [173], [163, Preface], [231] eventually came to share in viewing AIC as suspect. It is now

routine for investigators, perhaps through imitation, to use the AIC in establishing the order of the underlying model, but we refrain from doing so here because its use is apparently shaky. Even these algorithmic aspects of technology are evolving, but, fortunately, with longer time constants, in general, than those of hardware technologies. No field is static (unless it is dead)!

It may appear that an inordinate amount of attention was lavished on developing an "exacting simulator" and then successfully validating it. The reason for this emphasis is that all the alternative multichannel spectral estimation generalizations are apparently somewhat approximate in order to be tractably implemented and that multichannel spectral estimation is frequently vulnerable to cross-channel feedthrough. In performing validation of the two multichannel spectral estimation approaches and in making comparisons between the processing results of each, it would be awful if artifacts of simulator approximations and inaccuracies were to inadvertently taint the conclusions of this investigation into which is the more appropriate multichannel spectral estimator to be used for the Active Decoy application. To ensure against this unpleasant situation occurring, the new simulator design was pursued so that only exact mechanizations would be used that avoid use of uncalibrated approximations. Since documentation of the features of an "exacting simulator" had not been encountered in the open literature by the author but was forged instead from his industrial experience, it was completely documented here in Appendices D, E, F, and G.

# Bibliography

[1] Silverman, B. W., *Density Estimation for Statistics and Data Analysis,* Chapman and Hall, N.Y., 1986.

[2] Roy, R., "Binomial Identities and Hypergeometric Series," *American Mathematical Monthly,* Vol. 1, pp. 36-46, January 1987.

[3] Carter, G. C., and Ferrie, J. F., "A Coherence and Cross Spectral Estimation Program," in *Programs for Digital Signal Processing,* IEEE Press, N.Y., 1979.

[4] Nuttall, A. H., "On the Variance of the Phase Estimate of the Cross Spectrum and Coherence," NUSC Technical Memorandum TM No. 771112, New London, CT, 10 June 1977.

[5] Nuttall, A. H., and Carter, G. C., "Approximations for Statistics of Coherence Estimators," NUSC Technical Report No. 5291, New London, CT, 9 March 1976.

[6] Carter, G. C., "Estimation of the Magnitude Squared Coherence Function (Spectrum)," NUSC Technical Report No. 4343, New London, CT, 19 May 1972.

[7] Carter, G. C., Knapp, C. H., and Nuttall, A. H., "Estimation of the Magnitude-Squared Coherence Function via Overlapped Fast Fourier Transform Processing," *IEEE Transactions on Audio and Electroacoustics,* Vol. AU-21, No. 4, pp. 337-344, Aug. 1973.

[8] Knight, W. C., Pridham, R. G., and Kay, S. M., "Digital Signal Processing for Sonar," *Proceedings of the IEEE,* Vol. 69, No. 11, pp. 1451-1506, November 1981.

[9] Stearns, S. D., and Soloman, O. M., "A Comparison of the Methods for Estimating Coherence," *Proceedings of American Control Conference,* San Diego, CA, pp. 228-233, 1984.

[10] Bendat, J. S., and Piersol, A. G., *Random Data: Analysis and Measurement Procedures,* Wiley, N.Y., 1971.

[11] Cadzow, J. A., and Soloman,,O. M., "Linear Modeling and the Coherence Function," *IEEE Trans. on ASSP,* Vol. ASSP-35, No. 1, pp. 19-28, Jan. 1987.

[12] Carter, G. C., "Coherence and Time Delay Estimation," *Proceedings of the IEEE,* Vol. 75, No. 2, pp. 236-255, Feb. 1987.

[13] Stearns, S. D., "Tests of Coherence Unbiasing Methods," *IEEE Trans. on ASSP,* Vol. ASSP-29, April 1981.

[14] Holm, S., and Ottesen, G., "Bias in the Cross Spectrum and Time Delay Estimates Due to Misalignment," *IEEE Trans. on ASSP,* Vol. ASSP-34, No. 6, pp. 1662-1665, Dec 1986.

[15] Amos, D. E., and Koopmans, L. H., "Tables of the Distribution of the Coherence for the Stationary Bivariate Gaussian Process," Sandia Corporation Monograph SCR-483, Mathematics and Computers TID-4500 (19th Edition), March 1963.

[16] Deutsch, R., *Nonlinear Transformations of Random Processes,* Prentice-Hall, Englewood Cliffs, N.J., 1962.

[17] Betz, J. W. , "Comparison of the Deskewed Short-Time Correlator and the Maximum Likelihood Correlator," *IEEE Trans. on ASSP,* Vol. ASSP-32, No. 2, pp. 285-294, April 1984.

[18] Baggeroer, A. B., "Confidence Intervals for Regression (MEM) Spectral Estimates," *IEEE Trans. on Information Theory,* Vol. IT-22, No. 5, pp. 534-545, Sept. 1976.

[19] Burshtein, D. and Weinstein, E., "Confidence Intervals for the Maximum Entropy Spectrum," *IEEE Trans. on ASSP,* Vol. ASSP-35, No. 4, pp. 504-510, April 1987 (minor correction in Vol. ASSP-36, no. 5, p. 826, May 1988).

[20] Carter, G. C., and Nuttall, A. H., "Analysis of a Generalized Framework for Spectral Estimation – Part I: The Technique and Its Mean Value," *IEE Proceedings,* Vol. 130, Part F, No. 3, pp. 239-241, April 1983.

[21] Nuttall, A. H., "Analysis of a Generalized Framework for Spectral Estimation – Part II: Reshaping and Variance Results," *IEE Proceedings,* Vol. 130, Part F, No. 3, pp. 242-245, April 1983.

[22] Giannella, F., "C-R Bounds for AR Parameter Estimation as a Function of the Data Length," *IEEE Trans. on ASSP,* Vol. ASSP-34, No. 4, pp. 994-995, Aug. 1986.

[23] Norton, J. P., "Identification of Parameter Bounds for ARMAX Models from Records with Bounded Noise," *International Journal of Control,* Vol. 45, No. 2, pp. 375-390, 1987.

[24] Choi, B. S., "On the Relation Between the Maximum Entropy Probability Density Function and the Autoregressive Model," *IEEE Trans ASSP,* Vol. ASSP-34, No. 6, pp. 1659-1661, Dec. 1986.

[25] Rodriguez, C. C., and Van Ryzin, J., "Large Sample Properties of Maximum Entropy Histograms," *IEEE Trans. on Information Theory,* Vol. IT-32, No. 6, pp. 751-759, Nov. 1986.

[26] Masry, E., "Autoregressive Spectral Estimation in Additive Noise," to appear in *IEEE Trans. on Acoustics, Speech, and Signal Processing.*

[27] Kay, S. M., and Marple, S. L., "Spectrum Analysis – A Modern Perspective," *Proceedings of IEEE,* Vol. 69, pp. 1380-1419, November 1981.

[28] Moura, J. M. F., and Ribeira, M. I., "Parametric Spectral Estimation for ARMA Processes," *Proceedings of the Third ASSP Workshop on Spectrum Estimation and Modeling,* Northeastern Univ., Boston, MA, pp. 37-40, 17-18 Nov. 1986.

[29] Thomas, P., and Haykin, S., "Stochastic Modeling of Radar Returns," *IEE Proceedings,* Vol. 133, Part F, No. 5, pp. 476-481, August 1986.

[30] Farrier, D. R., and Jeffries, D. J., "Maximum Entropy Processing of Band-Limited Spectra. Part 2: Recovering a Spectrum from Noisy

Measurements," *IEE Proceedings,* Vol. 132, Part F, No. 6, pp. 498-504, Oct. 1985.

[31] Janssen, A. J. E. M., "Comments on 'Characterizing the Radar Ambiguity Functions'," *IEEE Transactions on Information Theory,* Vol. IT-33, No. 2, p. 298, March 1987.

[32] Auslander, L., and Tolimieri R., "Radar Ambiguity Functions and Group Theory," *SIAM Journal of Mathematical Analysis,* Vol. 16, pp. 577-601, May 1985.

[33] Kazakos, D., and Papantoni - Kazokos, P., "Spectral Distance Measures Between Gaussian Processes," *IEEE Transactions on Automatic Control,* Vol. AC-25, No. 5, pp. 950-959, October 1980.

[34] Preuss, R. D., "Testing Spectral Hypotheses in Noise," *Proceedings of Third ASSP Workshop on Spectrum Estimation and Modeling,* pp. 125-128, Boston, MA, 17-18 November 1986.

[35] Rosenblatt, M., "Higher Order Spectral Methods and Deconvolution," *Proceedings of Third ASSP Workshop on Spectrum Estimation and Modeling,* p. 1, Boston, MA, 17-18 November 1986.

[36] Kay, S. M., and Sengupta, D., "Spectral Estimation of Non-Gaussian Autoregressive Processes," *Proceedings of Third ASSP Workshop on Spectrum Estimation and Modeling,* pp. 10-13, Boston, MA, 17-18 November 1986.

[37] Marmarelis, V. Z., and Sheby, D., "Bispectral Analysis of Weakly Nonlinear Quadractic Systems," *Proceedings of Third ASSP Workshop on Spectrum Estimation and Modeling,* pp. 14-16, Boston, MA, 17-18 November 1986.

[38] Nikias, C. L., "Parametric Trispectrum Estimation," *Proceedings of Third ASSP Workshop on Spectrum Estimation and Modeling,* pp. 17-20, Boston, MA, 17-18 November 1986.

[39] Raghuveer, M., "Multichannel Bispectrum Estimation," *Proceedings of Third ASSP Workshop on Spectrum Estimation and Modeling,* pp. 21-24, Boston, MA, 17-18 November 1986.

[40] Rosenblatt, M., Van Ness, J. W., "Estimation of the Bispectrum," *Annals of Mathematical Statistics,* Vol. 36, pp. 1120-1136, 1965.

[41] Brillinger, D. R., Rosenblatt, M., "Asymptotic Theory of Estimates of kth Order Spectra," in *Spectral Analysis of Time Series,* B. Harris (ed.), pp. 158-188, Wiley, N.Y., 1967.

[42] Matsuoka, T., and Ulrych, T. J., "Phase Estimation Using the Bispectrum," *Proceedings of IEEE,* Vol. 72, pp. 1403-1411, October 1984.

[43] Rosenblatt, M., "Cumulants and Cumulant Spectra," in *Time Series in the Frequency Domain, D.* Brillinger and P. Krishnaiah (eds.), North Holland Press, pp. 369-382, 1983.

[44] Tryon, P. V., "Bispectrum and Higher Order Spectra: A Bibliography" National Bureau of Standards Tech Note 1036, National Eng. Lab, NBS, Boulder, Colorado (date unknown).

[45] Nikias, C. L., "Higher-Order Spectrum (Bispectrum, Trispectrum) Estimation," Session B, Central New England Council Miniconference on Acoustics, Speech, and Signal Processing, Embassy Suites Hotel, Boston, MA, 15, 16 May.

[46] Marple, S. L., *Digital Spectral Analysis with Applications,* Prentice-Hall, N.Y., 1987.

[47] Zurbenko, I. G., *The Spectral Analysis* of *Time Series* North Holland, N.Y., 1986.

[48] Miller, K. S., *Complex Stochastic Processes: An Introduction to Theory and Application,* Addison-Wesley, Reading, MA, 1974.

[49] Wax, M., and Kailath, T., "Detection of Signals by Information Theoretic Criteria," *IEEE Trans. on ASSP,* Vol. ASSP-33, No. 2, pp. 387-392, April 1985.

[50] Kashyap, R. L., "Inconsistency of the AIC Rule for Estimating the Order of Autoregressive Models," *IEEE Trans. on Automatic Control,* Vol. AC-25, No. 5, pp. 996-998, Oct. 1980.

[51] Akaike, H., "Markovian Representation of Stochastic Processes by Canonical Variables," *SIAM Journal of Control,* Vol. 13, No. 1, pp. 162-173, January 1975.

[52] Fuchs, J.-J., "ARMA Order Estimation Via Matrix Perturbation Theory," *IEEE Trans. on Automatic Control,* Vol. AC-32, No. 4, pp. 358-361, April 1987.

[53] Nakano, J., and Tagami, S., "Order Selection of a Multivariate Autoregressive Model by a Modification of the FPE Criterion," *International Journal of Control,,* Vol. 45, No. 2, pp. 589-596, 1987.

[54] Holm, S., and Omar, Z. I. A., "A Comparison of Autoregressive Order-Determining Criteria," in *Signal Processing 111: Theories and Applications, I. T.* Young, et al (eds.), Elsevier (North-Holland), N.Y., 1986.

[55] Akaike, H., "A New Look at Statistical Model Identification," *IEEE Trans. on Automatic Control,* Vol. AC-19, pp. 716-723, Dec. 1974.

[56] Chow, J. C., "On Estimating the Orders of an ARMA Process with Uncertain Observations," *IEEE Trans. on Automatic Control,* Vol. AC-17, pp. 707-709, 1972.

[57] Zhou, K., "Remarks on Stochastic Model Reduction," *IEEE Trans. on Automatic Control,* Vol. AC-32, No. 4, pp. 356-358, April 1987.

[58] Boram, Y., and Sandell, N. R., "Consistent Estimation on Finite Parameter Sets with Application to Linear Systems Identification," *IEEE Transactions on Automatic Control,* Vol. AC-32, No. 3, pp. 451-454, June 1978.

[59] Abramowitz, M., and Stegun, A., *Handbook of Mathematical Functions with Formula, Graphs, and Mathematical Tables,* Dover Publications, Inc., N.Y., 1970.

[60] Brownless, K. H., *Statistical Theory and Methodology in Science and Engineering,* Wiley, N.Y., 1965.

[61] Carter, G. C., *Time Delay Estimation,* NUSC Technical Report TR-5335, Naval Underwater Sciences Center, 9 April, 1976.

[62] Carter, G C., Scannell, E. H., "Confidence Bounds for MSC Estimators," IEEE ICASSP, 1978.

[63] Linhart, H., and Zucchini, W., *Model Selection,* John Wiley and Sons, N.Y., 1986.

[64] Drake, A., *Fundamentals of Applied Probability Theory.* McGraw-Hill, 1967.

[65] Gibbons, J. D., *Non-Parametric Statistical Inference.* Marcel Dekker, Inc., 2nd edition, 1971.

[66] Lilliefors, H. W., "On the Kolmogorov-Smirnov Test for Normality with Mean and Variance Unknown," *Journal of the Americal Statistical Association,* June 1967.

[67] Oppenheim, A. V., and Shafer, R. W., *Digital Signal Processing,* Prentice-Hall, 1975.

[68] Lim, J. A., and Malik, J. S., "A New Algorithm for Two-Dimensional Maximum Entropy Power Spectrum Estimation," *IEEE Trans. on ASSP,* ASSP-29, No. **3,** June 1981.

[69] Kerr, T. H., "Decentralized Filtering and Redundancy Management for Multisensor Navigation, *IEEE Trans. on Aerospace and Electronic Systems,* Vol. AES-23, No. 1, pp. 83-119, Jan. 1987 (minor corrections appear on p. 412 of May and on p. 599 of July 1987 issues of same journal).

[70] Stimson, G. W., *Introduction to Airborne Radar,* Huges Aircraft Company, El Segundo, CA, 1983.

[71] Proakis, J. G., *Digital Communications,* McGraw-Hill, N.Y., 1983.

[72] Blahut, R. E., *Fast Algorithms for Digital Signal Processing,* Addison-Wesley, Reading, MA, 1985.

[73] Mohanty, N., *Random Signals Estimation and Identification,* Van Nostrand Reinhold, Co., N.Y., 1986.

[74] Kunt, M., *Digital Signal Processing,* Artech House, Inc., Norwood, MA, 1980.

[75] Alexander, S. T., and Rhee, Z. M., "Spectrum Estimation Errors Due to Finite Precision Effects in Autocorrelation Based Methods," *Proceedings of Third ASSP Workshop on Spectrum Estimation and Modeling,* Northeastern Univ., Boston, MA, 17-18, Nov. 1986.

[76] Alexander, S. T., and Rhee, Z. M., "Analytical Finite Precision Results for Burg's Algorithm and the Autocorrelation Method for Linear Prediction," *IEEE Trans. on ASSP,* Vol. ASSP-35, No. 5, PP. 626-635, May 1987.

[77] Stoica, P., Nehorai, A., "On Stability and Root Location of Linear Prediction Models," *IEEE Trans. on ASSP,* Vol. ASSP-35, No. 4, pp. 582-584, April 1987.

[78] Sohie, G. R. L., and Sibul, L. H., "Stochastic Operator Norms for Two-Parameter Adaptive Lattice Filters," *IEEE Trans. on ASSP,* Vol. ASSP-34, No. 5, pp. 1162-1164, Oct. 1986.

[79] Friedlander, B., "Lattice Filters for Adaptive Processing," *Proceedings of the IEEE,* Vol. 70, pp. 102-107, Feb. 1984.

[80] Burg, J. P., "Maximum Entropy Spectral Analysis," *Proceedings of the* $37^{th}$ *Meeting of the Society of Exploration Geophysicists,* p. 34, 1967.

[81] Morf, M., Vieira, A., Lee, D. T. L., and Kailath, T. "Recursive Multichannel Maximum Entropy Spectral Estimation,". *IEEE Transactions on Geoscience Electronics,* Vol. GE–16, No. 2, pp. 85-94, April 1978.

[82] Friedlander, B., "Lattice Methods for Spectral Estimation,". *Proceedings of the IEEE,* Vol. 70, No. 9, ff. 990, September 1982.

[83] Jenkins, G. M., Watts, D. G., *Spectra Analysis and its Applications.* Holden-Day, 1968.

[84] Marple, S. L., and Nuttall, A. H., "Experimental Comparison of Three Multichannel Linear Prediction Spectral Estimators," *IEE Proceedings,* Vol. 130, No. 3, Part F, ff. 218, April 1983.

[85] Nuttall, A. H., "Positive Definite Spectral Estimate and Stable," NUSC Tech. Rep. 5729, Naval Underwater Syst. Center, New London, CT, 14 November 1977.

[86] Nuttall, A. H., "Multivariate Linear Predictive Spectral Analysis by Weighed Forward and Backward Averaging," Technical Report AD–A031 755, Naval Underwater Syst. Center, New London, CT, 13 October 1976.

[87] Papoulis, A., *Probability, Random Variables and Stochastic Processes,* McGraw–Hill, 2nd edition, 1984.

[88] Lewis, B. L., Kretschrner, F. F., and Shelton, W. W., *Aspects of Radar Signal Processing,* Artech House, Inc., Norwood, MA, 1986.

[89] Dudgeon D., and Mesereau, R., *Multidimensional Digital Signal Processing,* Prentice-Hall, Englewood Cliffs, N.J., 1985.

[90] Johnson, R. L., Miner, *G.* E., "Comparison of Superresolution Algorithms for Radio Direction Finding," in *IEEE Trans. on Aerospace and Electronic Systems,* Vol. AES-22, No. 4, July 1986.

[91] Lang, S. W., "Spectral Estimation of Sensor Arrays," Ph.D. Thesis, MIT, Cambridge, MA, Aug. 1981.

[92] Barabell, A. J., et al, "Performance Comparison of Superresolution Array Processing Algorithms," Project Report TST-72, MIT Lincoln Laboratory, Lexington, MA, 9 May 1984.

[93] Makhoul, J., "Stable and Efficient Methods of Linear Prediction," *IEEE Trans. on ASSP,* Vol. ASSP-25, No. 5, ff. 423, Oct. 1977.

[94] Lang, S. W., and McLellan, J. H., "Frequency Estimation with Maximum Entropy Spectral Estimation," *IEEE Trans. on ASSP,* Vol. ASSP-28, No. 6, pp. 716-724, Dec. 1980.

[95] Quamri, A., et al, "Comparison of High Resolution Spectral Methods Based on SVD," in *Signal Processing 111: Theories and Applications, I.* T. Young et al (editors), Elsevier, North-Holland, N.Y., pp. 337-340, 1986.

[96] Fougere, P. F., "A Solution to the Problem of Spontaneous Line Splitting in Maximum Entropy Spectrum Analysis," *Journal of Geophysical Research,* Vol. 82, pp. 1051-1054, 1977.

[97] Roberts, R. A., and Mullis, C. T., "Digital Signal Processing," in *Signal Processing III: Theories and Applications,* Addison-Wesley, Reading, MA, 1987.

[98] Fougere, P. F., "Applications of Maximum Entropy Spectrum Estimation to Air Force Problems," *Third ASSP Workshop on Spectrum Estimation and Modeling* Northeastern Univ., Boston, MA, pp. 77-80, 17-18, Nov. 1986.

[99] Ning, T., and Nikias, C. L., "Multichannel AR Spectrum Estimation: The Optimum Approach in the reflection Coefficient Domain," in *IEEE Trans. on ASSP,* Vol. ASSP-34, No. 5, pp. 1139-1152, Oct. 1986.

[100] Burg, J. P., "Maximum Entropy Spectral Analysis," Ph.D. thesis, Department of Geophysics, Stanford University, May 1975.

[101] Burdick, B., "BRV Active Decoy Base Replication (U)," Lincoln Laboratory Project Report No. PA-464 (RSATC-722), 1984 (SECRET).

[102] Nikias, C. L., and Raghuveer, M. R., "Bispectrum Estimation: A Digital Signal Processing Framework," *IEEE Trans. on ASSP,* Vol. ASSP-23, No. 7, July 1987.

[103] Stratonovich, R. L., *Topics in the Theory of Random Noise: Volume I,* Ed. by Richard Silverman, Gordon and Breach, N.Y., 1963.

[104] Roberts, R. A., Mullis, C. T., *Digital Signal Processing,* Addison-Wesley, Reading, MA, 1987.

[105] Kerr, T. H., "Testing Matrices for Definiteness and Application Examples that Spawn the Need," *AIAA Journal of Guidance, Control, and Dynamics,* Vol. 10, No. 5, Sept.-Oct., 1987.

[106] Kerr, T. H., "Computational Techniques for the Matrix Pseudoinverse in Minimum Variance Reduced-Order Filtering and Control," in *Control and Dynamic Systems,* Vol. XXVIII: Advances in Algorithms and computational Techniques for Dynamic Control Systems,

C. T. Leondes (Ed.), Academic Press, N.Y., 1988 (available from the author on request).

[107] Kerr, T. H., "A New Multivariable Cramer-Rao Inequality for Parameter Estimation (Application: Input Probing Function specification)," *Proceedings of IEEE Conference on Decision and Control,* December 1974.

[108] Kerr, T. H., "The Proper Computation of the Matrix Pseudo-Inverse and its Impact in MVRO Filtering," *IEEE Transactions on Aerospace and Electronic Systems,* Vol. AES-21, No. 5, September 1985.

[109] Jackson, L. B., and Chien, H. C., "Frequency and Bearing Estimation by Two-Dimensional Linear Prediction," *Proceedings of International Conference on Acoustics, Speech, and Signal Processing (ICASP),* pp. 665-668, Wash., D. C., 1979. Vol. AES-21, No. 5, September 1985.

[110] Kerr, T. H., "Overview Status of Cramer-Rao-Like Lower bounds for Nonlinear Filtering," submitted to *IEEE Trans. on Aerospace and Electronic Systems,* in Sept. 1986 (available from the author upon request).

[111] Newbold, P., "The Exact Likelihood Function for a Mixed Autoregressive Moving Average Process," *Biometrica,* Vol. 61, No. 3, pp. 423-426, 1974.

[112] Graupe, D., Krause, K. J., and Moore, J. B., "Identification of Autoregressive Moving-Average Parameters of Time Series," *IEEE Trans. on Automatic Control,* Vol. AC-20, *No.* 1, pp. 104-107, Feb. 1975.

[113] Kerr, T. H., and Chin, L., "The Theory and Techniques of Discrete-Time Decentralized Filters," in *Advances in the Techniques and Technology of the Application of Nonlinear Filters and Kalman Filters,* edited by C. T. Leondes, NATO Advisory Group of Aerospace Research and Development, AGARDograph, Noordhoff International Publishing, Leiden, 1982.

[114] Skolnik, M. I., *Radar Handbook,* McGraw-Hill, N.Y., 1970.

[115] Cook, C. E., and Bernfeld, M., *Radar Signab: An Introduction to Theory and Application,"* Academic Press, N.Y., 1967.

[116] Hannan, E. J., Kavalieris, L., "Multivariate Linear Time Models," *Advances in Applied Probability,* Vol. 16, pp. 492-561, 1984.

[117] Hannan, E. J., "The Estimation of the Order of an ARMA Process," *Annals of Statistics,* Vol. 8, pp. 1071-1081, 1980.

[118] Hannan, E. J., Rissanen, J., "Recursive Estimation of ARMA Order," *Biometrica,* Vol. 69, pp. 81-94, 1982.

[119] An, H.-Z., Chen, Z. -G., and Hannan, E. J., "Autocorrelation, Autoregression and Autoregressive Approximation," *Annals of Statistics,* Vol. 10, pp. 926-936, 1982.

[120] Chen, H. -F., and Guo, L., "Consistent Estimation of the Order of Stochastic Control Systems," *IEEE Trans. on Automatic control,* Vol. AC-32, No. 6, pp. 531-535, June 1987.

[121] Rihaczek, A. W., "Radar Resolution Properties of Pulse Trains," *Proceedings of IEEE,* Vol. 52, No. 2, pp. 153-164, Feb. 1964.

[122] Rihaczek, A. W., *Principles of High Resolution Radar,"* McGraw-Hill, N.Y., 1985.

[123] Brookner, E. (editor), *Radar Technology,* Artech, Dedham, MA, 1982.

[124] Haykin, S. S., *Detection and Estimation: Applications to Radar,* Halstead Press, John-Wiley and Sons, Inc., N.Y., 1976.

[125] Barnes, R. M., "Detection of a Randomly Polarized Target," Ph.D. thesis in Department of Electrical Engineering, Northeastern University, Boston, MA, June 1984.

[126] Whittle, P., "On the Filtering of Multivariate Autoregressions and the Approximate Canonical Factorization of a Spectral Density Matrix," *Biometrica,* Vol. 50, pp. 129-134, 1963.

[127] Wiggins, R. A., and Robinson, E. A., "Recursive Solution to the Multichannel Filtering Problems," *Journal of Geophysical Research,* Vol. 70, pp. 1885-1891, 1965.

[128] Mieras, H., "Optimal Polarizations of Simple Compound Targets," *IEEE Trans. on Antennas and Propagation,* Vol. AP-31, No. 6, pp. 996-999, Nov. 1983.

[129] Hinich, M. J., "Testing for Gaussianity and Linearity of a Stationary Time Series," *Journal of Time Series Analysis,* Vol. 3, No. 3, pp. 169-176, 1982.

[130] Skolnik, M. I., *Introduction to Radar Systems,"* Second Edition, McGraw-Hill, N.Y., 1980.

[131] Spanier, J., Oldham, K. B., *An Atlas of Functions,"* Hemisphere Publ. Corp. subsidiary of Harper and Row, N.Y., 1987.

[132] Hinich, M. J., Patterson, D. M., "Evidence of Nonlinearity in Daily Stock Returns, *Journal of Business and Economic Statistics,* Vol. 3, No. 1, pp. 69-77, January 1985.

[133] Verghese, G., and Kailath, T., "A Further Note on Backwards Markovian Models," *IEEE Transactions on Information Theory,* Vol. IT-25, No. 1, pp. 121-124, Jan. 1979.

[134] Verghese, G, and Kailath, T., " Correction to ' A Further Note on Backward Markovian Models'," *IEEE Transactions on Information Theory,* Vol. IT-25, No. 4, p. 501, July 1979.

[135] Bartlett, M. S., "A Note on the Multiplying Factors for various $\chi^2$ Approximations," *Journal of the Royal Society of Statistics,* Series B, Vol. 16, pp. 296-298, 1954.

[136] Lawley, D. N., "Tests of Significance of the Latent Roots of the Covariance and Correlation Matrices," *Biometrica,* Vol.' 43, pp. 128-136, 1956.

[137] Giri, N. C., *Multivariate Statistical Inference,* Academic Press, N. Y., 1977.

[138] Okamoto, M., "An Asymptotic Expansion for the Distribution of Linear Discriminant Function," *Annals of Mathematical Statistics,* Vol. 34, pp. 1286-1301, 1963 (Correction in Vol. 39, pp. 1358-1359).

[139] Chernoff, H., "Some Measures for Discriminating between Normal Multivariate Distribution with Unequal Covariance Matrices," in *Multivariate Analysis-III,* ed. by P. R. Krishnaiah, Academic Press, N.Y., 1973.

[140] Anderson, T. W., "Some Nonparametric Multivariate Procedures Based on Statistically Equivalent Blocks," *Multivariate Analysis,* ed. by P. R. Krishnaiah, Academic Press, N.Y., 1966.

[141] Olkin, I., and Sylvan, M., "Correlation Analysis When Some Variances and Covariances are Known," in *Multivariate Analysis-IV,* ed. by P. R. Krishnaiah, Academic Press, N.Y., 1977.

[142] Andrews, D. F., Gnanadesikan, P., and Warner, J. L., "Methods for Assessing Multivariate Normality," in *Multivariate Analysis-111,* ed. by *P.* R. Krishnaiah, Academic Press, N.Y., 1973.

[143] Kullback, S., *Information Theory and Statistics* John Wiley, N.Y., 1959.

[144] Kendall, M. G., and Stuart, A., *The Advanced Theory of Statistics,* Vol. 2, Hafner Publ. Co., N.Y., 1961.

[145] Kerr, T. H., "Real-Time Failure Detection: A Static Nonlinear Optimization Problem that Yields **a** Two Ellipsoid Overlap Test," in *Journal of Optimization Theory and Applications,* Vol. 22, No. 4, August 1977.

[146] Kerr, T. H., "Statistical Analysis of a Two Ellipsoid Overlap Test for Real-Time Failure Detection," *IEEE Transactions on Automatic Control,"* Vol. AC-25, No. 4, pp. 762-773, August 1980.

[147] Kerr, T. H., "False Alarm and Correct Detection Probabilities Over A Time Interval for Restricted Classes of Failure Detection Algorithms," *IEEE Transactions on Information Theory,* Vol. IT-28, No. 4, pp. 619-631, July 1982.

[148] Brumback, B. D., and Srinath, M. D., "A Chi-Square Test for Fault-Detection in Kalman Filters," *IEEE Transactions on Automatic Control,* Vol. AC-32, No. 6, pp. 552-554, June 1987.

[149] Gutowski, P. R., Robinson, E. A., and Treitel, S., "Spectral Estimation: Fact or Fiction," in *IEEE Transactions on Geoscience Electronics,* Vol. GE-16,No. 2, pp. 80-84, April 1978.

[150] Friedlander, B., and Porat, B., "On the computation of an Asymptotic bound for Estimating Autoregressive Signals in White Noise," *Signal Processing,* Vol. 8, pp. 291-302, 1985.

[151] Moses, R. L., and Beex, A. A. (L.), "A Comparison of Numerator Estimators for ARMA Spectra," *IEEE Transactions on ASSP,* Vol. ASSP-34, No. 6, pp. 1668-1671, Dec. 1986.

[152] Rihaczek, A. W., "The Maximum Entropy of Radar Resolution," *IEEE Transactions on Aerospace and Electronic Systems,"* Vol. AES-17, No. 1, p. 144, January 1981.

[153] Aki, K., and Richards, P. G., *Quantitative Seismology: Theory and Methods,* Vol. II, W. H. Freeman and Company, San Francisco, CA, 1980.

[154] Lacoss, R. T., "Data Adaptive Spectral Analysis Methods," *Geophysics,* Vol. 36, pp. 661-675, 1971.

[155] Schneider, W. A., Larner, K. L., Burg, J. P., and Backus, M. M., "A New Data-Processing Technique for the Elimination of Ghost Arrivals on Reflection Seismograms," *Geophysics,* Vol. 29, pp. 783-805, 1964.

[156] Claerbout, J. F., *Fundamentals of Geophysical Data Processing,* McGraw-Hill, N.Y., 1976.

[157] Burg, J. P., "Three-Dimensional Filtering with an Array of Seismometers," *Geophysics,* Vol. 29, pp. 693-713, 1964.

[158] Burg, J. P., "Maximum Entropy Spectral Analysis," A paper presented at the 37$^{th}$ Annual International SEG Meeting, Oklahoma City, Oklahoma, 31 Oct. 1967.

[159] Therrien, C. W., "Relations Between 2-D and Multichannel Linear Prediction," *IEEE Trans. of Acoustics, Speech, and Signal Processing,* Vol. ASSP-29, No. 3, pp. 454-456, June 1981.

[160] Fuller, W. A., *Measurement Error Models,* John Wiley and Sons, N.Y., 1987.

[161] Steinhardt, A., and Makhoul, J., "On Matching Correlation Sequences by Parametric Spectral Models," *Proceedings of the 1987 International Conference on Acoustics, Speech, and Signal Processing,* Dallas, TX, 6-9 April 1987.

[162] Bartels, R. H., and Stewart, G. W., "Algorithm 432: Solution of the Matrix Equation AX+XB=C [F4]," *Communications of the ACM* Vol. 15, No. 9, pp. 820-826, September 1972.

[163] Bittanti, S., ed., *Time Series and Linear Systems,* Springer-Verlag, N.Y., 1986.

[164] Jacovitti, G., Neri, A., Cusani, R., "Methods for Estimating the Autocorrelation Function of Complex Gaussian Stationary Processes," *IEEE Transactions on Acoustics, Speech, and Signal Processing,* Vol. ASSP-35, No. 8, pp. 1126-1138, Aug. 1987.

[165] Huang, W. Y., "Beamforming Using the Nuttall Algorithm," MIT Master of Science Thesis, Depts. of Electrical Engineering and Computer Science, May, 1987.

[166] Weiping, L., "Wigner Distribution Method Equivalent to Dechirp Method for Detecting a Chirp Signal," *IEEE Trans. on Acoustics, Speech, and Signal Processing,* Vol. ASSP-35, No. 8, pp. 1210-1211, Aug. 1987.

[167] Mertzios, B., G., and Paraskevopoulos, P. N., "Transfer Function Matrix of 2-D Systems," *IEEE Transactions on Automatic Control,* Vol. AC-26, No. 3, pp. 722-724, June 1981.

[168] Therrien, C. W., "The Analysis of Multichannel Two-Dimensional Random Signals," Naval Postgraduate School Report No. NPS 62-87-002, NPS, Monterey, CA, prepared for: Chief of Naval Research, Arlington, VA, 31 OCT. 1986.

[169] Hipel, K. W., "Geophysical Model Discrimination Using Akaike Information Criterion," *IEEE Transactions on Automatic Control,* Vol. AC-26, No. 2, pp. 358-378, April 1981.

[170] Catlin, D. E., "The Independence of Forward and Backward Estimation Errors in the Two-Filter Form of the Fixed Interval Kalman Smoother," *IEEE Trans. on Automatic Control,* Vol. AC-25, No. 6, pp. 1111-1115, Dec. 1980.

[171] Desai, U. B., Weinert, H. L., and Yusypchuk, G. H., "Discrete-Time Complementary Models and Smoothing Algorithms: The Correlated Noise Case," *IEEE Trans. on Automatic Control,* Vol. AC-28, No. 4, pp. 536-539, April 1983.

[172] Stoica, P., Soderstrom, T., Friedlander, B., "Optimal Instrumental Variable Estimates of the AR Parameters of an ARMA Process," *IEEE Transactions on Automatic Control,* Vol. AC-30, No. 11, pp. 1066-1074, November 1985.

[173] Fine, T. L., Hwang, W. G., "Consistent Estimation of System Order," *IEEE Trans. on Automatic Control,* Vol. AC-24, No. 3, pp. 387-402, June 1979.

[174] Ljung, L., *System Identification: Theory for the User,* Prentice-Hall, Inc., Englewood Cliffs, N.J., 1987.

[175] Bose, N. K., ed., *Multidimensional System Theory,* D. Reidel Publishing Co., Boston, MA, 1985.

[176] Gelb, A., ed., *Applied Optimal Estimation,* The *MIT Press,* Cambridge, MA, 1974.

[177] Hsia, T. C., "On Power Spectrum Identification Methods," *IEEE Trans. on Automatic Control,* Vol. AC-12, No. 6, pp. 781-782, December 1967.

[178] Kerr, T. H., "On Misstatements of the Test for Positive Semidefinite Matrices," *IEEE Transactions on Automatic Control,* submitted for publication review in September 1987 (available from the author upon request).

[179] Pagano, M., "Estimation of Models of Autoregressive Signal Plus Noise," *Annals of Statistics,* Vol. 2, No. 1, pp. 99-108, 1974.

[180] Stoica, P., Friedlander, B., Soderstrom, T., "Instrumental Variable Methods for ARMA Models," in *Control and Dynamic Systems:*

*Advances in Theory and Applications,* Vol. 25, Part 1, edited by C. T. Leondes, Academic Press, N.Y., 1987.

[181] Fuller, W. A., *Measurement Error Models,* John Wiley and Sons, N.Y., 1987.

[182] Ibrahim, M. K., "On Line-Splitting in the Optimum Tapered Burg Algorithm," *IEEE Transactions on Acoustics, Speech, and Signal Processing,* Vol. ASSP-35, No. 10, October 1987.

[183] Porat, B., Friedlander, B., "The Exact Cramer-Rao Bound for Gaussian Autoregressive Processes," *IEEE Transactions on Aerospace and Electronic Systems,* Vol. AES-23, No. 4, July 1987.

[184] Wu, N., "Properties of Power Spectrum Estimates in the Maximum Entropy Method," *IEEE Transactions on Acoustics, Speech, and Signal Processing,* Vol. ASSP-35, No. 9, pp. 1355-1358, September 1987.

[185] Stoica, P., Nehorai, A., Kay, S. M., "Statistical Analysis of the Least Squares Autoregressive Estimator in the Presence of Noise," *IEEE Transactions on Acoustics, Speech, and Signal Processing,* Vol. ASSP-35, No. 9, pp. 1273-1281, September 1987.

[186] Delsarte, P., Genin, Y., "On the Splitting of Classical Algorithms in Linear Prediction Theory," *IEEE Transaction on Acoustics, Speech, and Signal Processing,* Vol. ASSP-35, No. 5, p.645-653, May 1987.

[187] Kerr, T. H., "Multichannel Shaping Filter Formulations for Vector Random Process Modeling Using Matrix Spectral Factorization," MIT Lincoln Labatory Report No. PA-500, Lexington, MA, December 1987.

[188] Kalman, R.E., and Englar, T. S., *A User's Manual for the Automatic Synthesis Program (Program C),* NASA Contractor Report No. NASA CR-475, June 1966.

[189] Hutchinson, C. E., and Wondergem, H. M., *An Error Analysis Technique for Inertial Navigation Systems and Kalman Filters,* Report No. THEMIS-UM-68-2, University of Massachusetts, School of Engineering, Amherst, MA, September 1968.

[190] Kleinman, K. L., and Kleinman, A. K., "Computational Methods for the Steady-State Kalman Filter in High Order Navigation Models," Proceedings of Twelfth Annual Allerton Conference on Circuits and System Theory, October 1977.

[191] Moler, C., and Van Loan, C., "Nineteen Dubious Ways to Compute the Exponential of a Matrix," SIAM Review, Vol. 20, No. 4, pp. 801-836, October 1978.

[192] Ward, R. C., "Numerical Computation of the Matrix Exponential with Accuracy Estimate," SIAM J. of Numerical Analysis, Vol. 14, No. 4, pp. 600-610, September 1977.

[193] Ward, R. C., "Statistical Roundoff Error Analysis of a Pade Algorithm for Computing the Matrix Exponential," Pade and Rational Approximation, Edited by Saff, E. B., and Varga, R. S., pp. 449-460, Academic Press, N.Y., 1977.

[194] Kerr, T. H., "An Invalid Norm Appearing in Control and Estimation," IEEE Transactions on Automatic Control, Vol. AC-23, No. 1, pp. 73-74, Feb. 1978 (correction on pp. 1117-1118, Dec. 1978).

[195] Huynh, T. V., Hitzl, D. L., Kohfeld, J. J., "A New Method of Computing the State Transition Matrix for Linear Systems," AIAA Journal of Guidance, Control, and Dynamics, Vol. 10, No. 2, pp. 218-221, March-April 1987.

[196] Trankle, T. L., Vincent, J. H., and Franklin, S. N., "System Identification of Nonlinear Aerodynamic Models," Advances in the Techniques and Technology of the Application of Nonlinear Filters and Kalman Filters, Ed. by C. T. Leondes, NATO AGARDograph, No. AGARD-AG-256, Noordhoff International Publishing, Lieden, 1981.

[197] Kleinman, D. L., "A Description of Computer Programs for Use in Linear Systems Studies," Technical Report No. TR-77-2(under AFOSR Grant 77-3126), July 1977 (Revision 4, 8/31/83).

[198] Kalman, R. E., Englar, T. S., and Bucy, R. S., "Fundamental Study of Adaptive Control Systems," Report No. ASD-TR-61-27, Vol. 1, RAIS Division, The Martin Company, Baltimore, MD, for Flight Control Laboratory, Aeronautical Systems Division, AirForce Systems Command, Wright Patterson AFB, April 1962.

[199] Melsa, J. L., and Jones, S. K., Computer Programs for *Computational* Assistance in the Study of Linear Control Theory, McGraw)Hill Book Company, N.Y., 1973 (see subroutine STMST on p. 172).

[200] Mankin, J. B., and Hung, J. C., "On Round-off Errors in Computation of Transition Matrices," Joint Automatic Control Conference, Boulder, CO, pp. 60-64, 5-7 August 1969.

[201] Mandal, A. K., Choudhury, D. R., et al, "Numerical Computation Method for the Evaluation of the Transition Matrix," Proceedings of IEE, Vol. 116, No. 4, April 1969.

[202] McFarland, R. E., and Rochkind, A. B., "On Optimizing Computaitons for Transition Matrices," IEEE Trans. on Automatic Control, Vol. AC-23, No. 3, pp. 495-498, June 1978.

[203] Saha, R. K., and Boriotti, J. R., "Truncation and Round-off Errors in Computation of Matrix Exponentials," International Journal of Control, Vol. 33, No. 1, pp. 137-147, 1981.

[204] Levis, A. H., "Some Computational Aspects of the Matrix Exponential," IEEE Transactions on Automatic Control, Vol. AC-14, No. 4, pp. 410-411, Aug. 1969.

[205] Bierman, G. J., "Power Series Evaluation of Transition and Covariance Matrices," IEEE Transactions on Automatic Control, Vol. AC-17, No. 2, pp. 228-232, April 1972.

[206] Mehra, R., "Digital Simulation of Multidimensional Gauss-Markov Random Processes," IEEE Trans. on Automatic Control, Vol. AC-14, No. 1, pp. 112-113, Feb. 1969.

[207] Healy, M. J. R., Matrices for' Statistics, Clarendon Press, Oxford, England, 1986.

[208] Galvin, W. P., "Matrices with 'Custom-Built' Eigenspaces" SIAM Mathematical Monthly, pp. 308-309, May 1984.

[209] Graybill, F. A., Introduction to Matrices with Applications in Statistics, Wadsworth Publishing Co., Belmont, CA, 1969.

[210] Burlington, R. S., Handbook of Mathematical Tables and Formulas, McGraw-Hill, NY, 1962.

[211] Nering, E. D., Linear Algebra and Matrix Theory, John Wiley and Sons, NY, 1970.

[212] Fogel, E., "A Comment on the Use of Spectral Radius of a Matrix," IEEE Transactions on Automatic Control, Vol. AC-26, No. 3, pp. 798-799, June 1981.

[213] Norton, J. P., An Introduction to Identification, Academic Press, N.Y., 1986.

[214] Alengrin, G., and Zerubia, J., "A Method to Estimate the Parameters of an ARMA Model," IEEE Transactions on Automatic Control, Vol. AC-32, No. 12, pp. 1113-1115, December 1987.

[215] Prasad, S., and Hari, K. V. S., "Improved ARMA Spectral Estimation Using the Canonical Variate Method," IEEE Transactions on Acoustics, Speech, and Signal Processing, Vol. ASSP-35, No. 6, pp. 900-903, June 1987.

[216] Schweppe, F. C., Uncertain Dynamic Systems, Prentice-Hall, Englewood Cliffs, N.J., 1973.

[217] Fougere, P. F., "A Solution to the Problem of Spontaneous Line Splitting in Maximum Entropy Power Spectrum Analysis of Complex Signals," Proceedings of RADC Spectrum Estimation Workshop, Rome, N.Y., pp. 78-84, 24-26May 1978.

[218] Fougere, P. F., "Spectrum Model-Order Determination Via Significant Reflection Coefficients," Proceedings of IEEE International Conference on Acoustics, Speech, and Signal Processing, Tampa, FL, 26-29 March 1985.

[219] Khatri, C. G., "Classical Statistical Analysis based on a Certain Multivariate Complex Gaussian Distribution," Annals of Mathematical Statistics, Vol. 36, pp. 98-114, 1965.

[220] Tuel, W. G., "On the Transformation to (Phase-Variable) Cannonical Form," IEEE Transactions on Automatic Control, Vol. AC-11, No. 4, p. 607, July 1966.

[221] "KREMS Operational and Data Summary: Missions G.T. 85GB (U)," Report No. KOD-495, Lincoln Laboratory, Lexington, MA, 9 April 1982 (SECRET).

[222] "Tradex Data Users Manual," Lincoln Manual 112, Revision 2, Lincoln Laboratory, Lexington, MA, 15 December 1981.

[223] van Zyl, J. J., "On the Importance of Polarization in Radar Scattering Problems," Ph.D. Thesis, California Institute of Technology, Pasadena, CA, 1986 (submitted 10 December 1985).

[224] Therrien, C. W., "Coherrence Analysis and Modeling of MK12A Wake Signatures (U)," Report No. NPS62-88-001, Naval Postgraduate School, Monterey, CA, 30 October 1987 (SECRET).

[225] Huang, W. Y., "Implementation of Multichannel Linear Prediction Modelling of Time Series," Lincoln Laboratory Memo No. 95L-0046, MIT Lincoln Laboratory, Lexington, MA, 3 September 1986.

[226] Burdick, B., "BRV Active Decoy Base Replication (U)," Project Report No. PA-464 (RSATC-722), Lincoln Laboratory, Lexington, MA, 1984 (SECRET).

[227] DeMarco, T., Structured Analysis and System Specification, Yourdon Press (a subsidiary of Prentice-Hall), Englewoods Cliffs, N.J., 1979.

[228] Smith, G., "THE TEST AND MEASUREMENT NOTEBOOK: Using GPS as a Time and Frequency Reference," Microwave Systems News, Vol. 17, No. 13, pp. 72-82, December 1987.

[229] Ball, D., "Soviet Signals Intelligence," The International Countermeasures Handboolc, $12^{th}$ Edition, EW Communications, Inc., Palo Alto, CA, pp. 73-89, 1987.

[230] Golik, R. J., "A Methodology for Simulating Reentry Wake Signatures from Ballistic Range Data," TRW Report No. 40639-6032-UT-00, Redondo Beach, CA, 5 May 1983.

[231] Astrom, K. A., Soderstrom, T., "Uniqueness of the Maximum Likelihood Estimates of the Parameters of an ARMA Model," IEEE Transactions on Automatic Control, Vol. AC-19, No. 6, pp. 769-773, December 1974.

[232] Tan, S., and Vandewalle, J., "Separation of 2-D Nonsingular MIMO Digital Filters into a Cascade of 1-D Filters," *IEEE Transactions on Acoustics, Speech, and Signal Processing,* Vol. ASSP-36, No. 2, p. 301, February 1988 [abstract advertising current article in review and yet to appear].

[233] Fougere, P. A., "A Review of the Problem of Spontaneous Line Splitting in Maximum Entropy Power Spectral Analysis," pp. 301-315, in *Maximum-Entropy and Bayesian Methods in Inverse Problems,* C. Ray Smith and W. T. Grandy (eds.), D. Reidel Publishing Co., sold in the U.S. by Kluwer Academic Publishers, Hingham, MA, 1985.

[234] Maybeck, P. S., *Stochastic Models, Estimation, and Control,* Vol. 1, Academic Press, N.Y., 1979.

[235] Kleinman, D. L., "On an Iterative Technique for Riccati Equation Computation," *IEEE Transactions on Automatic Control,* Vol. AC-13, No. 1, pp. 114-115, February 19b8.

[236] Kleinman, D. L., "Stabilizing a Discrete, Constant, Linear System with Application to Iterative Methods for Solving the Riccati Equation," *IEEE Transactions on Automatic Control,* Vol. AC-19, No. 3, pp. 252-264, June 1974.

[237] Allwright, J. C., "A Lower Bound for the Solution of the Algebraic Riccati Equation of Optimal Control and a Geometric Convergence Rate for the Kleinman Algorithm," *IEEE Transactions on Automatic Control,* Vol. AC-25, No. 4, pp. 826-829, August 1980.

[238] Jazwinski, *A.* H., *Stochastic Processes and Filtering Theory,* ,Academic Press, NY, 1970.

[239] Fukunaga, K., *Introduction to Statistical Pattern Recognition,* Academic Press, NY, 1972.

[240] Kerr, T. H., "Theoretical Basis of an Algorithmic Subroutine for Steady-State Solution of the Matrix Riccati Equation and Recent Availability of Specialized Software to Support Modern Control and Estimation Algorithms," MIT Lincoln Laboratory Group Memo No. 95.3149, Lexington, MA, 9 March 1987.

[241] Kerr, T. H., "Cautions Concerning Occasional Misuse of Shaping Filters for Marginally Stable Systems," submitted to IEEE Transactions on Aerospace and Electronic Systems, in July 1987 (available from the author upon request).

[242] Tufts, D. W., and Melissinos, C. D., "Simple, Effective Computation of Principal Eigenvectors and their Eigenvalues and Applications to High-Resolution Estimation of Frequencies," IEEE Transactions on Acustics, Speech, and Signal Processing, Vol. ASSP-34, No. 5, pp. 1046-1053, 1986.

[243] Yang, J.-F., Kaveh, M., "Adaptive Eigensubspace Algorithms for Direction or Frequency Estimation and Tracking," IEEE Transactions on Acustics, Speech, and Signal Processing, Vol. ASSP-36, No. 2, pp. 241-251, February 1988.

[244] Mohnkern, G. L., "Maximum Likelihood Estimation of Magnitude-Squared Coherence," IEEE Transactions on Acustics, Speech, and Signal Processing, Vol. ASSP-36, No. 1, pp. 130-132, January 1988.

[245] Cadzow, J. A., Solomon, O. M., "Linear Modeling and the Coherence Function," IEEE Transactions on Acustics, Speech, and Signal Processing, Vol. ASSP-35, No. 1, pp. 19-28, January 1987.

[246] Gish, H., Cochran, D., "Invariance of the Magnitude-Squared Coherence Estimate with Respect to Second-Channel Statistics," IEEE Transactions on *Acustics*, Speech, and Signal Processing, Vol. ASSP-35, No. 12, pp. 1774-1776, December 1987.

[247] Kay, S. M., Modern Spectral Estimation, Prentice Hall, Englewood Cliffs, NJ, 1988.

[248] Kerr, T. H., "An Almost Completely Analytic Closed-Form Implementation Example of a Schweppe Likelihood Ratio Detector," submitted to IEEE Trans. on Aerospace and Electronic Systems, in Sept. 1987 (available from the author upon request).

[249] Huang, W. Y., "WMH Programs," Group 95 Memorandum No. 95a.3121, MIT Lincoln Laboratory, Lexington, MA, February 1987.

[250] Tufts, D. W., Giannella, F., Kirsteins, I., Scharf, L. L., "Cramer-Rao Bounds on the Accuracy of Autoregressive Parameter Estimators," Proceedings of $2^{nd}$ *ASSP* Spectrum Estimation Workshop, pp. 12-16, November 1983.

[251] Kikkawa, S., and Ishida, M., "Number of Degrees of Freedom, Correlation Times, and Equivalent Bandwidths of a Random Process," IEEE Transactions on *Information* Theory, Vol. IT-34, No. 1, pp. 151-155, January 1988.

[252] Schweppe, F. C., "Recursive State Estimation: Unknown but Bounded Errors and System Inputs," IEEE Transactions on Automatic Control, Vol. AC-13, No. 1, pp. 22-29, February 1968.

[253] Schlaepfer, F. M., and Schweppe, F. C., "Recursive State Estimation: Unknown but Bounded Errors and System Inputs," IEEE Transactions on Automatic Control, Vol. AC-17, No. 2, pp. 197-205 , April 1972.

[254] Fogel, E., and Huang, Y. F., "On the Value of Information in System Identification-Bounded Noise Case," *Automatica* Vol. 18, No. 2, pp. 229-238, 1982.

[255] Kanai, H., Abe, M., and Kido, K., "Accurate Autoregressive Spectrum Estimation at Low Signal-to Noise Ratio Using a Phase-Matching Technique," IEEE Transactions on Acustics, Speech, and Signal Processing, Vol. ASSP-35, No. 9, pp. 1264-1272, September 1987.

[256] Zhang, X.-D., and Takeda, H., "An Approach to Time Series Analysis and ARMA Spectral Estimation," IEEE Transactions on Acustics, Speech, and Signal Processing, Vol. ASSP-35, No. 9, pp. 1303-1313, September 1987.

[257] Kwakernaak, H. and Sivan, R., Linear Optimal *Control* Systems, Wiley-Interscience, N. Y., 1972.

[258] Ben-Tal, A., Borwein, J. M., and Teboulle, M., "A Dual Approach to Multidimensional $L_p$ Spectral Estimation Problems," SIAM Journal on Control and Optimization, Vol. 26, No. 4, pp. 985-996, July 1988.

[259] Kerr, T. H., "Meeting Report: Subcontractor Kick-off Meeting with Charles Therrien (NPS)," Group Memo No. 95.3155, Lincoln Laboratory, Lexington, MA, 18 March 1987.

[260] Kerr, T. H., "Meeting Report and Subsequent Status Update: June Technical Interchange Subcontractor Meeting with C. W. Therrien (NPS)," Group Memo No. 95.3277, Lincoln Laboratory, Lexington, MA, 27 July 1987.

[261] Kerr, T. H., "Meeting Report and Issues/Action Items: August Technical Interchange Subcontractor Meeting with C. W. Therrien (NPS)," Group Memo No. 95.3338, Lincoln Laboratory, Lexington, MA, 4 September 1987.

[262] Therrien, C. W., and Kerr, T. H., "Results of 2-D Spectrum and Correlation Analysis," Group Memo No. 95.3155, Lincoln Laboratory, Lexington, MA, 8 September 1987.

[263] Baggeroer, A. B., "Confidence Interval Determination for Spectral Estimates Using 'Tilted Densities'," IEEE International Conference on Acoustics, Speech, and Signal *Processing*, Vol. 3, pp. 1454-1457, Boston, MA, 14-16 April 1983.